Flinders UNIVERSITY
ADELAIDE · SOUTH AUSTRALIA

Streamflow generation for Intermittent Rivers and Ephemeral Streams

By

Karina Yazmin Gutiérrez Jurado

Thesis
Submitted to Flinders University
for the degree of

Doctor of Philosophy

College of Science and Engineering
October 2020

Declaration

I certify that this thesis does not incorporate without acknowledgment any material previously submitted for a degree or diploma in any university and that to the best of my knowledge and belief it does not contain any material previously published or written by another person except where due reference is made in the text.

.....

Karina Y. Gutiérrez Jurado

27 October 2020

Coauthorship

Karina Y. Gutierrez Jurado is the primary author of this thesis and all the enclosed documents. Chapter 2 was written as an independent manuscript in which the co-authors provided intellectual supervision and editorial comments.

Dedication

To Zack my star editor and accomplice through it all,

To Mum my greatest example, biggest motivation in life and the most badass person I know,

To Dad always fighting the windmills,

To Ivan who was lost but found his way back home,

To Hugo, Roshelly, and Adriel even though you punks left,

To Cesar always cheering for me,

To all my friends around the world for sharing this journey called life with me,

Finally, to you, graduate student,

Push back, stand for yourself, and fight the broken system,

This is your life, this is your journey,

You are the captain of this ship,

Run it like a Pirate and throw anyone overboard that wants to tell you otherwise,

Aaaarrrrgggghhhh,

Ahoy, Me Hearties!

All Hand Hoy!

YOU GOT THIS!

Dedicatoria

A Zackito, mi editor estrella y cómplice en esta aventura/tortura,

A Roskita, mi ejemplo a seguir, mi mayor motivación y la persona más chingona en todo el mundo,

A Roskito, siempre peleando contra los molinos de viento,

Al Mudis, que estuvo perdido, pero encontró su camino de vuelta a casa,

Al Chango, la Piswa y el Pukis, aunque me hayan abandonado mugrosos,

Al Querido Cuil, siempre echándome porras,

A mis amigos desparramados por todo el mundo por compartir esta aventura llamada vida,

Y finalmente a ti, estudiante de posgrado,

Pelea por lo que es justo,

No aceptes un "no" por respuesta de un sistema que está roto,

Hecha pa' delante y cámbialo,

Esta es tu vida, esta es tu aventura,

Tú eres el Capitán de este barco,

Navégalo como un Pirata echando al agua a cualquiera que quiera decirte lo contrario,

Aaaarrrrgggghhhh,

¡Ahoy, Compañero!

¡Todos a cubierta!

TU PUEDES!

Acknowledgements

To paraphrase a very wise (and modest) person "Every major accomplishment in life is rarely the result of a single person's effort but it rather stems from the support of an amazing group of people behind someone's journey" – KYGJ 2014

I would like to express my gratitude to my main supervisor, Dr. Margaret Shanafield, for giving me the opportunity to pursue this PhD and trusting me with a challenging and fascinating topic. I also want to thank my co-supervisors, Dr. Peter Cook and Dr. Okke Bateelan, for their invaluable support and insight throughout this thesis process.

A special mention to the brilliant professors, researchers, visiting academics, and post-docs of the College of Science and Engineering and the National Centre for Groundwater Research and Training (NCGRT) at Flinders University, from whom I learnt invaluable lessons both academically and personally. A huge thank you goes to Dan Partington for all his help and for sharing his modelling and programming wizardry, and to Romana Challans for "saving the day" more than once. I also would like to acknowledge the amazing support of the administrative and technical staff of the College of Science and Engineering and the NCGRT. A special shout out to Nick White for all his help, specially that time he helped me "dig out" sensors that were not even there and for walking alongside me endless kilometres of Pedler creek. Some of the best memories from this adventure will always be those from the field campaigns that promised (and delivered) "camping under the stars with a stimulating company", even if at first I did not understand a word of what he was saying.

I also want to thank the Australian Research Council for the funding provided for this research by the grant DE150100302 and to Flinders University for providing me with a 3-year tuition fee scholarship for my 4 year program and then kindly agreeing to extend it, after I fought them for it.

A profound thank you goes to all my friends who always helped me find some joy even through the rough times, you all made the somewhat torturous PhD journey a fun and memorable adventure. To my friends I left back on the other side of the ocean who supported me from afar, I am sorry I missed your weddings, birthdays, and graduations, and I hope you all know I keep you all close to my heart. A special shout out to the PONYS, the BGNS, the BB4Lyf, the 5oS crew, Ainhoa, Andrew, Antara, Miriam, and Rachael. When you are away from home for so long your

friends become your family, that is how I regard you all and I am very grateful for every single one of you. A special thank you goes to those of you also going through a PhD journey, struggling alongside you was at times the one thing that kept me afloat, if you were not giving up neither was I. A special mention goes to my office mates Sarah, Ferijal, Lanre, Cristina, Ajiao, Rena and Djamil, Aurélie, Yogita, Julie, Birte, and Marcio. I also want to thank everyone that participated in Cake-Club, one of my biggest achievements will always be to have been able to lure you out of your offices to meet over a piece of delicious cake, you nerds can be a tough crowd. Without a doubt Cake-club was the best weekly meeting throughout all this PhD. Thanks Marianina for taking over and continue this awesome tradition, I could not wish for a better "heiress for the Cake-Club throne". A very special mention goes to my social justice warrior teammate Robin, our little crusade against the Uni for their initially terrible response (or the lack thereof) to the COVID crisis gave me purpose when I needed it the most. I learnt so much from you and I can just hope that you never stop getting in "good and necessary trouble", in fact I am counting on it.

A huge thank you goes to my counsellor David. I would not had made it through the last part of this journey without him assuring me I was not completely crazy (just a healthy bit) and reminding me to "just breathe".

My deepest gratitude goes to my family, when everything else felt uncertain, it was their love, support, and faith in me that pushed me forward. I owe everything I am and every success to them. I am forever grateful to my parents for all their sacrifices and for always encouraging me to dream big even if those dreams were taking their little girl far away. The most heartfelt thank you goes to my brothers for showing me that with hard work, determination, and courage, any dream can come true. Thank you for setting the bar so high you punks!

A final and most special thank you goes to my partner in crime who was crazy enough to follow me across the world and who supported me through the roughest of times, sending me to work with a full belly and receiving me home with a warm dinner. Even if our journeys have taken different directions, I will always owe a big part of this accomplishment to you and I will be forever grateful for everything we shared.

Agradecimientos

Parafraseando a una persona sabia (y modesta) *"Cada logro importante en la vida es raramente el resultado del esfuerzo de una sola persona, más bien proviene del apoyo de un grupo increíble de personas que van detrás del caminar de alguien" – KYGJ 2014*

Primeramente, quiero expresar mi gratitud a mi supervisora la Dra. Margaret Shanafield, por darme la oportunidad de realizar este doctorado y por confiarme con un tema desafiante y fascinante. También quiero agradecer a mis co-supervisores, el Dr. Peter Cook y el Dr. Okke Bateelan, por sus invaluables consejos y apoyo a lo largo de esta tesis.

Una mención especial a los brillantes profesores, investigadores, académicos visitantes y postdoctores de la Facultad de Ciencias e Ingeniería y del Centro Nacional de Investigación y Capacitación de Aguas Subterráneas (NCGRT por sus siglas en ingles) de la Universidad de Flinders, de quienes aprendí lecciones invaluables tanto académicas como personales. En particular quiero agradecer a Dan Partington por toda su ayuda y por compartir sus mejores trucos de modelación y programación, y a Romana Challans por "salvar el día" más de una vez. También quiero agradecer el increíble apoyo del personal administrativo y técnico Facultad de Ciencias e Ingeniería y del NCGRT. Un agradecimiento especial a Nick White por su increíble ayuda, especialmente esa vez que me ayudó a "desenterrar" unos sensores que ni siquiera estaban allí y por caminar conmigo los interminables kilómetros del arroyo Pedler. Algunos de los mejores recuerdos de esta aventura serán siempre los de las campañas de campo que prometían "acampar bajo las estrellas con una compañía estimulante", aun cuando al principio no entendía le entendía media palabra a Nick.

Igualmente quiero agradecer al Consejo de Investigación Australiano por el financiamiento proporcionado para esta investigación y a la Universidad de Flinders por proporcionarme una beca de 3 años para la colegiatura, aunque el programa es de 4 años, pero que luego amablemente accedieron a extenderla, claro después de que les diera guerra por ello.

Un profundo agradecimiento a todos mis amigos por ayudarme a encontrar siempre algo de alegría aun en los momentos más difíciles, todos ustedes hicieron de esta tortuosa experiencia una aventura bonita y memorable. A mis amigos que dejé al otro lado del océano que me apoyaron desde lejos, lamento haberme perdido sus bodas, cumpleaños y graduaciones, pero espero que todos sepan que

los mantengo siempre cerca de mi corazón. Un agradecimiento especial a los PONYS, BGNS, BB4Lyf, la pandilla de 5oS, Ainhoa, Andrew, Antara, Miriam y Rachael. Cuando se está fuera de casa por tanto tiempo, los amigos se vuelven familia y yo así los considero a todos ustedes y estoy muy agradecida por lo poquito o mucho que he compartido con cada uno de ustedes. Un agradecimiento especial para aquellos de ustedes que también estuvieron o están en este condenado barco llamado doctorado, compartir esta aventura con ustedes fue a veces lo único que me mantuvo a flote, porque si ustedes no bajaban bandera, yo tampoco. Una mención especial para mis compañeros(as) de oficina Sarah, Cristina, Ajiao, Lanre, Rena y Djamil, Aurélie, Yogita, Julie, Birte y Marcio. También quiero agradecer a todos los que participaron en Cake-Club, uno de mis mejores logros fue lograr sacarlos de su oficina una vez por semana para compartir una rebanada de pastel. Sin duda la mejor junta semanal que tuve durante todo mi doctorado. Gracias Marianina por tomar la batuta y seguir con esta bonita tradición, no hubiera podido encontrar una mejor heredera al trono. Una mención muy especial para Robin, mi compañero de guerra de las causas de justicia. Nuestra pequeña cruzada contra la Uni por la terrible respuesta inicial (o la falta de ella) a la crisis del COVID me dio un propósito cuando más lo necesitaba. Aprendí mucho de ti y solo espero que nunca dejes de meterte en "problemas" de esos "buenos y necesarios" que se requieren para hacer de este mundo un lugar mejor, de hecho cuento con ello.

Un agradecimiento inmenso para mi terapeuta David, no hubiera logrado llegar al final de este viaje sin él asegurándome que no estaba completamente loca (solo un poquito y del lado izquierdo) y ayudándome a recordar que a veces solo hace falta parar y respirar.

Mi más profundo agradecimiento es para mi familia, cuando todo lo demás se sentía incierto, fue su amor, apoyo y fe en mí lo que me impulsó a seguir adelante. A ustedes les debo todo lo que soy y todos mis éxitos. Siempre estaré agradecida con mis padres por todos sus sacrificios y por siempre alentarme a soñar en grande incluso si esos sueños se iban a llevar a su niña tan lejos. El más sincero agradecimiento es para mis hermanos por mostrarme que con trabajo duro, determinación y coraje, cualquier sueño puede hacerse realidad. ¡Gracias por dejarme tan altas expectativas canijos!

Finalmente quiero expresar mi más grande gratitud para mi codelincuente en esta aventura que fue lo suficientemente loco para seguirme al final del mundo y que me apoyó en los momentos más difíciles, enviándome a trabajar con la barriguita llena y recibiéndome a casa con una cena calientita. Aun si nuestro caminar ha tomado direcciones diferentes, siempre te deberé una gran parte de este logro y estaré eternamente agradecida por todo lo que compartimos juntos.

Summary

Intermittent rivers and ephemeral streams (IRES) account for over 50% of the world's river network and are expected to increase with climate change and the increasing pressure on water resources. In a world of increasing water scarcity, understanding the hydrology of IRES from arid and semi-arid regions, including those in Mediterranean climates, has become increasingly important. The biggest limitations for hydrological studies in IRES stem from the difficulties to monitor them resulting in the lack of long-term-spatially-distributed streamflow observations. The most significant challenges to better manage IRES in semiarid catchments with Mediterranean climates are to understand the threshold behaviour of streamflow generation and to improve our capacity to monitor their flow/no-flow transitions.

This research aims to advance the understanding of streamflow generation in IRES from semiarid catchments with Mediterranean climates, with a focus on understanding hydrological processes and to advance a simple method to infer flow/no-flow conditions from streambed temperature measurements. In particular, this work investigates: [1] what triggers streamflow for Intermittent Rivers and Ephemeral Streams in Low-Gradient Catchments in Mediterranean Climates? [2] can an integrated model be used to capture the conceptualized streamflow generation processes of an intermittent stream at the catchment scale?, and [3] can we use only streambed temperature data to monitor intermittent streamflow in an intermittent Mediterranean-climate catchment?

For the first and second part of this study we used fully Integrated Surface-Subsurface Hydrological Models (ISSHMs) to investigate streamflow generation in IRES. We focused on understanding the dominant flow generation mechanisms and the development and spatial extent of flow generating areas at the threshold of flow generation. In the first study we followed a concept-development approach to explore the effect of a range of catchment and climatic controls representative of low-gradient Mediterranean-climate IRES on the threshold of flow. In the second study, we implemented an ISSHM for a medium-size Mediterranean-climate catchment in South Australia to test how streamflow generation concepts and theories from the smaller and simplified models would apply in a real

catchment. Results from both studies showed that soil type and topography exerts the greatest influence on streamflow generation and dictate the spatiotemporal development of flow by a given flow generation mechanism. These studies provided important insight into the pathways and thresholds of flow generation which were visible from the distinct flow generation mechanisms.

The third part of this study we applied a novel temperature-based method on a continuous wavelet transform (CWT) analysis to a field dataset to develop guidelines to estimate a flow/no-flow threshold and to evaluate its application and performance capturing streamflow in an intermittent Mediterranean-climate catchment in South Australia. We showed that the CWT method with the developed guidelines had a good performance capturing intermittent flow and that there is the potential to infer ponding conditions and hydrograph peaks and recession periods from the CWT results.

Overall, the results on capturing the dominant flow processes are promising and provide important insights on the hydrology of IRES and on the challenges of implementing ISSHMs for process understanding in these systems. The results from the CWT showed the method's potential to generate a better understanding of the seasonal flow variability in IRES. Future work should build upon the lessons learned from this PhD to continue advancing our understanding of the threshold behavior of streamflow generation in IRES.

Contents

List of Figures

List of Tables

Chapter 1

Introduction

Overview of key information relevant for the study of intermittent rivers and ephemeral streams (IRES) is presented in this section. The following sections include main hydrological and general concepts, and a review of studies highlighting the most relevant research and most important knowledge gaps.

1.1 IRES Hydrology

Streams are defined by their flow duration into perennial and non-perennial. Perennial streams are those that flow continuously supported by baseflow (i.e. groundwater contributions) and are more common on the lower sections of a catchment. Non-perennial streams flow discontinuously and can be further classified as ephemeral and intermittent streams. Ephemeral streams are disconnected from the groundwater lacking a source of baseflow and therefore flow only during or directly after intense precipitation events. Intermittent streams refer to channels that flow continuously for a period of the year, usually as a response to the onset of snowmelt on alpine areas or seasonal runoff and elevated groundwater tables product of the rainy season on a region (Levick et al., 2008). In many areas, seasonal groundwater table fluctuation is a main driver for intermittent flow. During the dry season, groundwater tables are usually low and therefore located below the stream bed. During the wet season groundwater tables increase in response to seasonal precipitation, the decreased of evapotranspiration or a combination of both. As the groundwater table rises and intersects the stream channel, the reach becomes a gaining stream with a source of base flow. In other areas, flow intermittency is supported by delayed subsurface flow from delayed from areas with higher infiltration capacities.

An important hydrologic characteristic of IRES are the highly complex longitudinal dynamics given by the onset and cessation of flow. Such dynamics encompass the development, expansion, and contraction of the wetted fronts, the hydrological connections-disconnections in time and space, and flow permanence (Larned et al., 2010).

1.2 IRES Distribution

IRES are one of the most widespread water systems accounting for over half of the world's river network (McDonough., 2011; Sheldon et al., 2010; Datry et al., 2014). They exist in all continents and through all climates. While they are prevalent in arid-semiarid and Mediterranean-climate regions, they are found across all the terrestrial biomes and throughout the river system. (Costigan et al., 2016; Larned et al., 2010; Skoulikidis et al., 2017; Steward et al., 2012). Their extensive distribution has been recognized in previous studies. Davies et al. (1993) mentions that about 40% of the river channels in South Africa present periods of no-flow. For the United States, IRES are estimated to account for roughly 60% of the total stream network (excluding Alaska) at the 1:100 000 scale, and more than 80% in most of the Southwest region (Nadeau & Rains, 2007). In Australia, the driest inhabited continent on earth, around 70% of the rivers measured at the 1:250 000 scale are "dryland" rivers and can be considered ephemeral (Sheldon et al., 2010).

Additionally, in the last 50 years most of the formerly perennial rivers in arid and semiarid regions have become intermittent, including some major rivers such as the Nile in Africa, Yellow in Asia, and the Rio Grande bordering the US and Mexico (Datry et al., 2014). With projected climate shifts and the increasing demand on water supply, more perennial rivers are likely to become intermittent (Costigan et al., 2016; Datry et al., 2014; Larned et al., 2010; McDonough et al., 2011).

1.3 IRES Terminology

Due to their extensive and diverse distribution from alpine zones to tropical areas, and from large first order rivers in wide alluvial corridors to small headwaters in steep mountainous catchments (Costigan et al., 2016; Larned et al., 2010; Skoulikidis et al., 2017; Steward et al., 2012), IRES have a wide range of catchment characteristics and hydrological regimes. For instance, temporary systems in Australia were classified into eight distinctive flow regimes for varying degrees of flow permanence, seasonality, flood characteristics, and flow variability and predictability (Kennard et al., 2010).

For the context of this thesis, and aligned with current research networks in IRES around the world (Costigan et al., 2017; Datry et al., 2016) at the start of this work, we define IRES as

flowing watercourses in which flow cessation occurs and which remain dry at some point in time and space along their courses.

Figure 1.1 Different names for intermittent and ephemeral streams around the world

1.4 IRES Significance

The importance of IRES has been documented in a broad set of disciplines including river ecology, hydrology and geohydrology, and socioeconomics. Historically, for over 3000 years, IRES have been a source of irrigation supporting agriculture around the world (Larned et al., 2010; Nabhan, 1979; Sandor et al., 2007). In most arid and semi-arid regions IRES represent an important source of water which is critical to meet water demands in local communities (Lange, 1998; Levick et al., 2008; Seely et al., 2003). Similarly, IRES provide important environmental services supporting key biotic communities. The transformation from terrestrial to aquatic habitat mosaics highly influence biotic communities by providing unique habitat to a wide diversity of species and serving as dietary "hot spots". Even during the dry periods it has been documented that dry riverbeds are an important habitat and refuge for mammals and persisting pools serve as refuge for aquatic and semi-aquatic organisms (Sheldon et al., 2010). Additionally,

IRES enhance the transport of nutrients and organic matter processing (Datry et al., 2014; Larned et al., 2010) which are key for water quality.

Accounting for over 50 % of the total river network and discharge globally, IRES are closely linked to perennial streams networks and highly influence the global hydrological cycle. Freeman (2007) highlighted the importance of these systems in the hydrologic connectivity in the broader regional and global scales for the "water-mediated transport of matter, energy, and organisms within or between the elements of the hydrologic cycle." Finally, in arid and semi-arid regions, seepage from IRES is thought to represent the main source of groundwater recharge (Batlle-Aguilar et al., 2015; Costa et al., 2013; Shanafield & Cook, 2014; Shanafield et al., 2014).

1.5 IRES Main Knowledge Gaps

With climate change and an increasing global population the world's water resources are expected to become more stressed (Thomas et al., 2016). This is particularly true for arid and semiarid regions where IRES are dominant. In a world of increasing water scarcity, understanding the hydrology of dryland rivers has become ever more important.

Increasing awareness of their importance and their vulnerability to climate change has been at the centre of a surge of research on IRES over the past decades (Assendelft & van Meerveld, 2019). However, the bulk of these studies have been done under the scope of ecological and biological research (Acuña et al., 2014; Bond & Cottingham, 2008; Costigan et al., 2016; Datry et al., 2016, 2014; Kennard et al., 2010; Larned et al., 2010; Skoulikidis et al., 2017; Steward et al., 2012; Stubbington et al., 2018) and important knowledge gaps of the hydrological functioning of IRES remain.

The highly variable flow regimes, often flashy and erosive flows, their unpredictable flood timing and the often-difficult access to the remote areas where they are found makes research challenging and has historically led to neglecting IRES. Indeed, it has been shown that streamflow gauges, which provide the most fundamental data to understanding the hydrology of rivers, are preferentially located on perennial rivers (Fekete & Vörösmarty, 2002; Poff, Bledsoe, & Cuhaciyan, 2006). These limitations have resulted on the lack of long-term-spatially-distributed streamflow observations for IRES (Fekete & Vörösmarty, 2002; Poff, Bledsoe, & Cuhaciyan, 2006; Tzoraki & Nikolaidis, 2007). A few studies have attempted to advance new

techniques and methodologies to capture and monitor streamflow in IRES (Arismendi et al., 2017; Assendelft & van Meerveld, 2019; Blasch et al., 2002, 2004; Constantz et al., 2001; C. S. Goulsbra et al., 2009; Gungle, 2006). However, to date, all methods require time consuming calibration periods, the calculation of complicated and site-specific set of parameters, or complicated installations which hinder their implementation.

Resulting from all these challenges, many studies on IRES have derived from research of perennial streams which contain intermittent or ephemeral sections common in small mountainous headwater catchments in temperate-humid climates. The majority of these studies have therefore focused on understanding streamflow dynamics on IRES from the expansion and contraction of the drainage network (Durighetto et al., 2020; Fritz et al., 2013, 2008; Godsey & Kirchner, 2014; C. Goulsbra et al., 2014; Peirce & Lindsay, 2015; Prancevic & Kirchner, 2019; Ward et al., 2018; Whiting & Godsey, 2016; Wigington et al., 2005; Zimmer & McGlynn, 2017). However, in many arid-semiarid and Mediterranean-climate catchments, IRES do not originate from the expansion of an already flowing stream but rather developed from completely dry stream network sections. Under these conditions, the development of flow generating areas at the catchment scale occur fragmented across the stream network resulting in highly variable flow patterns. Coupled with the lack of data, the added difficulties of characterising unsaturated flow, the natural wetting and drying cycles, and other highly non-linear processes, there are still large knowledge gaps in our understanding of the processes that lead to streamflow generation in IRES. Arguably one of the most important gaps in our understanding of the hydrology of arid-semiarid and Mediterranean-climate IRES is how they transition from dry to flowing and back to dry (i.e. onset and cessation of flow) and the streamflow processes associated with these transitions (Costigan et al., 2016, 2017; Shanafield et al [in prep]).

1.6 Research aims

This PhD aims to advance the understanding of streamflow generation of intermittent rivers and ephemeral streams from semiarid catchments with Mediterranean climates with a focus on investigating the transition from a dry to a flowing state. The foundations of this research are to [1] understand the threshold of streamflow generation in IRES, with an emphasis on the spatiotemporal variability of the hydrological processes occurring and contributing to this threshold and [2] to investigate an alternative methodology that would improve our capability to monitor streamflow generation in IRES. To accomplish these overall goals, we used a combination of physically based Integrated Surface-Subsurface Hydrological Models (ISSHMs) and the analysis of historical field data of an Intermittent Mediterranean-climate catchment located in South Australia. The specific goals of this PhD are to provide insight to the following three research questions:

Question 1. What triggers streamflow for Intermittent Rivers and Ephemeral Streams in Low-Gradient Catchments in Mediterranean Climates?
Method. A Concept-development approach implementing an ISSHM in a theoretical catchment to investigate streamflow generation processes.

Question 2. Can an integrated model be used to capture the conceptualized streamflow generation processes of an intermittent stream at the catchment scale?
Method. Development of a conceptual model for flow generation in an intermittent Mediterranean-climate catchment to test against the results from an ISSHM.

Question 3. Can streambed temperature data alone be used to monitor intermittent streamflow in an intermittent Mediterranean-climate catchment?
Method. Testing and advancing the use of Continuous Wavelet Transforms to identify streamflow in an intermittent Mediterranean-climate catchment.

These specific knowledge gaps and methodologies are the focus of Chapters 2 through 4. Chapter 2 is a manuscript now in press and Chapters 3 and 4 are in preparation for publication. Conference proceedings and supplementary data and analysis from preliminary work contained in this thesis are presented in Appendices A through L.

Chapter 2

What triggers streamflow for Intermittent Rivers and Ephemeral Streams in Low-Gradient Catchments in Mediterranean Climates

Accepted in Water Resources Research and reproduced with permission. Gutiérrez-Jurado, K. Y., Partington, D., Batelaan, O., Cook, P., & Shanafield, M. (2019). What triggers streamflow for intermittent rivers and ephemeral streams in low-gradient catchments in Mediterranean climates.

doi: 10.1029/2019WR025041.

1.7 Abstract

Intermittent rivers and ephemeral streams (IRES) account for over 50% of the world's river network and are expected to increase with climate change and the increasing pressure on water resources. One significant challenge to better manage IRES is unraveling the threshold behavior of streamflow generation, by understanding what controls the triggers of streamflow. This study aimed to understand the influence of groundwater depth, soil hydraulic properties, and rainfall on streamflow generation in IRES, through analyzing the spatiotemporal development of active areas (where flow generation processes are occurring) and determining the dominant flow generation mechanisms. In a concept-development approach, we used fully Integrated Surface-Subsurface Hydrological Models to investigate streamflow generation for a range of characteristics representative of IRES in low-gradient catchments with Mediterranean climates. The results showed that soil type exerts the greatest overall influence on streamflow generation and is the main factor determining the spatiotemporal development of active areas by a given flow generation mechanism and threshold contributing processes. The identified dominant mechanism for each soil demonstrated the effect of the initial groundwater head and rainfall scenarios on the timing and processes that trigger streamflow onset. These results reaffirm the importance of unsaturated storage dynamics to explain thresholds and pathways of flow and

suggest that knowledge of the development of active areas and prediction of the dominant flow generation mechanisms is critical to understand streamflow generation in IRES. Future research should identify the influence of catchment morphology, geologic constraints, and aquifer heterogeneity and anisotropy on streamflow generation in IRES.

1.8 Plain Language Summary

"Temporary rivers" is a broad term used to classify waterways that are dry for some part of the year. They contribute roughly 50% of all the world's available river water, are important for groundwater replenishment, and maintain key environmental services. To manage them, we need to understand how they transition from a dry to a flowing state. In this study, we use computer models to explore how rainfall, soil properties, and the depth to groundwater affect the processes that trigger when this transition occurs. We tested over 1,600 scenarios to explore the effect of different factors on when, where, and why these rivers will flow. Results showed that soil type was the main control determining when and where flow is generated and is the governing factor dictating the different ways water gets to the river. For this, we identified distinct pathways that water takes to get to the river for each of the tested soils. Understanding the different pathways in which water moves through the catchment can help manage vulnerability of temporary rivers to the impacts of land use changes, soil erosion, and prolonged droughts. Future studies should investigate the effects of catchment morphology and heterogeneity on streamflow generation in IRES.

1.9 Introduction

Intermittent rivers and ephemeral streams (IRES) are one of the most widespread and dynamic water systems. They are present in all continents and climates and account for over 50% of the world's river network and global discharge (Acuña et al., 2014; Costigan et al., 2016; McDonough et al., 2011; Sheldon et al., 2010). While they are the predominant feature in arid - semiarid and Mediterranean-climate regions, they are found across all terrestrial biomes and throughout the river system. Due to their extensive distribution and diversity from alpine zones to tropical areas, and from large first order rivers in wide alluvial corridors to small headwaters in steep mountainous catchments (Costigan et al., 2016; Larned et al., 2010; Skoulikidis et al., 2017; Steward et al., 2012), IRES have a wide range of catchment characteristics and

hydrological regimes. For instance, temporary systems in Australia were classified into eight distinctive flow regimes for varying degrees of flow permanence, seasonality, flood characteristics, and flow variability and predictability (Kennard et al., 2010). For the context of this paper, and aligned with current research networks in IRES around the world (Costigan et al., 2017; Datry et al., 2016), we define IRES as flowing watercourses in which flow cessation occurs and which remain dry at some point in time and space along their courses.

The variability of their flow regimes, flashy and erosive flows, and their unpredictable flood timing have restricted IRES research (Constantz et al., 2001; Levick et al., 2008). While there are some studies related to streamflow generation for IRES, there has been little focus on understanding the hydrological processes that determine the threshold for flow generation. Most studies have focused instead on understanding the dynamics and patterns of expansion and contraction of the drainage network (Godsey & Kirchner, 2014; Goulsbra et al., 2014; Peirce & Lindsay, 2015; Prancevic & Kirchner, 2019; Ward et al., 2018), the effects of flow permanence (Fritz et al., 2008; Fritz et al., 2013), and in advancing techniques and new methodologies to capture and monitor streamflow (Blasch et al., 2002, 2004; Constantz et al., 2001; Goulsbra et al., 2009). The few process - based studies on streamflow generation for IRES have mainly been conducted in small headwater catchments, often in temperate or humid climates (Zimmer & McGlynn, 2017; Zimmermann et al., 2014). In such systems, streamflow generation processes are primarily driven by soil moisture content and catchment topography (Penna et al., 2011). However, in semiarid, low - gradient catchments in Mediterranean climates, such as those commonly found in Australia, California, and Africa, the questions of when, where, and why do IRES start to flow remain unanswered.

Traditionally, streamflow generation has been investigated through hillslope studies on perennial systems. Although the hydrological principles that underpin these studies apply to IRES, the assumptions and scope under which such studies were developed raise important questions and leave key knowledge gaps to understand IRES. One important limitation is that traditional hillslope studies only offer localized insight. Even for perennial systems, it is well recognized that the localized approach of hillslope studies does not provide a comprehensive understanding of the hydrological response at the catchment scale (Frisbee et al., 2011). For instance, Ambroise (2004) argues that the common concept of variable source area, which was

largely used to explain streamflow generation in small catchments in humid climates, does not capture the spatiotemporal variabilities that control catchment dynamics.

A second issue with traditional hillslope studies is that the typical conceptualization of hillslope hydrology assumes rainfall always results in surface or subsurface runoff ("rainfall - runoff" approach) or replenishes storage, generally with the inherent assumption of a baseflow component and therefore a permanently saturated area contributing to streamflow. Under this approach, the generation of "some" runoff-streamflow in response to rainfall is virtually guaranteed. Hence, the river hydrograph is evaluated in terms of volumetric flows or peak-recession dynamics (Freeze, 1974; Hallema et al., 2016; Mosley, 1979; Pearce, 1990). This is problematic for IRES, which typically have dry initial conditions. Moreover, they are often disconnected from groundwater (GW), which buffers the streamflow response to precipitation. Although streamflow in IRES can be generated in response to single extreme precipitation events, in many catchments, flow is mostly linked to a series of precipitation events overtime; as water moves though the system, certain thresholds must be reached before streamflow is generated (Figure 0.1). Moreover, without the baseflow component and/or a saturated contributing area, streamflow is often generated discontinuously along a segmented drainage network. The complexity of the development, expansion, contraction, and fragmentation of the partially saturated areas and the drainage network results in intricate spatiotemporal variability of hydrological processes (e.g., Partington et al., 2013). These complex dynamics raise key questions regarding the development of areas where flow generation processes are occurring and how they influence the integrated catchment response leading to streamflow generation in IRES. For the context of this paper, these areas where flow is generated at a given time by a given flow generation mechanism are defined as "active areas"; a variation on this term as first used by Ambroise (2004). Defining the development of these active areas and the mechanisms that trigger the onset of streamflow is one of the most important challenges to better understand the hydrology of IRES (Bond & Cottingham, 2008; Costigan et al., 2016; McDonough et al., 2011).

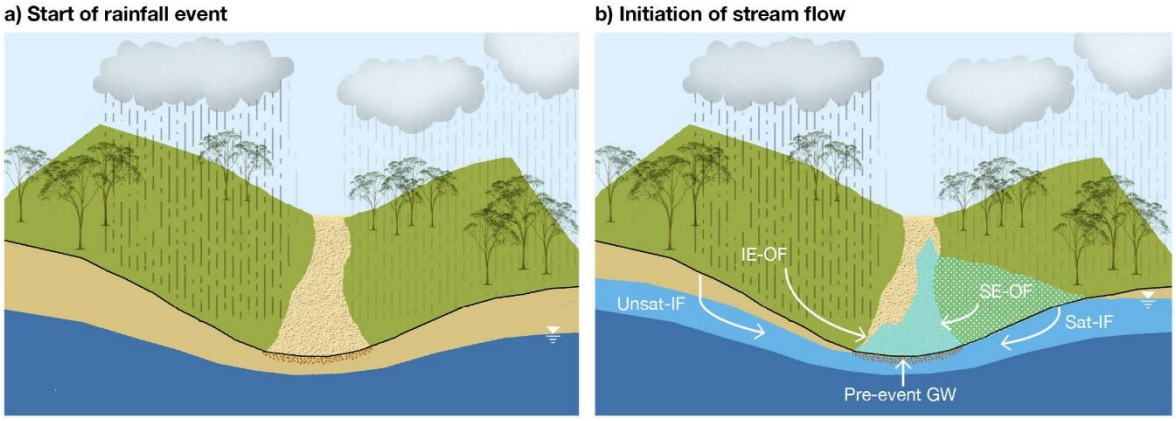

Figure 0.1 Conceptual diagram showing the transition from a dry (a) to a flowing stream (b). The main processes contributing to the initiation of streamflow typical of intermittent rivers and ephemeral streams are shown, although additional processes occur within the hydrologic cycle. Flow generation mechanisms include infiltration excess overland flow (IE-OF), saturation excess overland flow (SE-OF), interflow generating from saturated and unsaturated soil profiles (unsaturated interflow [Unsat-IF]/saturated interflow [Sat-IF]) and pre-event groundwater (GW). All generation mechanisms can occur directly on the stream and on the hillslope, but for clarity, they are only denoted once.

The data paucity of most IRES, as they are often part of ungauged basins, leads to insufficient long-term, comprehensive data sets and contributes to the lack of understanding of the controls and processes leading to streamflow generation in IRES (Constantz et al., 2001; Tzoraki & Nikolaidis, 2007). In the context of limited data availability, fully Integrated Surface-Subsurface Hydrological Models (ISSHMs) (Sebben et al., 2013) have been used in recent years for concept-development studies (Loague et al., 2010; Mirus et al., 2011) to advance the understanding of catchment processes (Loague et al., 2006; Mirus et al., 2011; Mirus & Loague, 2013; Partington et al., 2013; VanderKwaak & Loague, 2001). The latest generation of ISSHMs have surpassed the original "blueprint" proposed by Freeze and Harlan (1969) (Loague et al., 2010), demonstrating their ability to fully integrate the surface and subsurface flow domains and produce physically consistent simulations (Fatichi et al., 2016; Kollet et al., 2017). The integration of surface-subsurface processes is particularly important for streamflow generation studies in IRES, where the feedbacks between the surface and subsurface domains are requisite to understanding the underlying hydrological processes.

The fully integrated approach of ISSHMs, together with advancements in computational efficiency (Brunner & Simmons, 2012; Trudel et al., 2014), led to widespread use of ISSHMs for studies simulating streamflow generation over the last two decades. These studies were able

to identify and differentiate dominant controls of streamflow generation (VanderKwaak & Loague, 2001), the spatiotemporal variability of the hydrological processes (Park et al., 2011), and the overall surface-subsurface hydrodynamic processes (Sudicky et al., 2008). Further studies have provided an insight on the effects of topography (Frei et al., 2010; Frei & Fleckenstein, 2014; Ivanov et al., 2004; Weill et al., 2013); the spatial variability of saturated hydraulic conductivity (Maxwell, 2010; Maxwell & Kollet, 2008; Meyerhoff & Maxwell, 2011); fractured bedrock flow contributions (Ebel et al., 2007, 2008); and rainfall characteristics (Mirus & Loague, 2013) on the controls of streamflow generation.

Although ISSHMs have been used in IRES or under scenarios representative of these temporary systems (with dry initial conditions and a disconnected GW domain), often the simulations are conceptualized as a single event forced hydrologic response (rainfall-runoff) with the main aim of testing the discharge response at the outlet rather than to understand the processes and longer term hydrological responses critical for IRES (Di Giammarco et al., 1996; Kollet et al., 2017; Panday & Huyakorn, 2004). In other cases, the focus is on trying to reproduce an integrated catchment response (Heppner et al., 2007; Mirus et al., 2009) and to evaluate how this response varies under different scenarios (Carr et al., 2014; Heppner & Loague, 2008). Nevertheless, by far, the majority of hydrological modeling has been done on perennial streams, or in the case of theoretical simulations, under the assumptions typical for perennial streams. This is evident when considering that the bulk of streamflow generation studies, benchmark cases, and modeling research is conceptualized as rainfall-runoff simulations of partially saturated catchments (Aquanty, 2016; Jones et al., 2006; Kollet et al., 2017; Sebben et al., 2013). Subsequently, ISSHMs model performance diagnosis is based on the catchment outflow hydrograph and water balance (Ala-aho et al., 2017; Sebben et al., 2013), both of which are evaluated in a similar fashion to those in traditional rainfall-runoff modeling.

While valuable insight on streamflow generation has been gained from these previous process-based and modeling studies for perennial and non-perennial systems, their scope, approach, and limitations have not addressed one of the fundamental components of IRES: understanding the transition from a dry to a flowing system. In a review on intermittent river research, Costigan et al. (2016) highlighted the need for future work on understanding the threshold behavior of

streamflow generation, with a focus on identifying the spatiotemporal variability of the hydrological processes occurring and contributing to this threshold.

To identify how active areas develop, streamflow thresholds are reached, and streamflow begins, it is paramount to track the water as it moves though the system. The Hydraulic Mixing-Cell (HMC) method developed by Partington et al. (2011) offers this capability, allowing insight into the spatiotemporal variability of the hydrological processes and identification of the dominant mechanisms contributing to the threshold of streamflow generation (this method is detailed below). Therefore, the goal of this study is to make a first step toward developing a quantitative understanding of the controls on the threshold behavior of streamflow generation and the associated relationships of these thresholds to certain catchment characteristics and climatic controls.

We follow a concept-development approach implementing an ISSHM coupled with the HMC method to investigate the controls that dictate the threshold behavior of streamflow generation for a range of catchment and climatic characteristics representative of the particular cases of IRES in low gradient catchments with Mediterranean climates. The main objectives of this study are to provide insight into when, where, and why these IRES start to flow by determining the extent to which:

1. Initial depth to GW, soil hydraulic properties, and different precipitation rates and durations dictate streamflow generation and time to flow.

2. Dominant flow generation mechanisms are clearly identifiable in IRES streamflow generation.

3. The development of the active areas and processes impacts the threshold of streamflow generation.

1.10 Methods

1.10.1 The Fully Integrated Modeling Platform and HMC Method

The selected model platform for simulating flow in this study is the three-dimensional (3D), fully integrated, surface-subsurface model HydroGeoSphere (HGS) (Aquanty, 2016). HGS uses

the control-volume finite element method, a mass conservative modeling approach, to couple surface/subsurface flow and transport. The numerical formulation for subsurface 3D saturated/unsaturated flow is based on a modified Richards' equation, while surface water flow is simulated though the depth-integrated diffusion-wave approximation of the Saint-Venant equations. Detailed information on HGS physical conceptualization, discretization, and numerical implementation can be found in Aquanty Inc. (2016) and the review by Brunner and Simmons (2012). Flow generation mechanisms are tracked with the HMC method, which is based on the modified mixing-cell method of Campana and Simpson (1984). Originally developed to extract the GW component of streamflow at any point along the stream using standard hydrological output from ISSHMs (Partington et al., 2011), it was later used to investigate baseflow dynamics (Li et al., 2013, 2014; Li et al., 2015; Partington et al., 2012). In a later work, Partington et al. (2013) extended the HMC analysis to quantify flow generation processes by area (i.e., hillslope or in-stream) and showed the need for distinction between active and contributing processes to understand streamflow generation. Put basically, the HMC method tracks water entering the model domain in a given area and through a given boundary condition. In doing so, it is possible to attribute flow at any position within the model to the source of water (i.e., boundary condition) and the location from where it originates (i.e., hillslope, in-stream, or the porous media).

In this study, the delineation for the hillslope and in-stream fractions also includes the internal model state of saturation. This allows differentiation of overland flow by saturation/infiltration excess, interflow (IF) originated from infiltration on saturated/unsaturated areas, and pre-event GW (old GW) (Table 1). Infiltration excess overland flow (IE-OF), commonly known as Horton overland flow (Horton, 1945), refers to flow originating from rainfall exceeding the infiltration capacity of the soil and the rill storage capacity (depression storage that must be filled before lateral surface flow occurs). Saturation excess overland flow (SE-OF), referred as Dunne overland flow (Dunne & Black, 1970), occurs when the soil becomes saturated limiting the infiltration capacity of the soil and producing flow once the rill storage is full. IF, also called subsurface stormflow or lateral flow, refers to infiltrated water that moves laterally through the saturated shallow subsurface toward the stream (Sophocleous, 2002). Depending on where the

infiltration occurred, the IF fraction is subdivided into: saturated IF (Sat-IF) and unsaturated IF (Unsat-IF), for flow originating over a saturated or unsaturated soil profile, respectively.

Table 0.1 Flow Generation Mechanisms Delineated for the HMC Method

Flow generation mechanism	Fraction	Fraction origin
Saturation excess overland flow	SE-OF (Dunne)*	In-stream and hillslope
Infiltration excess overland flow	IE-OF (Horton)	In-stream and hillslope
Saturated interflow	Sat-IF	In-stream and hillslope
Unsaturated interflow	Unsat-IF	In-stream and hillslope
Pre-event GW	Pre-event GW (old GW)	Porous media

Note. HMC = Hydraulic Mixing-Cell; IF = interflow; SE-OF = saturation excess overland flow; IE-OF = infiltration excess overland flow; GW = groundwater.

*Common names used for the fractions are shown in parenthesis

After each time step of the HGS flow simulation, the prevailing flow generation mechanism is identified at each node. Then, the HMC fraction $f_{k,i}^{N}$ of water derived from each flow generation mechanism *k* at time *N* in cell *i*, is calculated as follows:

For k in [SE-OF, IE-OF, Sat-IF, Unsat-IF, Pre-event GW]:

$$f_{k,i}^{N} = f_{k,i}^{N-1} + \frac{1}{V_i^N}\left(\sum_{j\epsilon\, Inflow} f_{k,j}^{N-1} V_{IN,j} - \sum_{j\epsilon\, Outflow} f_{k,i}^{N-1} V_{OUT,j} + V_{FGM} - V_{BC\ OUT} f_{k,i}^{N-1}\right) \quad \textbf{(2.1)}$$

Where $f_{k,i}^{N}$ is the fraction for a particular flow generation mechanism [-]; V_i^N is the total volume of water in cell i at time *N* [L3/T]; $f_{k,j}^{N-1}$ is the fraction of the same flow generation mechanism k present in the set of neighboring cells *j* at time-step *N-1*; $V_{IN,j}$ is the volume of water that flows into cell *i* from the set of neighbor cells $j\epsilon\ Inflow$ [L3/T]; $V_{OUT,j}$ is the volume of water that flows out from cell *i* into the set of neighbor cells $j\epsilon\ Outflow$ [L3/T]; V_{FGM} is the volume of water entering cell i that is from flow generation mechanism *k* [L3/T]; $V_{BC\ OUT}$ is the volume of water leaving cell *i* through all boundary conditions such as critical depth outflow and evapotranspiration [L3/T].

1.10.2 Concept-Development Simulations Setup

We used the field-scale experimental site used by Abdul (1985) as the conceptual study site for the simulations. The experimental site consists of a plot approximately 80 m by 16 m with a maximum depth of 4.5 m in the northeast corner. The stream channel is described in the original work as approximately 0.6 m wide and located 1.2 m below the surrounding floodplain. With the understanding that river channels are a dynamic feature (particularly in low-gradient catchments), in this study, we extended the selection of river nodes to average a 2 m width channel following a change in elevation of approximately 0.1 m from the lowest point in the channel. A full description of the original experimental site can be found in VanderKwaak and Sudicky (2000). We used the Manning's roughness coefficients (n) presented in the aforementioned study, which were derived from Chow (1959), and values from the original experiments by Abdul (1985) and Abdul and Gillham (1984) for values typical of a clean-straight natural stream (0.03 s/m1/3) for the river, and of short grass for the floodplain areas (0.3 s/m1/3). Rill storage height was set to 0.002 m for both the river and floodplain zones and no obstruction height was implemented. The surface topography is discretized with a triangular grid containing 1,372 nodes and 2,651 triangular elements (Aquanty, 2016). Horizontal discretization goes from 0.5 m along the riverine area to 2 m at the domain boundary. A total of 15 layers were generated to provide a discretization of 0.1 m near the surface and increasing to approximately 0.6 m at depth. Sets of nodes comprising a river cross section were selected at four locations along the river channel and tagged as hydrograph nodes to track streamflow generation (Figure 0.2.a).

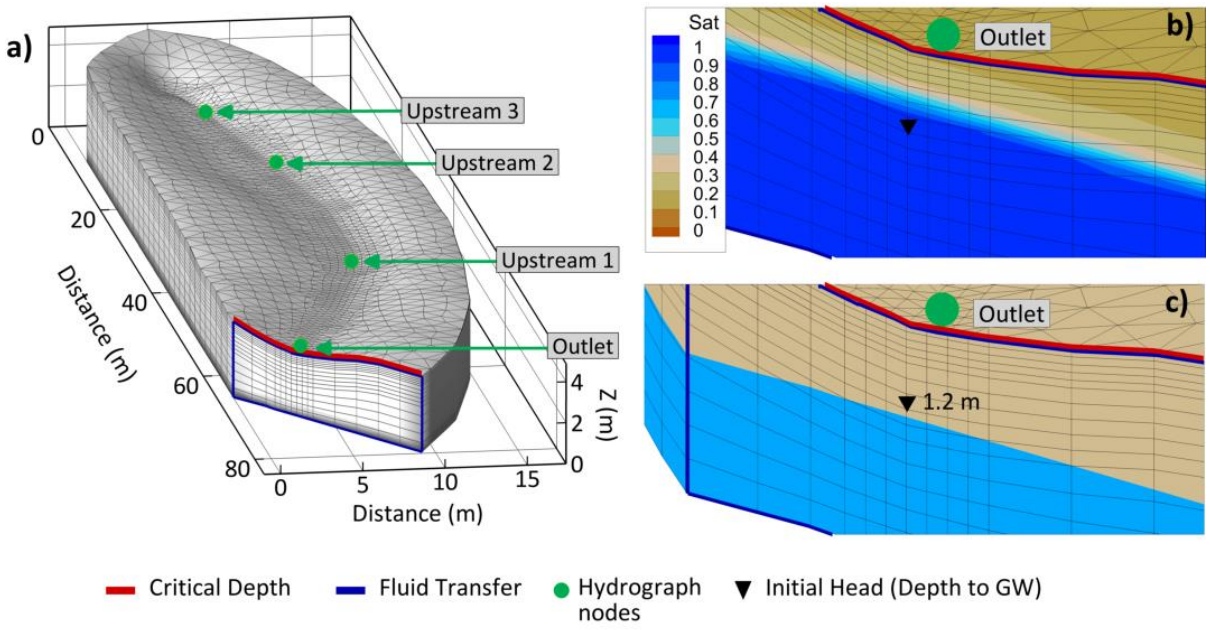

Figure 0.2 (a) Three-dimensional representation of the Abdul catchment showing the mesh discretization, model boundary conditions, and hydrograph node locations. Two inserts from the outlet show the (b) initial saturation and (c) initial depth to groundwater (GW) given by one of the 60 initial subsurface heads for the sandy soil.

The soil is homogeneous throughout the catchment and three soil types (sand, sandy gravel, and sandy loam) were used to test the effect of soil properties in the threshold of streamflow generation. Soil physical and hydraulic properties for each soil type were obtained from previous published work where extensive soil analysis was available and are shown in Table 2 (Aquanty, 2016; Mirus, Ebel, et al., 2011; Smith & Woolhiser, 1971; Thoma et al., 2014; VanderKwaak, 1999). Functional constitutive relationships for pressure-saturation and saturation-relative hydraulic conductivity (K) were defined using the van Genuchten function parameters (van Genuchten, 1980) in HGS. Outflow model boundary conditions for the surface domain were set as a critical-depth boundary condition at the catchment's outlet and as a no-flow boundary condition for the rest of the domain.

Table 0.2 Surface-Subsurface Parameters for Theoretical Models

Media	Parameter	Value
	Surface	
Overland	Manning's roughness n	0.3 $s/m^{1/3}$
	Rill storage	0.002 m
	Obstruction storage	0.0 m
Stream	Manning's roughness n	0.03 $s/m^{1/3}$
	Rill storage	0.002 m
	Obstruction storage	0.0 m
Surface-Subsurface Coupling	Coupling length	0.002 m
	Subsurface	
Sand	Hydraulic conductivity K_{sat}	1.00 E-05 m/s
	Porosity	0.37
	van Genuchten a	1.9 m^{-1}
	van Genuchten β	6
	Residual saturation θ_r	0.18
Sandy Gravel	Hydraulic conductivity K_{sat}	1.08 E-03 m/s
	Porosity	0.41
	van Genuchten a	16 m^{-1}
	van Genuchten β	1.79
	Residual saturation θ_r	0.045
Sandy Loam	Hydraulic conductivity K_{sat}	2.00 E-07 m/s
	Porosity	0.38
	van Genuchten a	4.5 m^{-1}
	van Genuchten β	2
	Residual saturation θ_r	0.11

To test the effect of depth to GW in streamflow generation, we used a series of 60 subsurface heads as the porous media initial boundary conditions. The heads were obtained by initiating a simulation with a fully saturated subsurface domain and applying a fluid transfer boundary condition to drain the model, saving the subsurface heads each time the depth to GW at the outlet increased by 0.05 m. The antecedent soil moisture conditions were computed from the subsurface heads using the constitutive relationships for the van Genuchten model. To mimic a natural system, a fluid transfer gradient was set at the outlet faces to allow GW to flow out of the domain (Figure 0.2). The gradient was given by setting the head 0.2 m lower than the initial GW head at a distance of 5 m from the outlet faces.

We tested a total of nine precipitation rates within three duration blocks to explore the effects of climatic controls (Table 3). Aiming to obtain realistic and representative precipitations, we used the annual exceedance probability (AEP) records of six randomly selected sites in arid and semiarid regions where IRES dominate the landscape. We selected three sites in arid regions of Australia (Stations 23876, 15643, and 13022, Australian Government Bureau of Meteorology, 2018) and three from the southwest United States (Stations 29-3649, 02-7751, and 26-3671, NOAA's National Weather Service, 2018). We chose 1, 6, and 24 h storm durations to ensure a range of precipitation from short-duration-high intensity to long-duration-low-intensity. Within these durations, we selected three precipitation intensities matching a common occurrence (50% AEP), rare (2% AEP), and an extreme precipitation intensity (0.2% AEP). The final values for each precipitation rate were calculated through an arithmetic mean of the six sites.

Table 0.3 Catchment and Climatic Controls Used for Simulations

Controls	Parameter	Value	
	Catchment		
Soil	Sand	See table 2	
	Sandy Gravel	See table 2	
	Sandy Loam	See table 2	
Depth to GW		0.05 m increments from 0 to 2.95 m	
	Climatic		
Precipitation	*Duration*	*Rate mm/h* [a] *(AEP)**	Depth [b] (mm)
	1 h	18.6 (50%)	18.6
		49.8 (2%)	49.8
		69.3 (0.2%)	69.3
	6 h	4.7 (50%)	28.2
		12.9 (2%)	77.4
		16.3 (0.2%)	97.8
	24 h	1.7 (50%)	40.8
		4.5 (2%)	108.0
		6.9 (0.2%)	165.6

GW = groundwater; AEP = annual exceedance probability.

[a]For simplicity precipitation rates are referenced in their rounded value from herein.

[b]Total amount for each application (i.e., rate * duration).

The precipitation needed to be intermittent throughout the simulation to allow the flow generation processes to develop and progress overtime in a more realistic way. To achieve this, each precipitation scenario (rate and duration) was implemented at three separate occasions (Figure 0.3). The applications were considered effective precipitation and were applied uniformly to the entire surface domain. With the premise of winter dominated precipitation (typical for Mediterranean climates), we assumed that ET would be negligible, and therefore, it was not included in this study.

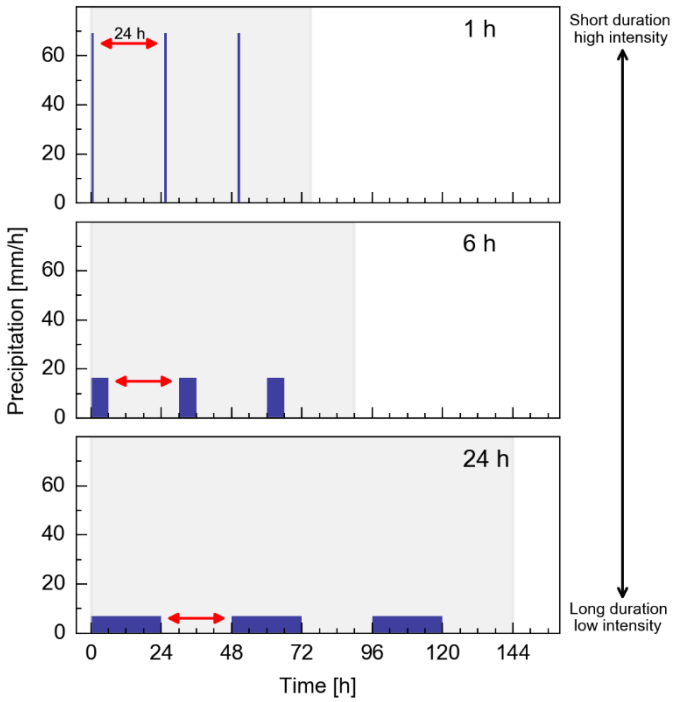

Figure 0.3 Precipitation scenarios for the extreme annual exceedance probability rainfalls and all storm durations (1, 6, and 24 h). Three rainfall applications (precipitation rate * precipitation duration) were prescribed to each simulation. The first application occurred at time 0 and following applications 24 h after the end of the previous application. The shaded area depicts the simulation time for each scenario, from time 0 to 24 h after last precipitation application.

1.10.2.1 Simulation Implementation

The simulations were performed in HGS using the control-volume finite element mode and dual-node approach for surface-subsurface coupling with a coupling length of 0.002 m across the entire domain. An adaptive time step with a computed under-relaxation factor scheme was used in the simulations to aid the computational efforts. As the aim of this study was to capture the highly time sensitive threshold of flow generation, adaptive time stepping was applied by an

initial step size of 0.5 s, a maximum step multiplier factor of 2.0, and a maximum time step of 100 s.

1.10.2.2 Computational Demand

The combination of the three different soils, nine precipitation applications, and 60 initial depths to GW yielded a total of 1,620 unique simulation scenarios. To meet the computational requirements, we used the high-performance computing services of TANGO provided by eResearch SA Ltd, distributing the 1,620 simulations over 50 cores. A set of specific input files are required to run the preprocessor, which generates HGS compatible files to perform each unique model simulation. We developed scripts in Python to automate the generation of the input model files, launch the execution of the simulations, and extract the simulated hydrograph output files. Computational time for model simulations ranged from 0.5–13 h. All preprocessing and postprocessing scripts are provided in the Supporting Information.

1.11 Data Analysis

1.11.1 Streamflow Generation Analysis

For each simulation, we obtained a set of four hydrograph output files with the values of the unique fractions from the HMC method at the locations specified in Figure 0.2. Python scripts were used to examine the 6,480 hydrograph files to determine if flow was generated. If flow was detected, the time of the first flow occurrence (time to flow) and the HMC components for that first flow were extracted. A minimum of 0.001 m3/s as total flow (i.e., summation of all HMC fractions) was used to determine the time to flow; values smaller than this threshold were considered numerical noise. A consolidated list of all the first flows information (HMC fractions) for each hydrograph node and their respective simulation information (soil type, precipitation, and depth to GW) is a first approach to understand the effect of the different controls on initiation of streamflow.

The spatiotemporal variability of streamflow generation at the threshold of flow was investigated by comparing the times to the first flow for the four hydrograph node locations, the different depths to GW, precipitation applications, and soils. Additionally, we compared the variation in the times to flow for all these hydrograph locations for each soil and precipitation

application. For all simulations where flow was generated at more than one hydrograph location, we calculated the time lag for the first flow occurrence among the different locations.

1.11.2 Cluster Analysis of the Dominant Flow Generation Mechanism

Because the HMC method was developed to decompose the hydrograph into flow generation components, the output is given in terms of volumetric flow for each fraction (generation mechanism) comprising the total flow. To determine the dominant mechanisms, we converted the HMC flow components back into their fractions by dividing their value over the total flow (i.e., normalization). We performed a cluster analysis through the Scikit-learn package in Python (Pedregosa et al., 2011) to analyze the relationship between the different controls and the dominant mechanisms at the threshold of flow. We chose the K-means clustering algorithm, which uses the Euclidian distance measure (straight-line distance between two points) to partition the data into a number of specified clusters (k). The key concept for the K-means algorithm is the grouping of data (observations) into clusters of similar attributes by using the mean attribute values of all training instances (variables) assigned to that cluster in order to minimize the sum of the squared errors for each cluster (inertia). The aim of the cluster analysis is basically to group the first flow observations by their dominant flow generation mechanism (using the HMC fractions as the training instances) to identify their relation to the different simulation controls (soil type, GW depth, and rainfall).

1.11.3 Analysis of the Development of Active Areas and Processes

Model output from the streamflow generation analysis was setup at 30-min intervals to keep output data manageable despite 1,620 model runs. A subset of models were rerun with finer output times for overland (two-dimensional) and porous media (3D) information to evaluate the spatial and temporal development of active areas in specific simulations where streamflow was generated. For each of the three soils, we selected scenarios (the combination of soil, GW depth, and precipitation rate) where flow was observed for the deepest initial GW head for all soils within each precipitation duration group (1, 6, and 24 h). In the reran models, output times were specified at 5-min intervals for up to 1 h prior to the time to flow at the outlet, for the sand and sandy gravel soils. For the sandy loam scenarios, which resulted in the shortest times to flow, outputs times ranged from every 5 s to 5 min prior to the first flow.

The overland output files for these simulations were further processed to integrate a new column with the determined dominant flow generation mechanism for every active node from the surface domain at each output time. A threshold of 0.001 m water depth was used to identify and filter the activated areas. This allowed us to visualize and quantify the development and spatial extent of the dominant processes at and leading to the threshold of flow generation at the outlet location.

The porous media output was used to evaluate whether surface water-GW interactions impacted the thresholds for the catchment's activation and subsequent streamflow generation.

1.12 Results

1.12.1 Streamflow Generation

Flow occurred for most simulations (623) at the catchment outlet (Figure 0.4), and the number of simulations for which flow occurred for the upstream locations decreased linearly with increasing distance from the outlet to the top of the catchment. The sandy loam scenarios resulted in more flow events and the sandy gravel the least. For the furthest upstream location, only the rare and extreme short-duration-high-intensity precipitation events (50 and 69 mm/h for 1 h) produced flow for the sand and sandy loam soils. The 2 mm/h for 1 h precipitation did not generate flow for any scenarios of the sandy and sandy loam, and flow was simulated only at the outlet location for the 5 mm/h rates for both durations (6 and 24 h). Flow for the sandy gravel soil was generated at the Upstream 3 location for all rainfall rates but only for the scenarios where the initial head was a surface elevation. The same was observed for all the common AEP rainfalls for this soil type where flow was generated in all the hydrograph locations but only for that initially fully saturated scenario.

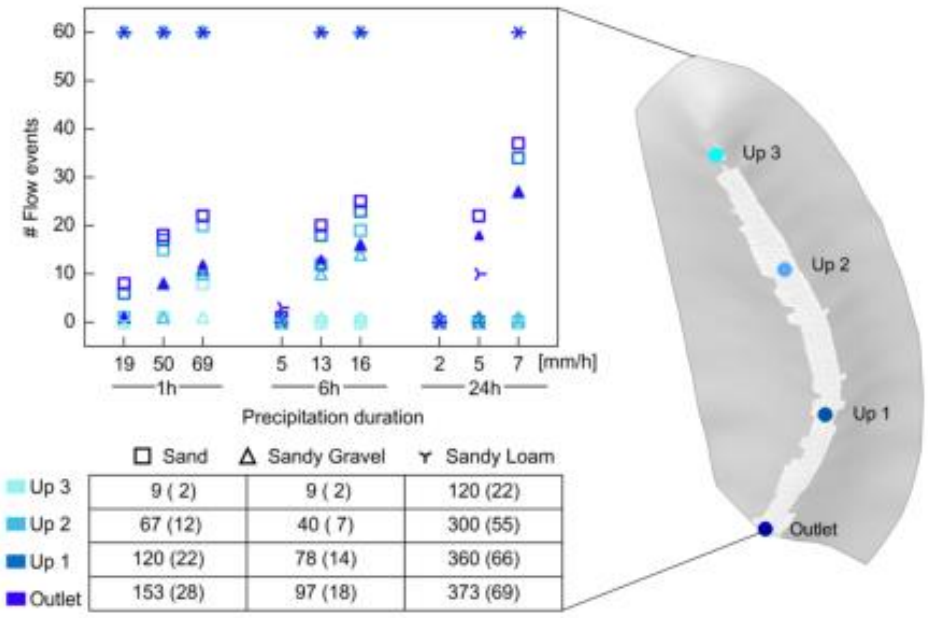

	Sand	Sandy Gravel	Sandy Loam
Up 3	9 (2)	9 (2)	120 (22)
Up 2	67 (12)	40 (7)	300 (55)
Up 1	120 (22)	78 (14)	360 (66)
Outlet	153 (28)	97 (18)	373 (69)

Figure 0.4 Simulated flows at each hydrograph location for all simulations by precipitation scenario (x axis). Symbols denote the soil type and different colors depict the hydrograph locations as shown in the map. Note that different orientation for the markers of the sandy loam are used due to data aliasing (creating a "*" shape) on all but the 5mm/h precipitation rates. Summary table shows the total simulated flows which is given as a percentage in parenthesis by soil type and hydrograph location.

The range of initial depth to GW in combination with precipitation had a greater influence on flow generation for the sand and sandy gravel soils where long-duration-low-intensity precipitation events (i.e., 5 and 7 mm/h for 24 h) produced flows for deeper initial GW heads. The deepest initial depth to GW where flow was simulated was 1.80 m for sand and 1.30 m for the sandy gravel, both in response to the 7 mm/h for 24 h precipitation. Conversely, the 19 mm/h for 1 h generated flow only up to an initial GW depth of 0.35 m for the sand, and no-flow was simulated for the sandy gravel for initial GW depths below surface elevation. When flow was simulated at a location for the sandy loam scenarios, it was simulated for all the different initial GW head scenarios, with the exception of the 5 mm/h for 6 h and 5 mm/h for 24 h precipitation, where flows were not simulated for initial GW heads below 0.10 and 0.45 m, respectively.

In terms of precipitation and considering total flows as the summation of simulated flows at each location, the short-duration-high-intensity applications produced the most flows and the

long-duration-low-intensity the least for the sand and sandy loam soil. The opposite was observed for the sandy gravel, where more flow events happened in response to the long-duration-low-intensity 7 mm/h for 24 h precipitation.

1.12.2 Time to Flow

Soil type influenced the time it took for streamflow to occur at the different hydrograph locations. The simulations for the sandy loam soil resulted in the fastest times to flow, followed by the sandy soil, and the longest times were simulated for the sandy gravel (Figure 0.5). Similarly, short-duration-high-intensity (1 h duration) rainfall events took the shortest time to produce flow among soils and locations and the long-duration-low-intensity rainfalls (24 h duration) the longest time. The relationship between time to flow and initial depth to GW was exponential for the sandy loam soil and logarithmic for the sand and sandy gravel soils.

In terms of location, flow generally occurred first at the outlet; we observed an increasing time lag for flow generation at the upstream locations, with the exception of the rare and extreme 1 h events for the sandy loam where flow was simulated at the Upstream 2 location a few seconds to a few minutes before the Upstream 1 location. The time lag magnitude varied greatly among soils. Time lags were largest for the sandy soil simulations with time differences up to 50 h and the shortest for the sandy loam scenarios where the maximum time lag was 7 h. Among precipitation scenarios, time lags were larger for the smaller precipitation rates (50% AEP) and shorter for the rare and extreme rates within each duration group (1, 6, and 24 h).

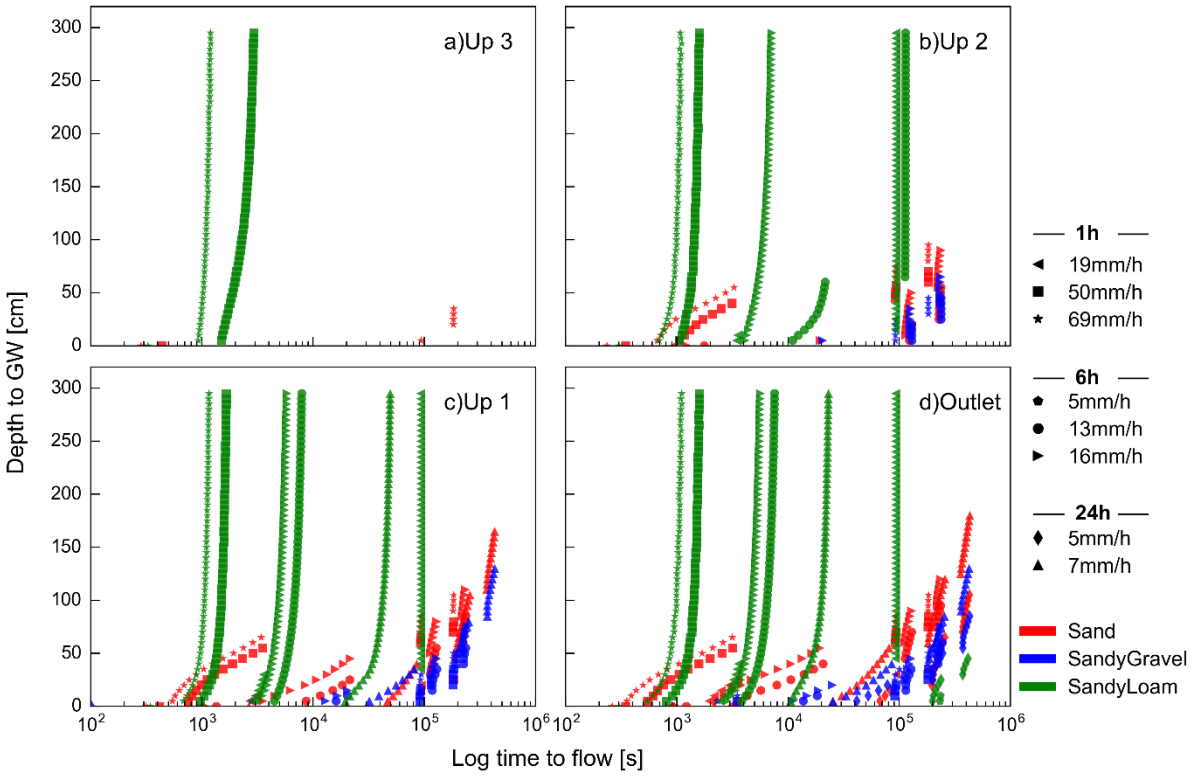

Figure 0.5 Time to flow (log scale) versus depth to groundwater (GW) for all soils (depicted in different colors), precipitation rates (different markers), and hydrograph node locations (subplots a-d).

1.12.3 Dominant Flow Generation Mechanism: Cluster Analysis

The cluster analysis grouped the simulated flows into three clusters. This allowed us to identify the partitioning of the contributing HMC fractions to determine dominant flow generation mechanisms at the threshold of streamflow generation for each cluster. We observed a distinctive dominant mechanism for each cluster that was consistent across all hydrograph node locations (Figure 0.6). SE-OF, referred as Dunne overland flow, from both the river and hillslope areas was the dominant mechanism for Cluster 1 (Figure 0.6.c-f), accounting on average, for over 80% of the flow. Cluster 2 had three major HMC contributing components, all occurring directly in the riverine area (Figure 0.6.b-e). In order of contribution from high to low, the components are IF originated from unsaturated areas (UNSAT-IF), pre-event GW, and Dunne overland flow. The dominant mechanism for Cluster 3 was IE-OF, referred as Horton overland flow, occurring both at the floodplain and riverine areas and contributing on average for over 98% of the flow (Figure 0.6.a-d).

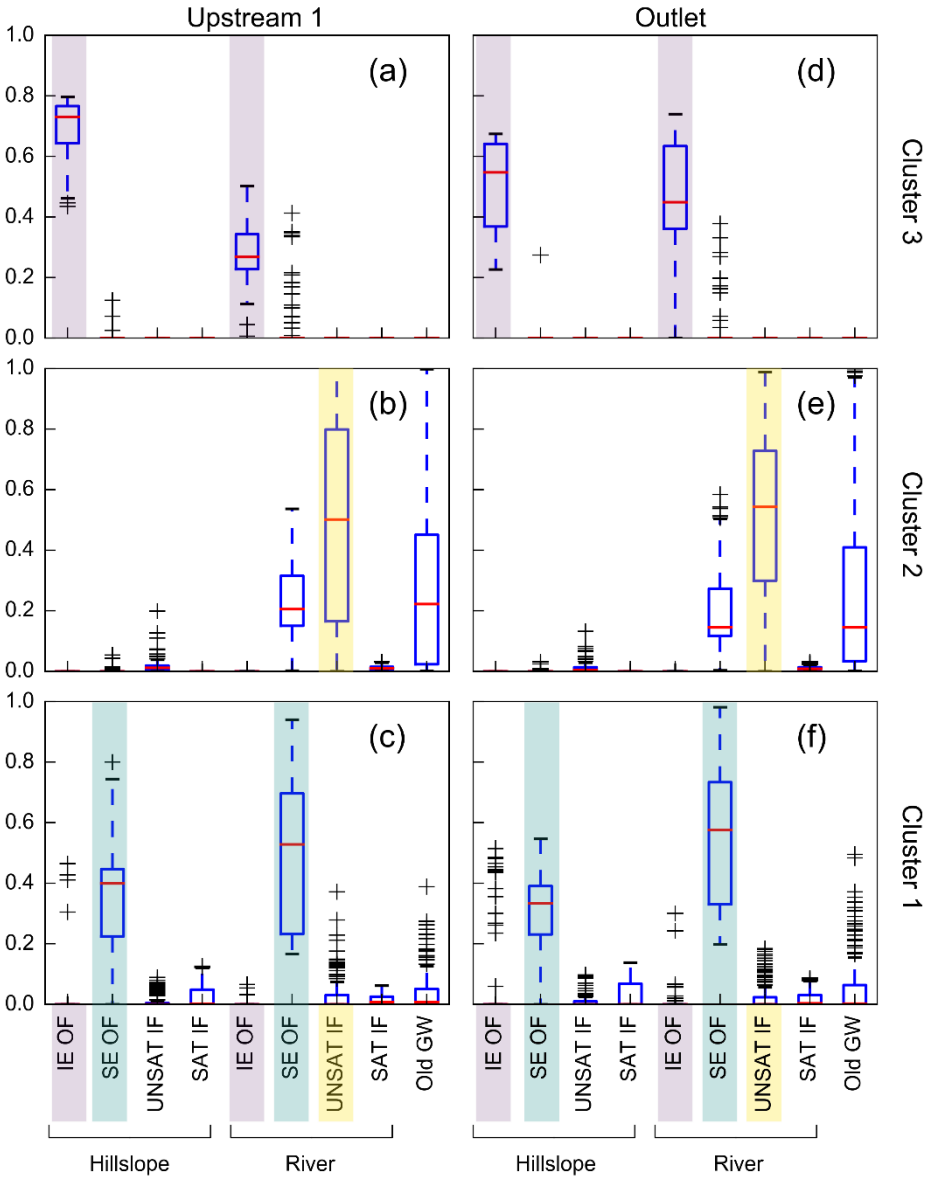

Figure 0.6 Composition and distribution of streamflow generation mechanisms by their contribution (fraction of flow) at the onset of flow for the Upstream 1 (a-c) and outlet (d-f) locations for each cluster. The area within the boxplots represents the interquartile range (25th-75th percentile), the median is shown in red. The whiskers indicate the min - max values that are within 1.5 of the interquartile range; values outside of the whiskers are considered outliers (represented by the "+" symbols). Dominant mechanisms are highlighted with a different background color for each cluster.

The simulated flows were replotted by soil type and color coded using the results from the cluster analysis. This yielded a distinct cluster group and hence a dominant flow generation mechanism, for each soil type (Figure 0.7). The dominant mechanism for the sandy loam soil

was Horton overland flow (Figure 0.7.a-d), while Dunne overland flow dominated flow generation for the sandy soil (Figure 0.7c-f), and subsurface flow from unsaturated areas was the major contributor for the sandy gravel soil (Figure 0.7.b-e). A few exceptions are noted for scenarios of the sandy gravel and sandy loam soils with shallow initial GW depths where Dunne overland flow was dominant.

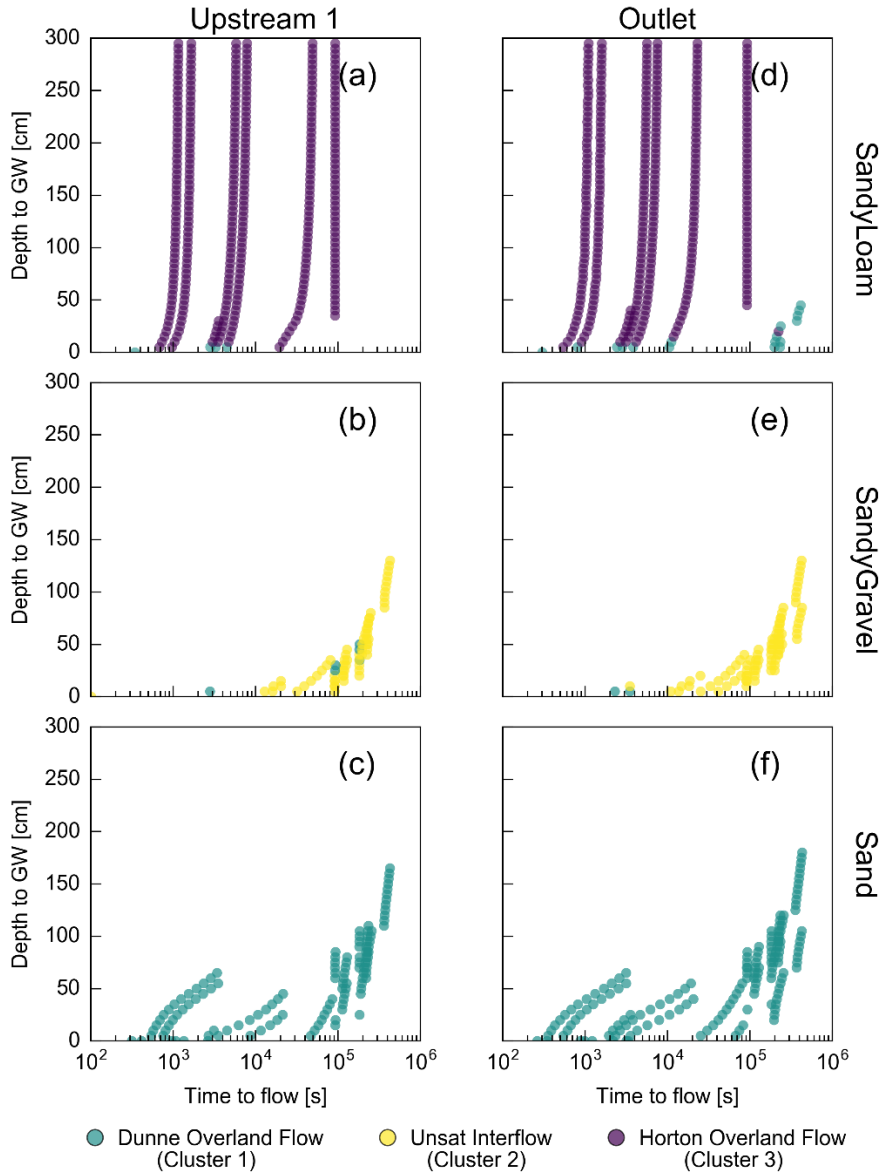

Figure 0.7 Time to flow (log scale) versus initial depth to groundwater (GW) for each soil showing the dominant mechanisms as per their cluster classification shown in different colors for the Upstream 1 (a-c) and outlet (d-f) locations.

1.12.4 Active Areas

The smallest spatial extents of active areas at the time of runoff initiation were simulated for the sandy soil scenarios, while the smallest extents at the time to flow at the outlet resulted for the sandy gravel simulations (Figure 0.8). The development of active areas for the sandy loam occurred uniformly across the entire surface domain (100% catchment became active) and remained constant from runoff initiation until the onset of flow.

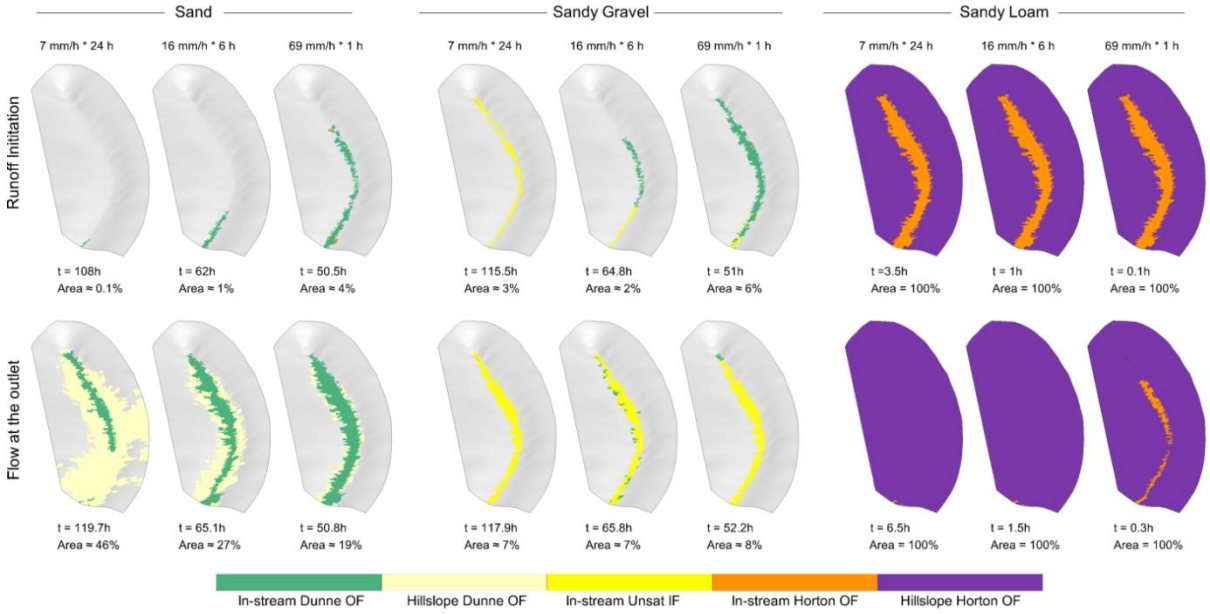

Figure 0.8 Development and spatial extent of active areas by their dominant HMC component from runoff initiation (development of first active areas) to onset of streamflow at the outlet location. Times and the spatial extent as percentage of the catchment area, is shown below the snapshots. Colors show both the dominant process and the origin of the water contributing to the flow in each cell. For example, all green areas are from water originating at the river by the Dunne mechanism (some of which can contribute to active areas in the river banks).

The development of active areas for the sandy soil simulations was considerably different among the precipitation scenarios. At the time of runoff initiation, the extent of active areas ranged from 42 m^2 (≈4%) to less than 1m^2 (≈0.1%) for the short-duration-high-intensity (69 mm/h for 1 h) to the long-duration-low-intensity (7 mm/h for 24 h), respectively. The opposite trend was observed for the spatial extent at the onset of flow where the largest active areas corresponded to the long-duration-low-intensity scenarios. The extent of active areas from long-duration-low-intensity to short-duration-high-intensity precipitations were 487 m^2 (≈46%), 287 m^2 (≈27%),

and 206 m^2 (≈19%). The development of the first active areas for this soil type was restricted to the riverine area. However, by the time flow was generated at the outlet, the active areas extended to the adjacent hillslope anywhere from 1 m to the full extent of the model boundaries in the midlower parts of the catchment.

For the sandy gravel, the development of active areas differed at the time of runoff initiation, however, the extent at the onset of flow was similar among the different precipitation scenarios. The active extent at runoff initiation ranged from 68m^2 (≈6%) to 21m^2 (≈2%), and the largest active area was shown for the short-duration- high-intensity precipitation. At the onset of flow, the average extent of active areas was 81 m^2 (≈7%). The active area extent for these scenarios was consistently restricted to the river zone.

The development of the first active areas in the catchment occurred within the first precipitation application for all the sandy loam scenarios, whereas for the sand and sandy gravel soils, the first active areas developed in response to the last application. The time lags between the development of active areas until flow was observed at the outlet (i.e., from runoff initiation to flow at the outlet) were generally shorter for the sandy loam and longest for the sandy soil scenarios. The shorter lags among precipitations were shown mostly for the short-duration-high-intensity precipitations and the longest for the long-duration-low-intensity scenarios. Time lags from long duration low intensity to short duration high intensity precipitations ranged from 11.7 to 0.3 h for the sand; 2.4 to 1.2 h for the sandy gravel; and 3 to 0.2 h for the sandy loam.

Dominant flow generation processes across the active areas at both runoff initiation and at the time to flow at the outlet were overall consistent to those identified as the main contributors of streamflow generation at the threshold of flow for all soil types (Figure 0.8). A few exceptions were noted for the sandy gravel soil, where in-stream Dunne overland flow accounted for over 90% of the active areas for the 69 mm/h precipitation and roughly for 50% for the 16 mm/h scenario at the time of runoff initiation. However, within an hour, over 90% of the active area was dominated by IF from the unsaturated riverine area in both scenarios.

The thresholds for the development of the first active areas in the catchment varied mostly among soils. For the sandy loam, the almost immediate activation by the Horton overland mechanism occurred solely due to the precipitation rate exceeding the infiltration capacity of

the soil. For both the sand and sandy gravel scenarios, the activation of areas by the Dunne mechanism occurred in response to the gradual rise in GW levels which resulted in the subsurface saturation to build up until intersecting the surface (Figure 0.9). Similarly, the development of active areas for the sandy gravel scenarios by IF originating from unsaturated parts of the riverine area occurred in response to GW levels rising and connecting to the river.

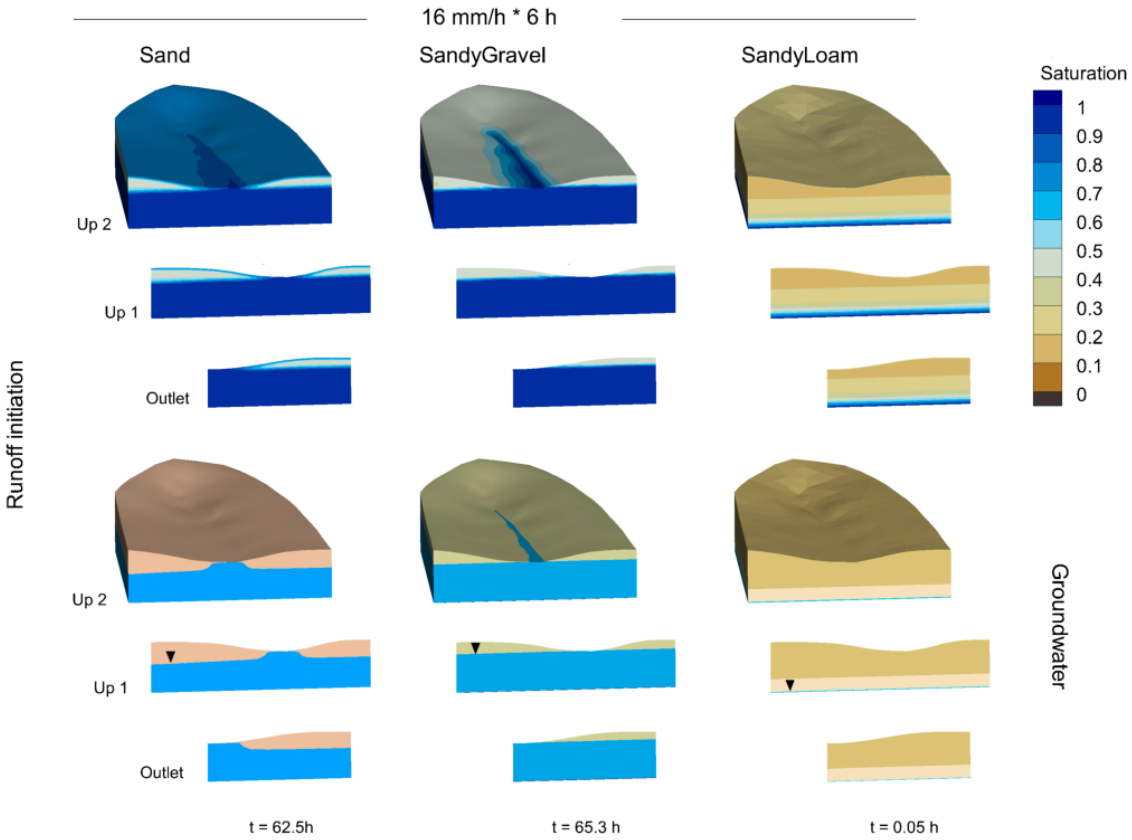

Figure 0.9 Slices of the subsurface domain at three of the hydrograph locations showing a snapshot of the saturation (top row) and groundwater level (bottom row) at time of runoff initiation (development of first active areas) for each soil for one of the precipitation scenarios.

An important observation was the markedly different unsaturated storage dynamics in the sand and sandy gravel scenarios which impacted the spatial extent, dominant processes, and thresholds of activation. The increase in GW levels for the sandy soil occurred faster along the river resulting in GW mounding in the riverine area (Figure 0.9). The mounding effect promoted the increase of the soil saturation around the river which controlled the threshold for the initiation of the first active areas by the Dunne mechanism and subsequent streamflow generation. Conversely, the GW rise in the sandy gravel developed uniformly across the

catchment allowing the river to develop into a gaining state where infiltrated water moving as IF discharged into the stream. Changes in the saturation and GW level from the start of the simulation until runoff initiation were minimal for the sandy loam due to the fast response given by the Horton overland flow mechanism.

1.13 Discussion

The goals of this study were to provide insight into the main factors controlling the threshold behavior of streamflow generation in IRES by analyzing the development and spatial extent of active areas and determining the dominant flow generation mechanisms. The effects of initial depth to GW, soil hydraulic properties, and different precipitation scenarios were investigated to assess how they impact streamflow onset on IRES in low-gradient catchments in Mediterranean climates.

1.13.1 Streamflow Generation Major Controls and Dominant Processes

The results of the simplified simulation scenarios presented here showed that soil type is a key control on streamflow generation and is the major factor determining the development and spatial extent of active areas by a given flow generation mechanism and the contributing processes at the threshold of flow generation (Figure 0.6). The importance of soil type in streamflow onset is consistent with previous work by Mirus and Loague (2013), who quantitatively showed that hydraulic conductivity is a leading factor in runoff generation. In this study, we gain further insight on the extent to which soil properties dictate the development and spatial extent of active areas and the contributing processes for flow generation.

This is a major step toward understanding the thresholds of flow generation by different flow generation mechanisms and the effects other controls have on such thresholds for IRES. For instance, as expected, we observed that initial depth to GW was not a defining factor in the threshold of flow generation when the dominant mechanism was Horton overland flow (sandy loam soil scenarios). Conversely, the cutoffs on streamflow generation after a given initial GW depth for scenarios dominated by Dunne and IF mechanisms (sandy and sandy gravel soils), indicated that in such scenarios, GW depth is a key constraint for streamflow generation (Figure 0.5). Furthermore, the results showed that the unsaturated storage dynamics, as observed by the response of the GW levels, helped explain the spatial extent of active areas, dominant processes,

and thresholds of activation for the sand and sandy gravel soils. These results are consistent with previous studies which found that unsaturated storage dynamics largely dictate the processes by which runoff is generated (Mirus & Loague, 2013; Smith & Hebbert, 1983; Vanderkwaak & Loague, 2001).

The linear decrease in simulated flows by hydrograph location from the outlet to the top of the catchment for the sand and sandy gravel soils was the result of the catchment topography due to differences in the impermeable basal boundary depth across the domain. With the impermeable boundary depth increasing from the outlet toward the top of the catchment, the initial depth to GW, and therefore the soil water storage, was greater at the upstream locations. The decrease in flows by hydrograph location reconfirmed our observation that unsaturated storage dynamics are major controls for flow generation when the dominant generation mechanisms are Dunnian and IF. Depth to a low-permeable bedrock or soil layer is known to be an important feature controlling hydrological processes (Shangguan et al., 2017). Several studies have shown the influence of bedrock geology as a major contributor of streamflow generation through subsurface processes (Huntington & Niswonger, 2012), and other studies have shown that contrasting soil layers and soil heterogeneity can promote subsurface storm flow by restricting vertical flow and favoring the development of a perched aquifer (Maxwell & Kollet, 2008; Smith & Hebbert, 1983). The importance of unsaturated flow dynamics are stressed by Mirus and Loague (2013) as their results showed that contrast among soil layers is a critical control on the threshold of runoff generation. Moreover, several studies mention the relevance of the underlying geologic structure in water storage and permeability, which controls not only the wetting but also the drying thresholds in stream length dynamics (Godsey & Kirchner, 2014; Jensen et al., 2017; Ward et al., 2018). Saft et al. (2016) found that soil depth was related to shifts in the rainfall-runoff response and pointed out that deeper soils with larger soil water capacity might need more time to respond. For the case of the sandy loam, where the dominant flow generation mechanism was Horton overland flow, we attribute the decrease in observed flows to the reduction in the catchment area with potential to contribute overland flow at the upstream locations.

Understanding the impacts of unsaturated storage dynamics for streamflow generation is of particular relevance for IRES, where water table depths can range from a couple of meters to

tens of meters, and where GW decline is a constant risk due to overextraction of GW and the cumulative impact from prolonged droughts. Our results suggest that impacts of GW declines in streamflow generation would be larger in IRES dominated by Dunne and subsurface processes. Several studies have shown the impacts of GW level declines and changes in catchment storage in reducing runoff, affecting the stream-aquifer interactions, and potentially changing long term watershed dynamics (Falke et al., 2011; Saft et al., 2016; Vivoni et al., 2007). Our results reaffirm the need to understand unsaturated flow dynamics and storage controls from soil stratigraphy and geologic settings in order to understand streamflow generation in IRES.

As expected, extreme precipitation intensities (0.2% AEP) within each application duration generated the maximum number of flows simulated for all soils (Figure 0.4). However, comparisons among all the application rates within the three duration blocks, show that not only the total application depth, but how the precipitation occurs (intensity and duration), is important for streamflow generation in IRES. When comparing the number of simulated flow events by total application amount among common precipitations intensities (50% AEP), we observed the most streamflow events simulated for the 1 h duration, which also has the lowest total application (56 mm); conversely, with more than double the total amount for the 24 h duration (122 mm), only four simulations generated flow under this application rate. Moreover, we observed that the effect of precipitation rate and application duration on flow generation differed among soils and hence among different flow generation mechanisms. Results for the sandy loam (Hortonian flow) showed that precipitation intensity is more important to predict flow than the total amount, whereas for the sand and sandy gravel (Dunnian and subsurface flow), the long-duration-low-intensity applications generated flows for more simulations (deeper initial GW depths). These results are consistent with other studies that have shown that precipitation intensity influences the overall catchment hydrologic response. For instance, Park et al. (2011) simulated a decrease in subsurface flow contributions with increasing precipitation intensity, and Thomas et al. (2016) identified significant changes in the recharge-precipitation ratio with decreasing precipitation intensity. Moreover, in a concept-development simulation, Loague et al. (2010) directly linked the generation of Dunnian flow to precipitation rates on saturated areas. The impacts of precipitation rates on flow generation are an important consideration for IRES as it is widely recognized that climate change is likely to affect not only

the variance of the total precipitation amount but also the precipitation characteristics (Dore, 2005; Guilbert et al., 2015; Huntington & Niswonger, 2012; Trenberth et al., 2003). Our results reaffirm one of the major concerns regarding the high vulnerability of IRES to climate change associated not only to rising temperatures but also to changes in precipitation patterns (Chiu et al., 2017).

1.13.2 Threshold of Time to Flow

The threshold of time to flow (when flow was detected at a hydrograph location) for the different initial GW heads was also largely affected by the development of active areas and dominant flow generation mechanism given by the soil type, in combination with the rainfall rate. As anticipated, the higher precipitation rates showed the fastest times to flow, and the lower rates took longer for flow to be generated. This trend of time to flow versus precipitation rates was consistent among soils (Figure 0.5). However, the time lag for decreasing initial GW depth and among hydrograph locations was significantly different among soils (Figure 0.5) and was explained by the dominant flow generation mechanisms. The time lags for the sandy loam dominated by Hortonian flow were minimal (within minutes to hours for most application rates), and most flows occurred in response to the first precipitation application resulting from precipitation rates exceeding infiltration capacity. The opposite was observed for the sand and sandy gravel scenarios dominated by Dunnian and IF mechanisms, respectively, where time lags ranged from 2 to 5 days for the deeper initial GW depths and 1 to 2 days among the hydrograph nodes. For these soils, the variability of soil water content and the position and development of the water table was the major factor influencing the time (and hence the amount of water needed) for flow to be generated. The increasing time lags on time to flow by hydrograph location from the outlet to the top of the catchment for the sand and sandy gravel soils are explained by the unsaturated storage dynamics discussed in the previous section.

1.13.3 Active Areas Development and Spatial Extent

Results from the active areas analysis demonstrated the underlying processes contributing to the threshold of runoff initiation and subsequent streamflow generation. The importance of the areas contributing to streamflow (source areas) has been discussed extensively in traditional streamflow generation studies (Betson, 1964; Cappus, 1960; Dunne & Black, 1970; Hewlett & Hibbert, 1967; Ragan, 1968). Concepts arising from these studies, such as the "variable source

area" revolutionized the efforts to understand streamflow generation processes. However, as previously mentioned, traditional studies were developed for perennial systems where the presence of a saturated area within the catchment (the baseflow contribution) is inherently present or assumed. Moreover, it has been recognized that to better understand the spatiotemporal variability controlling catchment dynamics, we need to re-evaluate the validity of the "variable source area" concept (Ambroise, 2004). Ambroise addressed this by introducing the concepts of variably "active" and "contributing" areas to differentiate the areas where processes are occurring (are active) at a given time and point in space but that do not necessarily contribute to the hydrological output at another point of interest, to areas that are both active and effectively contributing to flow at a given time and space. While the active and contributing processes might be the same in small-scale systems (i.e., at the hillslope scale) for larger scale studies, and particularly in areas with significant flow depletion and retention processes, this distinction is necessary (Partington et al., 2013). This is particularly relevant for IRES where high infiltration and transmission losses are common, as well as ET losses in arid and semiarid regions (Levick et al., 2008; Shanafield & Cook, 2014; Snelder et al., 2013). Therefore, the understanding of how active areas develop within in a catchment and the processes involved in their progression before contributing to streamflow is essential to understand streamflow generation in IRES. Although in this study we were not able to differentiate between active and contributing areas, our results offer an initial insight to understand the development of active areas under a given dominant flow generation mechanism and the contributing processes at the threshold of flow for a range of scenarios pertaining to low-gradient catchments in Mediterranean climates under idealized soil properties conditions. By analyzing the progression of the active areas and their dominant generation mechanisms, we were able to identify the underlying hydrological processes that explained how certain thresholds were reached for both runoff initiation and the onset of streamflow.

1.13.4 Study Limitations and Future Work

As is the case for all theoretical models, these simulations present a simplified version of what we recognize are complex and diverse natural systems. Nevertheless, similar simplified and idealized approaches have proven useful as "diagnostic tools" to provide insight into "threshold processes" in hydrological research (Ward et al., 2018; Zehe & Sivapalan, 2009), to emphasize the effects of a given parameter on runoff processes (Frei et al., 2010; Maxwell & Kollet, 2008;

Meyerhoff & Maxwell, 2011), and as an alternative approach for improving process conceptualization in general (Hopp & McDonnell, 2009).

IRES occur all around the world, from humid temperate climates, to arid and Mediterranean ones; and from small headwater streams to major rivers. In these simulations, we have focused on parameters that would be appropriate to low-gradient catchments in Mediterranean climates with weathered geology, therefore, the initial conditions and GW levels might not be appropriate for IRES in humid climates and alpine systems, such as are commonly found in western Europe and the United States. Moreover, with the aim of isolating the effects of contrasting soil characteristics, rainfall types, and different initial GW depths on streamflow generation and find commonalities, we excluded the effects of soil heterogeneity, catchment topography, and ET.

It results evident that the distinct influence of soil type on the active and contributing flow generation mechanisms and times to flow were amplified by our simplifying assumption of soil homogeneity. While this was an expected result, we recognize that soil heterogeneity is the predominant feature of natural systems, and we expect that in real catchments, the development of active areas and dominant processes would be more complex and lead to more intricate interactions. For instance, results by Meyerhoff and Maxwell (2011) showed that Hortonian flow was controlled by the degree of heterogeneity in the subsurface, while Maxwell and Kollet (2008) indicated the development of shallow perching caused by the presence of low hydraulic conductivity layers in the subsurface. Moreover, other studies have shown that under heterogeneous hydraulic conductivities, runoff is generated earlier and flow durations are longer due to the delayed runoff response from areas with higher infiltration capacities (Ebel et al., 2016; Luce & Cundy, 1994; Smith & Hebbert, 1979). Although catchments in real scenarios are highly heterogeneous, often dominant soil types can be identified, and therefore, understanding the role of soil properties (mostly Ksat) on streamflow generation under a given mechanism could be valuable. Further studies that explore the effects of soil heterogeneity on the development of active areas would be extremely valuable, not only to understand the thresholds of flow generation, but to explain how the transition from ephemeral to intermittent flow occurs for certain IRES. Our results focused on the dominant mechanisms from catchment activation to streamflow initiation, although other mechanisms may have also contributed to the catchment's response at that or a later time. Future work on differentiating between active and

contributing areas would be essential, especially for larger and more complex systems where depletion processes might play a more critical role.

Future studies that include the impact of vegetation through ET on streamflow generation are necessary to better represent system dynamics for arid and semiarid catchments where IRES are the most common feature. The impact of ET is especially important for areas where rainfall occurs during the summer months such as the Sonoran and Chihuahuan Deserts in North America (Pierini et al., 2014), where ET demands are high and exacerbate initial losses. Moreover, with precipitation and flow regime shifts predicted by most climate scenarios (Head et al., 2014; Trenberth et al., 2003), understanding the effects of ET on streamflow generation is vital to predicting if and how climate change could affect streamflow generation in all IRES. Lastly, understanding the effects of ET along with soil heterogeneity, would be necessary for looking at the transition from ephemeral to intermittent streamflow that occurs in many arid systems, as well as for assessing the risk of perennial systems becoming intermittent.

Another area for further research is the role of longer term precipitation patterns. Due to the high computational demand of this exercise, we limited the simulations to relatively short precipitation applications within an overall short simulation period. A seasonal or even a multiyear simulation would be ideal to explore the effect of the memory of the system, that is, how important a previous year's rainfall season was to the next year threshold behavior for flow generation.

Finally, future simulations should include a larger scale catchment to explore the variability in time and space of flow generation processes in IRES in more detail and also consider testing other catchment controls. From the seminal paper on "drainage basin characteristics" by Horton (1932) to a recent work on the extension and contraction of stream networks by Prancevic and Kirchner (2019), the importance of topographic controls on streamflow generation is well documented in the literature. Therefore, it is paramount for future work to explore the effects of a range of topographic controls such as catchment shape, slope, mean soil thickness, and contributing drainage area.

1.14 Conclusion

A concept-development approach was used to explore the effect of a range of catchment and climatic controls representative of low-gradient Mediterranean-climate IRES on the variability on the threshold of flow by determining the dominant flow generation mechanisms and the development and spatial extent of active areas. This approach was implemented through a physically based ISSHM in a well-established experimental catchment setup, allowing us to examine over 1,600 unique "hypothetical realities" to gain insight into the hydrological processes that influence streamflow generation in IRES. Results from this study showed the importance of soil properties for streamflow generation, particularly, for determining the development and spatial extent of active areas and the dominant streamflow generation mechanisms. Understanding the extent to which soil properties dictate the dominant active and contributing processes for streamflow generation is important not only to explain the threshold of flow generation, but how other controls such as depth to GW and different precipitations characteristics influence this threshold. Furthermore, the results reaffirm the importance of unsaturated storage dynamics to explain the thresholds and pathways of flow. The insight gained from these results have important implications for understanding IRES. Our findings show the importance of considering soil type and depth to GW when modeling or managing streamflows in low gradient, Mediterranean-climate type IRES. In a broader sense, these findings can aid management decisions when evaluating the vulnerability of a catchment dominated by a given mechanism to impacts from factors such as GW level declines, land use changes, soil erosion, and shifts on precipitation patterns. Additionally, flow generation mechanisms are key to understand flow pathways which highly influence ecosystems functions, water quality, and land surface processes (Alexander et al., 2007; Freeze, 1974; Haria & Shand, 2004; Liu et al., 2008; Zimmer & McGlynn, 2018). This is an initial step toward a more complete explanation of streamflow generation for some IRES; future work should complement this study by expanding on the effects of other controls for more complex and larger catchments.

Chapter 3

Taking theory to the field: streamflow generation mechanisms in an intermittent, Mediterranean-climate catchment.

1.15 Introduction

In a world of increasing water scarcity, understanding the hydrology of rivers in drylands has become increasingly important. It is widely recognised that our hydrologic understanding of these IRES is still insufficient (Costigan et al., 2017; Boulton et al., 2017). This is partly due to lack of appropriate data; indeed, it has been shown that streamflow gauges, which provide the most fundamental data to understanding the hydrology of rivers, are preferentially located on perennial rivers (Fekete & Vörösmarty, 2002; Poff, Bledsoe, & Cuhaciyan, 2006). Data availability for the many other parameters needed to accurately understand the water balance of IRES is also lacking. Coupled with the added difficulties of characterising unsaturated flow, the natural wetting and drying cycles, and other highly non-linear processes, there are still large knowledge gaps in our understanding of the processes that lead to streamflow generation in IRES.

Numerical models offer one method to better explore the complex drivers that lead to streamflow production in a catchment (Appendix E). By exploring relationships in theoretical or simplified models, data paucity constraints to study streamflow-runoff generation in IRES can be circumvented. Past modelling studies have used fully integrated Surface-Subsurface Hydrological Models (ISSHMs) in IRES have provided insight on the role of soil cover, topography, and soil heterogeneity on runoff generation (Pierni et al., 2014; Ebel et al., 2016; Maxwell & Kollet, 2008) and on the evolution of saturated area patterns (Weill et al., 2013), as well as the importance of unsaturated storage dynamics as major controls on the processes of runoff generation (Vanderkwaak & Loague 2001; Mirus & Loague 2013). In an idealized concept development study, Gutierrez-Jurado et al. (2019) concluded that soil hydraulic

properties control streamflow generation and determine the spatiotemporal development of runoff generating areas and dominant flow generation mechanisms.

While these studies have advanced our understanding on the hydrology of IRES, the required level of information to adequately parameterize boundary value problems have restricted the use of ISSHMs in IRES to mostly small-scale hillslope or headwater catchments (0.001-0.9 km^2). A limitation of the localized insight from these studies is that it does not capture key spatiotemporal processes that control catchment dynamics. For instance, in small-scale systems, the hydrological processes occurring at a given time and place (i.e. 'active' processes [Ambroise, 2004]) might be the same as those contributing to flow generation at that same time. However, in large-scale systems the hydrologic response is influenced by different surface water-groundwater travel times, initial losses (e.g. evapotranspiration or infiltration) and the connectivity of the areas where hydrological processes are occurring. Consequently, the active processes occurring at a time and place does not necessarily contribute to the integrated catchment response at another given point at that or a later time. This is particularly important for IRES where a defining characteristic of the dry-wet transition is that the dry initial conditions exacerbate initial losses causing the development of saturated areas and generation runoff and streamflow to occur discontinuously throughout the catchment. In their study, Gutierrez-Jurado et al. (2019) highlighted the importance of understanding the development and progression of active areas (i.e. where processes are active) and their dominant flow generation mechanisms to understand the pathways and threshold of streamflow generation for IRES.

Another limitation of previous modelling efforts for IRES is that most studies have been set up in a rainfall-runoff approach with relatively short modelling periods (2h – 330 days). Under this approach, the aim is to investigate the integrated system response to a set of distinctive scenarios and/or conditions (Carr et al., 2014; Di Giammarco et al., 1996; Heppner et al., 2007; Kollet et al., 2017; Mirus et al., 2009; Panday & Huyakorn, 2004) rather than to understand longer-term hydrological processes that control the dry-wet transition. In the case of the few process-oriented and concept development studies, the assumptions and simplifications make it difficult to assess how the theory would apply to real, more complex and, larger-scale catchments.

The goal of this study is to investigate the physical processes leading to and at the threshold of stream flow generation in a medium-sized catchment with a temporary stream network, to

evaluate how the theory of previous modelling efforts applies to a real case scenario. To do this, we use an ISSHM coupled with the Hydraulic Mixing-Cell method (HMC) developed by Partington et al. (2011) to capture the physical processes to explain the thresholds of streamflow generation in a temporary stream network within a larger-scale Mediterranean-climate catchment in South Australia. The HMC method tracks the water as it enters the system allowing the identification of active areas by a given flow generation mechanism and the quantification of contributing flow generation mechanisms at selected locations along the catchment (further details on the HMC are provided in the methods section).

Given the inherent difficulties of modelling a large unsaturated domain with contrasting soil layers to capture the physical processes at a rather sudden state change (dry to wet), the goal of this study is not to exactly reproduce the field observations, which in temporary rivers are strongly a function of antecedent moisture conditions. Instead, we present a conceptual model of our understanding of the potential physical flow processes, based on field data combined with our understanding of the geology, topography, and water levels of the catchment. We use the conceptual model to compare the integrated model results to re-evaluate our conceptual understanding of the physical processes occurring in the catchment. The specific objectives of this chapter are to:

1. Develop a conceptual model of the stream system based on available data to build hypotheses about flow generation that can be tested with the integrated model.
2. Use the conceptual model to inform the integrated model setup to identify the development of active areas and determine the dominant flow generating mechanism given distinct differences in geology, topography, and groundwater level within the catchment.
3. Provide insight into the challenges faced in modelling streamflow generation in IRES and how to overcome them.

1.16 Methods

1.16.1 Study Site

The catchment used for this model is Pedler Creek which is part of the larger Willunga basin located roughly 30 km south of Adelaide, South Australia (Figure 3.1). Pedler Creek lies within the McLaren Vale region, an area of high agricultural value mainly for the viticulture industry.

The catchment area is approximately 107 km^2 and discharges into the sea on the Gulf of St Vincent to the west of the catchment. A wastewater treatment plant located in the town of McLaren Vale discharges water into the creek; therefore, we only considered the area upstream of the creek before it passes through the town for this study. The Pedler sub-basin has an area of 69 km^2, encompassing over 60% of the catchment and more importantly, it contains roughly 80% of the total length of the stream network. The creek flow regime is generally intermittent from July to September in response to the winter rains and ephemeral during the rest of the year, flowing only after extreme rainfall events. For the period of record 2000-2018 at gauge ID A5030543, the creek flows on average 120 days per year, ranging from 33 to 199 d yr^{-1}. Mean annual discharge is 3.88 x 10^6 m^3 with the higher flows occurring between July and September (Water Data Services, 2019). Mean annual precipitation for the basin is 550 mm ranging from 289 to 812 mm for the period of record 1900-2018 at the McLaren Vale station 232729 (SILO - Australian Climate Data, 2019). Mean daily temperatures range from 37 to 5 °C, with higher daily temperatures occurring in January and lower daily temperatures registered during June and July (SILO - Australian Climate Data, 2019).

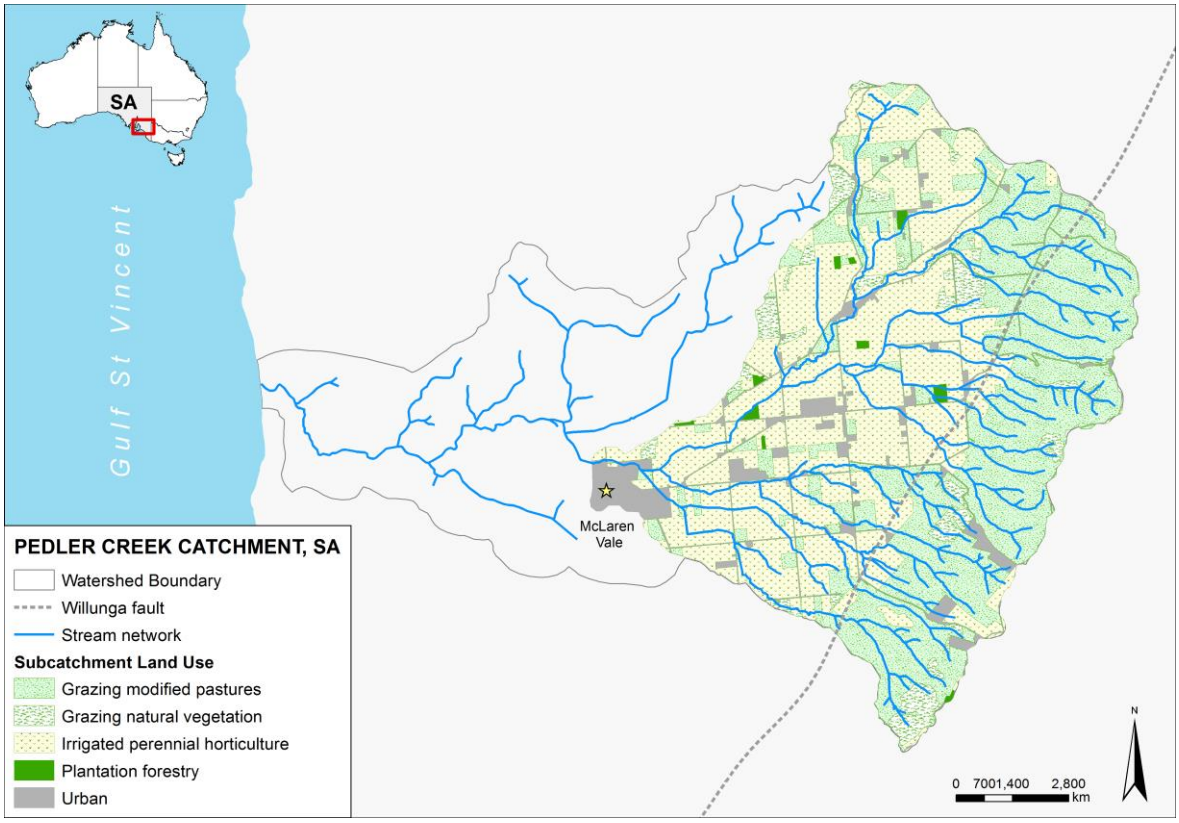

Figure 0.1 Pedler Creek catchment location showing the original watershed boundary, the stream network, and the Willunga Fault. The five major land uses are shown for the model sub-catchment area.

As part of the Willunga basin, Pedler catchment presents a complex multi-aquifer system. The groundwater system consists of four main aquifers: Quaternary sediments, Port Willunga Formation, the Maslin Sands, and the Basement Fractured Rocks (Aldam, 1989). The Maslin Sands and the Port Willunga aquifer are separated in some locations by the Blanch Point Formation which acts as an aquitard. All the hydrogeological units outcrop at the surface and regional groundwater flow towards the coast from northeast to southwest.

The catchment topography consists of a low-lying coastal plain with mild undulating hills towards the north of the catchment and separated by the Willunga Fault to the steep hills located on the east of the catchment (Figure 3.2). Elevation ranges from ≈400 m on the northeast of the sub-catchment (steep hills) to ≈50 m at the sub-catchment's outlet (Figure 0.3.c). The hills area on the east of the fault is characterized by having a shallow sediment profile (0.5 - 2 m) which is underlain by the basement rocks while west of the fault the sediments thicken seaward (Figure 3.2.b). Shallow soil types in the sub-catchment can be clustered into three major soil groups: loam, sand, and clay. Covering roughly 62% (42.36 km^2) of the sub-catchment, the loam soils are distributed on the middle-eastern area; sandy soils cover around 32% (21.7 km^2) and are located mainly on the north part of the sub-catchment with some patches present in the middle section (valleys); the clay soils account for only 6% (3.94 km^2) of the sub-catchment area and are located on the further downstream section towards the west of the sub-catchment (Figure 3.2.a). Most of the stream network (over 80%) is located within the loam soil. Detailed soil profiles obtained from the Department of Environment Water and Natural Resources (DEWNR) consistently show a distinctive clay layer starting from 1.1 to 1.5 meters depth in the sandy soil areas and at around 0.5 m within the loam areas. From the 4 major land uses in the sub-catchment, agriculture (45%-30.4 km^2) and grazing (46%-31.8km^2) dominate over 90% of the landscape. Urban (residential and commercial) account only for 8% (5.4 km^2), and plantation forestry covers less than 1% (0.38 km^2) of the sub-catchment (Figure 3.1).

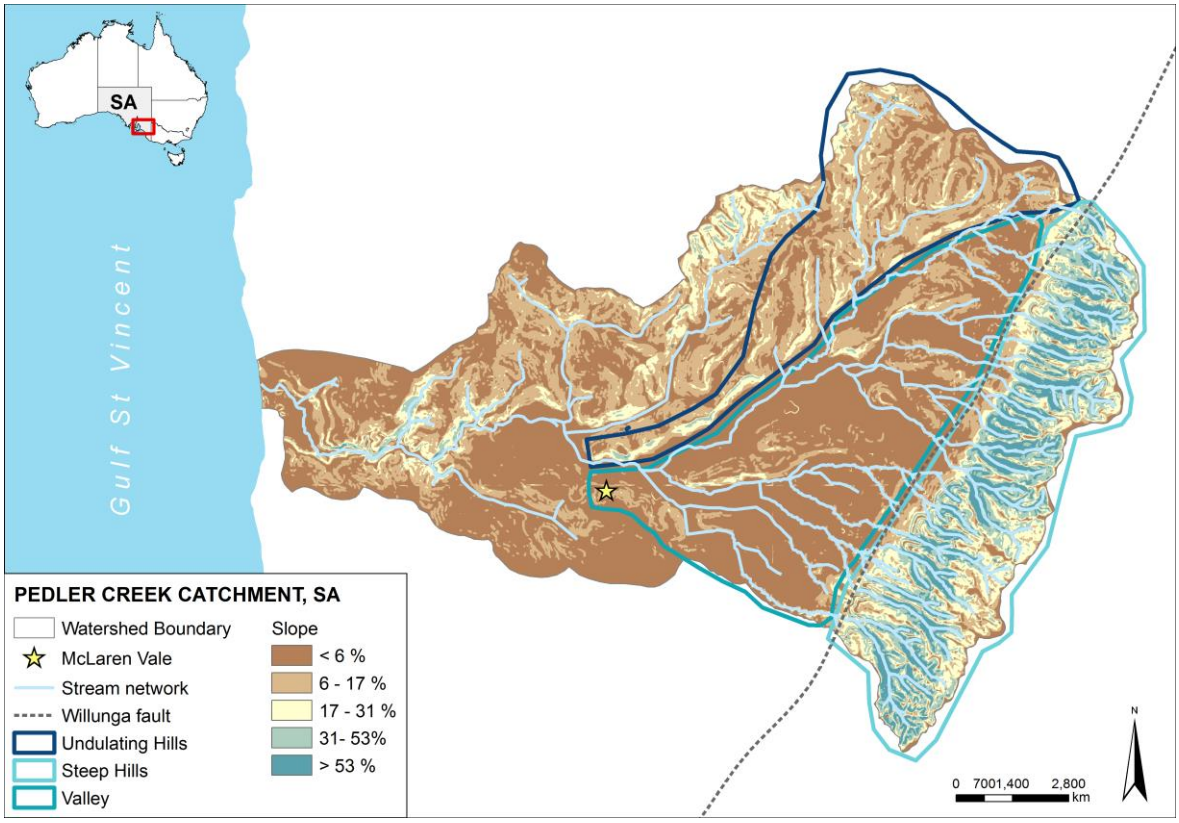

Figure 0.2 Pedler catchment slopes highlighting the three distinctive areas for the sub-catchment area: undulating hills on the north, the steep hills on the east and the low gradient valley.

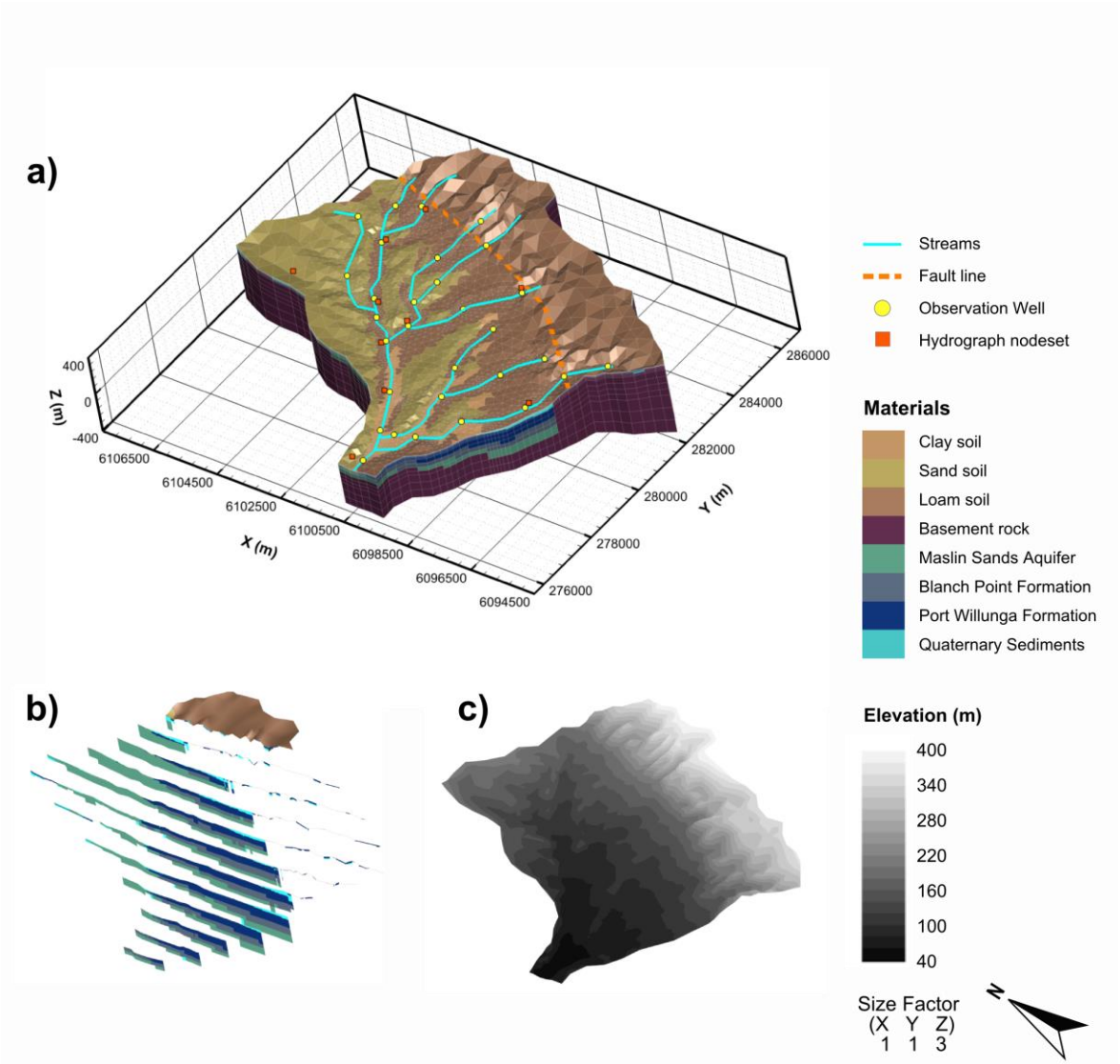

Figure 0.3 a) Three-dimensional representation of Pedler catchment showing the mesh discretization, the spatial distribution of shallow soil types, and the location of observation wells and hydrograph nodes. b) Slices showing the distribution and thickness of the hydrogeological layers. c) Digital elevation model showing the surface topography.
* Approximated location of the discretised stream network and the fault line are over imposed for illustration purposes.

Surface water-groundwater interactions within Pedler catchment have been documented in previous studies to play a critical role in the creek flow's regime. Sereda and Martin (2000) observed rapid groundwater level rises in response to large precipitation events in some shallow monitoring wells adjacent to creeks while noting that GW level declines in the Quaternary aquifer during 1995-1999 could be attributed to a decrease of yearly precipitation during that

period. Moreover, Harrington (2002) observed that groundwater levels seemed to mirror streamflow records for the Creek. While these observations confirm that GW recharge occurs from precipitation and creek seepage, these and other studies have also indicated that GW discharge occurs in some areas of the creek (Harrington 2002, Anders 2012). Further studies have indicated that the creek presents both gaining and losing stream sections, which are not only spatially but temporally variable and which are dependent on rainfall and shallow groundwater levels (Harrington 2002; Brown 2004; Irvine 2016; Anders 2012).

1.16.2 Conceptual Model of Streamflow Generation Process in Pedler Creek

For medium to large size catchments, like Pedler Creek, the interactions of varying topographic features such as slope and mean soil thickness in conjunction with heterogeneous shallow soils and aquifers properties and a variable depth to GW are likely to result in different streamflow generation processes developing at different spatiotemporal scales throughout the catchment. To understand the integrated catchment response as well as the stream network dynamics (development, expansion, and contraction) it is paramount to capture the spatiotemporal occurrence of the different streamflow generation mechanisms. In a similar classification to Gutierrez-Jurado et al. (2019) the streamflow generation mechanisms include: infiltration excess overland flow (IE-OF), saturation excess overland flow (SE-OF), unsat/sat interflow (Sat-IF, Unsat-IF) and pre-event GW (old GW). Further details on the streamflow generations mechanisms can be found in Gutierrez-Jurado et al. (2019).

Based on field data and available soil and aquifer information we developed a conceptual model to outline the most likely processes leading to streamflow generation and what the dominant streamflow generation mechanisms might be for Pedler Creek. We identified three major areas with distinctive characteristics; 1) the steep hills on the east, 2) the undulating hills on the north, and 3) the flat valley on the south-west area of the catchment (

.a). We hypothesize that contrasts in the topography, soil characteristics, and groundwater level among these three areas will lead to differences in the physical recharge and discharge processes that occur within these regions of the catchment, ultimately creating the observed seasonal patterns of ephemeral and intermittent streamflow responses.

Figure 0.4 **a)** Conceptual diagram showing the three major areas that are likely to develop distinct streamflow generation mechanisms during the intermittent flow season. **b-d)** 2D soil profiles for the three major areas detailing the processes developing from the initial conditions until the threshold of flow (modified from Gutierrez-Jurado et al., 2019) **e)** Typical hydrograph during the intermittent season highlighting the hypothesized 'fast' and

The three main areas patial understanding of the most likely streamflow generatin flows in Pedler Creek occur in direct response to extreme precipitation events (characterized by low-duration, high-intensity precipitation), the temporal component can be considered negligible. Instead, flow is mostly linked to the spatial characteristics of the catchment where we hypothesize that the dominant flow generation mechanism is infiltration excess overland flow originating from the loam and clay soils throughout the catchment. Conversely, it is paramount to include the temporal component to understand how these processes develop and the threshold of flow is reached for intermittent flow during the rainy season. We hypothesize that the dry conditions at the

beginning of the rainy season will result in most of the rainfall to infiltrate due to the high infiltration capacity of the soil. However, differences in topography and soil characteristics will promote different processes to develop as the rainy season progresses. A detailed description of the processes for each area and the spatiotemporal development of the most likely dominant streamflow generation components for intermittent flow are provided below (Figure 3.3.b-d).

1.16.2.1 Steep Hills; Fast Flow:

The steep hills are characterized by a permeable, shallow, loam soil underlain by a heavy clay profile with steep slopes (Figure 3.2 and Figure 3.3.b). The combination of the soil permeability, the high infiltration capacity, and the steep slopes are likely to allow the water to infiltrate and to flow relatively fast as unsat-IF towards the stream (Figure 3.3b.1-2). We hypothesize that the shallow soil profile and the water holding capacity of the loam will promote a perched GW mounding along the riverine area which will result in SE-OF from the riverine area and the adjacent hillslope to develop as the dominant streamflow generation mechanism (Figure 3.3.b.3).

1.16.2.2 Undulating Hills; Slow Flow:

The undulating hills consist of a highly permeable deep sandy soil profile underlain by a heavy clay layer with mild slopes (Figure 3.2 and Figure 3.3.b). The high soil infiltration capacity and permeability will result in a large infiltration rate allowing most of the precipitation to infiltrate in this area (Figure 3.3.c.4). As the infiltrated water reach the low permeable clay layer it will move in the subsurface as IF towards the low-gradient areas (Figure 3.3.c.5). We hypothesize that the high infiltration rates in combination with the mild slopes (or low-gradient areas in the valley) will favour the development of a perched GW that will rise uniformly allowing the river to develop into a gaining condition. As the infiltrated water moves as IF it will discharge into the downstream areas (Figure 3.3.c.6). Due to the larger unsaturated storage and the mild slopes, this area will likely take longer to contribute to flow (i.e. more water will be needed and therefore more time to reach the threshold of flow generation). We hypothesize that these areas will provide the "slow flows" necessary to sustain intermittent flow for the days without rainfall during the intermittent season and conversely, they are not likely to contribute to flow during ephemeral events (Figure 3.3.e).

1.16.2.3 Flat Valley; Mixed Flows:

The flat valley comprises a mix of the previous two soil profiles (deep sand and shallow loam both underlain by heavy clay) and heavy clay small area, all located in a low-gradient topography (Figure 3.2 and Figure 3.3.d). The GW becomes shallower near the riverine areas in the valley and depth to GW decreases towards the outlet area (the shallowest bore is located near the outlet with the GW ≈2 m below surface elevation). This zone has the largest draining area with both the steep and undulating hills draining towards it. The diversity of conditions in this area is likely to result in a combination of the processes previously discussed as well as additional ones. We hypothesize that the processes originating on the sandy soil areas on the valley will be similar to those on the undulating hills with the difference that the unsat-IF that might originate early during the season might only contribute with a small amount of flow that might reflect further downstream. We also expect to see some sat/unsat-IF originating early in the season in the loam areas on the valley (Figure 3.3.d.8-9). However, we hypothesize that the low-gradient terrain along with the water holding capacity of the soil will slow down water moving as interflow and rather promote the soil saturation to build up in the shallow soil profile. As the saturation increases, we expect the dominant streamflow generation mechanism will switch to saturation excess overland flow from both the hillslope and the river area.

The low permeability of the soil will limit infiltration and favour water to pond on the surface for the clay areas, which will eventually result in infiltration excess overland flow (Table 3.3.d.10-11). The large draining area of the valley combined with the low-gradient topography is likely to promote the development of a perched GW along the riverine area which will result in SE-OF along some sections of the river (Figure 3.3.d.9). During wet years, sections of the creek near the outlet where GW is shallow, are likely to develop into a gaining state with old-GW contributing to streamflow (Figure 3.3.d.10). Once the saturation threshold has been met along the riverine area in the steep hills and throughout the loam areas in the valley, SE-OF and the IE-OF from the clay are likely to contribute with the "fast flows" as travel times for overland flow are generally smaller than those for subsurface processes (Figure 3.3.b).

1.16.2.4 Impacts of these Processes on the Hydrograph:

We hypothesize that the development of these "fast" and "slow" streamflow generation mechanisms across the catchment is reflected on the hydrograph (Figure 3.3.e). The peaks showing a "fast" rise followed by a sharp recession are likely to reflect large precipitation events

that result on overland flow (SE-OF and IE-OF) mechanisms occurring from the loam and clay areas across the catchment. We believe that it is the subsurface processes, mainly the interflow originating from the sandy soil areas that contribute the flows that maintain streamflow during periods of small rainfall events or in the absence of rainfall during the intermittent flow season.

1.16.3 Modelling Platform and HMC Method

To explore the potential for streamflow within the structure of the conceptual model, we built a fully integrated, numerical model of the catchment. For this study, we used HydroGeosphere (HGS), a 3-D fully integrated surface-subsurface hydrological model (ISSHM). HGS's fully integrated approach allows producing physically-based simulations of hydrological processes by using the control-volume finite element method to simultaneously solve the surface and subsurface flow equations. The numerical code uses the diffusion wave approximation to the St Venant equations for 2D surface flow and a modified form of Richard's equation to solve the variably saturated subsurface flow. Further details on the physical and mathematical conceptualization and the implementation of the HGS code can be found in Aquanty Inc. (2016) and the review by Brunner and Simmons (2012).

The decomposition of flow into the different generation mechanisms is provided by coupling HGS with the HMC method which is based on the modified mixing-cell method (Campana & Simpson, 1984). Using the standard hydrological output from a numerical model, the HMC method allows the partition of flow in any node within the catchment. To do this partition the HMC method tags the existing water at the beginning of the simulation and any new water as it enters the model domain by area of origin (i.e. stream, hillslope, and the porous media), by boundary condition (i.e. the source of water) and for the case of the new water, by the internal model state of saturation of the area of origin (i.e. saturated or unsaturated soil profile). This allows the partition to include all previously mentioned streamflow generation mechanisms stated in section 3.3.2 for each of the specified areas of origin. Using these tags, the water is tracked as it moves through the model domain and after each time step of the flow simulation the method calculates the fraction of water in each cell that derives from the different flow components. Detail information on the numerical formulation and application of the HMC method are given in Partington et al. (2011), Partington et al. (2013), and Gutierrez-Jurado et al. (2019).

To test the hypothesis outlined in our conceptual model (section 3.3.2) the hillslope fraction was further divided into the three dominant soil types (sand, loam, and clay). A summary of the flow generation mechanisms covered by the resulting fractions and the fractions origin are detailed in Table 3.1.

Table 0.1 Hydraulic Mixing-Cell delineated fractions

Flow generation mechanism	Fraction name	Fraction origin
Saturation excess overland flow	SE-OF (Dunne)*	In-stream and sand, clay and loam hillslopes
Infiltration excess overland flow	IE-OF (Horton)	In-stream and sand, clay and loam hillslopes
Saturated interflow	Sat-IF	In-stream and sand, clay and loam hillslopes
Unsaturated interflow	Unsat-IF	In-stream and sand, clay and loam hillslopes
Pre-event GW	Pre-event GW (old GW)	Porous media

Note. HMC = Hydraulic Mixing-Cell; IF = interflow; SE-OF = saturation excess overland flow; IE-OF = infiltration excess overland flow; GW = groundwater.
*Common names used for the fractions are shown in parenthesis

1.16.4 Model Setup

1.16.4.1 Model Discretization

Two major considerations preceded the 2D model discretization: 1) the stream network extent represented in the mesh, and 2) the mesh refinement along the stream network. A representative stream network was needed to be able to capture the development of active areas leading to streamflow generation in different parts of the catchment (Appendix F), while smaller elements along the streams were needed to better capture the topographic features allowing a more accurate representation of the hydrodynamic processes.

Initially, we created a 2D mesh which consisted of 57,978 nodes and 115,168 triangular elements with a ≈5-10 m nodal spacing around the streams in comparison to the ≈0.5-3 m stream width observed in the field (**Error! Reference source not found.**.a). The coarser resolution along the stream sections was a compromise to include a larger stream network which would be representative of the three major areas in the catchment (Figure 0.3). A preliminary model test

showed that the model convergence was extremely slow, and we decided to relax the 2D surface discretization. A selected set of additional meshes that were tested are shown in **Error! Reference source not found.**.b-d.

The final 2D surface domain discretisation consisted of 3015 nodes and 5869 triangles with the nodal spacing ranging from ≈40-70 m around the streams and up to ≈500 m at the catchment boundary (**Error! Reference source not found.**.c). Vertically, the subsurface domain was discretised into 28 layers with a finer resolution implemented for the upper 20 m (within the range of the shallow aquifer's water table for most of the shallow observation wells). For the first two layers the resolution was 0.05 m, followed by 0.2 m up to a depth of 2.1 m (layers 1-13), and grading to 5 m at a depth of 20 meters (layers 14-18). The consecutive layers ranged from 12 to 120 m at the bottom of the domain (layers 19-28). The final 3D grid consisted of 84,420 total nodes and 159,192 total triangular elements. The topography for the surface elevation was implemented by using a digital elevation model based from 5 m contours with a final resolution of 10 m. To compensate for the coarser nodal spacing around the stream network we subjected the digital elevation model to a post-processing routine using Python to depress the elevation along the stream and incise the stream nodes (Appendix G). We tested four different scenarios by incising the stream nodes by 4, 6, 8 and 10 m respectively.

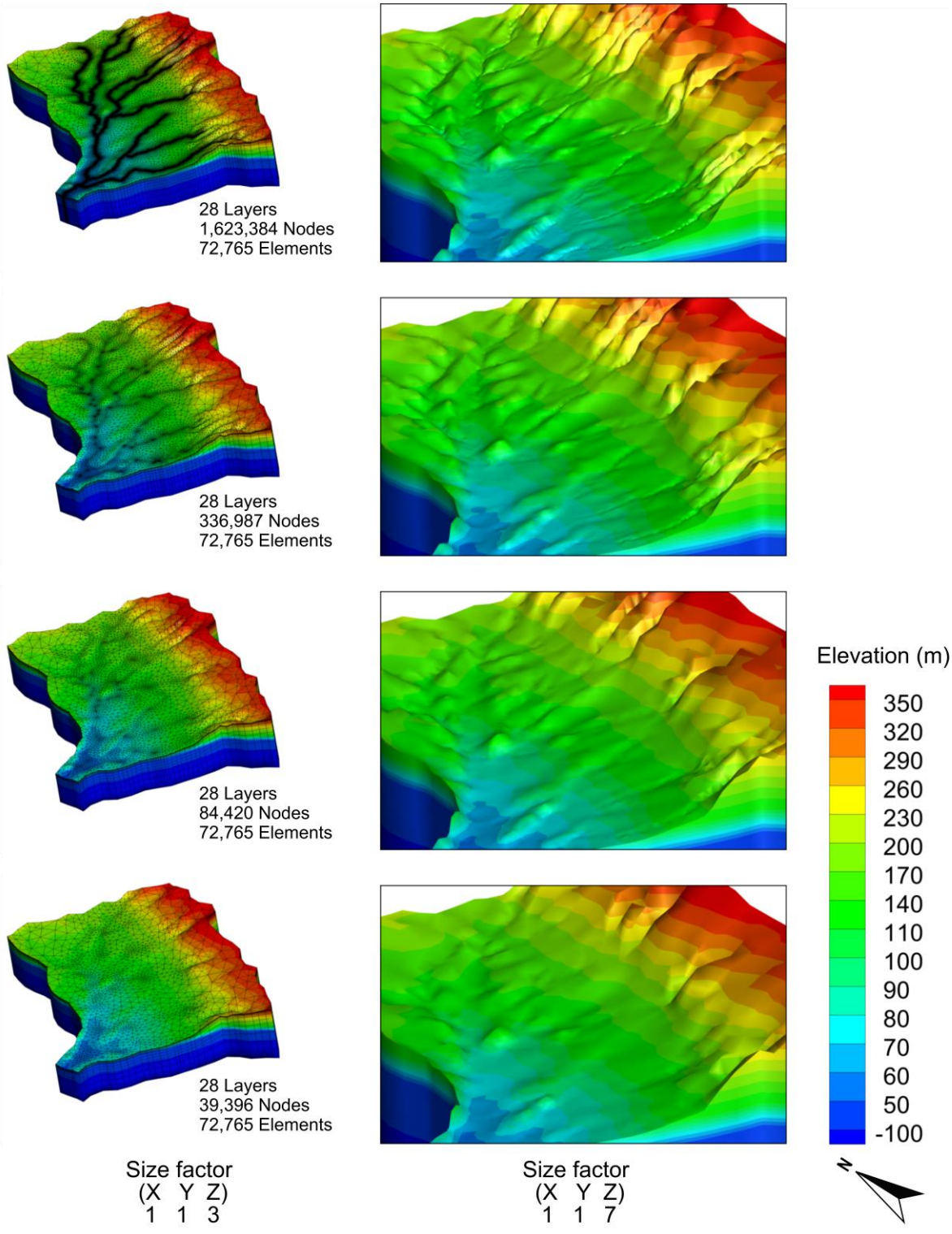

Figure 0.5 Selection of a set of tested 3D meshes showing the impact of the 2D discretization on the topography representation from fine to coarse (top to bottom). The figures on the left have the mesh mapped to provide a visual of the discretization around the streams. The right column shows a zoomed view of the catchment with a larger vertical exaggeration and without the grid to provide a better view of the resulting topography. A summary of the total number of layers, nodes, and elements is provided for each 3D mesh.

1.16.4.2 Porous Media Properties

Soil physical and hydraulic properties were applied to the subsurface to capture the horizontal and vertical soil heterogeneity for both the shallow soils and the Quaternary Sediments, Port Willunga Formation, Blanche Point formation and the Maslin Sands hydrogeological layers. Since the aims of this research are mostly linked to surface water-groundwater processes occurring in the shallow subsurface and to improve computational time, we chose to not include the basement fracture rock and therefore the elements corresponding to this unit were made inactive. Although we know from field observations that east of the fracture, the basement contributes flow to some areas, there is not enough information to inform the model about these occurrences.

To select and apply the properties to the hydrogeological units we used rasters of the top and bottom elevations for each unit generated from a previous study. Hydraulic conductivity, porosity and specific storage for the selected hydrogeological units were obtained from literature estimates (Aldam 1990; Anders 2012; Irvine 2016; Martin 1998, 2006) and are reported in Table 3.2. Values for the unsaturated functions were not available, therefore we used values obtained from the soils from Carsel and Parrish (1988) and Mirus et al. (2011) which had the closest hydraulic conductivity values to the estimates for each hydrogeological unit.

Table 0.2 Surface-Subsurface Parameters for Pedler Creek

Media	Parameter	Value
	Surface	
Floodplain Agriculture	Manning's roughness n	4.05 E-7 $s/m^{1/3}$
	Rill storage	0.01 m
	Obstruction storage	0.0 m
Floodplain Pasture	Manning's roughness n	3.47 E-7 $s/m^{1/3}$
	Rill storage	0.01 m
	Obstruction storage	0.0 m
Floodplain Urban	Manning's roughness n	1.85 E-7 $s/m^{1/3}$
	Rill storage	0.01 m
	Obstruction storage	0.0 m
Creek Valley	Manning's roughness n	1.15 E-6 $s/m^{1/3}$
	Rill storage	0.01 m
	Obstruction storage	0.0 m
Creek Headwaters	Manning's roughness n	4.05 E-7 $s/m^{1/3}$
	Rill storage	0.01 m
	Obstruction storage	0.0 m
Surface-Subsurface Coupling	Coupling length	0.001 m
	Subsurface	
Sand	Hydraulic conductivity K_{sat}	0.314, 1.06, 7.128 m/d

	Porosity	0.43
	van Genuchten *a*	5.9, 7.5, 14.5 m^{-1}
	van Genuchten β	1.48, 1.89, 2.68
	Residual saturation θ_r	0.045
Loam	Hydraulic conductivity K_{sat}	0.0624, 0.108, 0.2496 m/d
	Porosity	0.46
	van Genuchten *a*	1.9, 2.0, 3.6 m^{-1}
	van Genuchten β	1.31, 1.41, 1.56
	Residual saturation θ_r	0.067, 0.095, 0.078
Clay	Hydraulic conductivity K_{sat}	0.0624, 0.0009 m/d
	Porosity	0.475
	van Genuchten *a*	1.9, 0.6 m^{-1}
	van Genuchten β	1.31.
	Residual saturation θ_r	0.095
Quaternary Sediments	Hydraulic conductivity K_{sat}	0.86301 m/d
	Porosity	0.3
	van Genuchten *a*	7.5
	van Genuchten β	1.89
	Residual saturation θ_r	0.065
Port Willunga Formation	Hydraulic conductivity K_{sat}	4.1095 m/d
	Porosity	0.3
	van Genuchten *a*	12.4 m^{-1}
	van Genuchten β	2.28
	Residual saturation θ_r	0.057
Blanch Point Formation	Hydraulic conductivity K_{sat}	$8.6E^{-05}$ m/d
	Porosity	0.3
	van Genuchten *a*	4.3 m^{-1}
	van Genuchten β	1.25
	Residual saturation θ_r	0.02
Maslin Sands	Hydraulic conductivity K_{sat}	0.86 m/s
	Porosity	0.3
	van Genuchten *a*	7.5 m^{-1}
	van Genuchten β	1.89
	Residual saturation θ_r	0.065
	Evapotranspiration	
Grass	Evaporation depth	1 m
	Root depth	1 m
	Leaf area index	1
	Transpiration fitting parameter c1	0.5
	Transpiration fitting parameter c2	0.0
	Transpiration fitting parameter c3	1.0
	Wilting point	0.29
	Field capacity	0.56
	Oxic limit	0.75
	Anoxic limit	0.9
	Limiting saturation (minimum)	0.25
	Limiting saturation (maximum)	0.9
	Canopy storage parameter	0.0 m
	Initial interception storage	0.0 m
Eucalyptus	Evaporation depth	3 m
	Root depth	5 m

Leaf area index (LAI)	2.08
Transpiration fitting parameter c1	0.6
Transpiration fitting parameter c2	0.0
Transpiration fitting parameter c3	1.0
Wilting point θ_{wp}	0.29
Field capacity θfc	0.56
Oxic limit θ_o	0.8
Anoxic limit θ_{an}	0.95
Limiting saturation (minimum)	0.25
Limiting saturation (maximum)	0.9
Canopy storage parameter	0.00045
Initial interception storage	0.0003

We used a digital soil-landscape map obtained from the Department for Environment, Water and Natural Resources of South Australia (DWLBC 2004; Hall et al., 2009) to differentiate the spatial distribution of the three dominant shallow soil types. The vertical heterogeneity was determined by analysing soil characterisation datasheets from detailed soil profiles available within the Pedler sub-catchment (Appendix H, [DEWNR 2016]). The shallow soils were considered as the top 1.5 m of the subsurface domain which was the average depth reported in the soil characterisation datasheets. Consistently, the soil profiles for the loam and sandy areas showed a distinct transition into a clay layer at an average depth of 1.1 m for the sand and from 0.3 m for the loamy areas. The information of the horizontal and vertical distribution of soils was assigned into the model using 2D overlays (horizontal) for the three main soil areas and the mesh layers generated during the grid discretization (vertical). As quantitative soil hydraulic properties were not available in the soil datasheets, we tested a range hydraulic parameters representative of the three main soil types (sand, loam and clay) obtained from Carsel and Parrish (1988) as shown in Table 3.1. Data of particle size distribution at two different depths (soil layers) was available for two of the soil profiles within the catchments and four additional sites nearby. We used the ROSETTA model H2 (Schaap et al., 2002) to estimate the soil hydraulic parameters and to validate the selected range of values that were tested (Appendix I).

1.16.4.3 Overland Flow Properties

Manning's roughness coefficients (n) derived from Chow (1959) were implemented for the three prevalent land uses (i.e. agricultural, pasture, and urban) which account for over 99.5% of the sub-catchment area. We used the values for cultivated areas with mature row crops (4.05E-7 $d/m^{1/3}$) for the agricultural areas, for pasture with no bush and short grass (3.47E-7 $d/m^{1/3}$), and the value of asphalt (1.85E-7 $d/m^{1/3}$) was applied to the urban area (Table 3.2). For the

stream network, we used values for a clean and straight natural channel for the headwater sections (4.05E-7 $d/m^{1/3}$) and of weedy reaches for the middle-lower sections (1.15E-6 $d/m^{1/3}$). Rill storage height was set to 0.01 m uniformly across the domain and no obstruction storage height was implemented. The coupling length was set at 0.001 to warrant a good coupling of the surface-subsurface domains which is paramount to capture streamflow generation processes (Liggett et al., 2014).

1.16.4.4 Simulation Period and Initial Conditions

We selected a 4-year simulation period from January 2015 to December 2018 to ensure a representative set of years with average (2017 ≈ 500 mm/y), below average (2015 and 2018 ≈400 mm/y) and above-average (2016 ≈ 800 mm/y) rainfall amounts. Precipitation records from the McLaren Vale and the McLaren Flat stations (located in the valley and close to the steep hills respectively) were averaged and applied as a fluid flux to the surface of the model domain (MEA, 2019). To determine the optimal time resolution for the precipitation forcing we tested preliminary models with quarterly-hour, 1-hour and 24-hour inputs. Results from the preliminary models show better convergence and smaller errors in the water balance for the hourly precipitation inputs. Estimates of potential evapotranspiration (ET_0) were only available at a daily time step, therefore we used values of solar radiation to approximate ET_0 at hourly intervals to match the precipitation inputs. Values of ET_0 that were less than 0.0001 m/h were considered numerical noise and were excluded from the input dataset. The resulting ET_0 dataset was applied to the surface domain. Actual evapotranspiration (ET) and interception are simulated as mechanistic processes within HGS using the concepts by Kristensen and Jensen (1975) and Wigmosta et al. (1994) which require plant and soil conditions (Aquanty, 2016). Vegetation characteristics cited in the literature for Eucalyptus were used on the riverine area and values typical of grass where used for the rest of the catchment (Table 3.2). Although a large area on the catchment consists of vineyards, during the winter months the vines are dormant without leaves and grass is commonly used as an inter-row soil cover. For the scope of this study, we did not include the effects of irrigation, ET and interception during the vines growing season as we considered the overall effects for streamflow generation would be negligible since they occur during the driest and hottest months of the year when streamflow is practically non-existent.

With the simulation starting in January (the hottest month) we assumed completely dry initial conditions for the surface domain. For the subsurface domain, we first tried to approximate the initial GW heads using GW levels from all the available shallow wells in the area (Appendix J). Due to the lack of spatial coverage of wells across the catchment the approximated GW raster was considered unrealistic and it was discarded. Subsequently, we opted for approximating the initial groundwater heads by draining a fully saturated model domain. We applied a fluid transfer around the catchment outlet and a constant evapotranspiration rate to drain the model. Observation wells were set up in the model domain in all the locations where shallow GW elevation data were available. The convergence of water draining from the hills towards the valley where the catchment becomes narrower coinciding with the fact that the elements around the outlet consisted of the Blanch point aquitard (low K_{sat}), resulted in 'bottle-neck' effect at the outlet. To counter this issue, we modified the K_{sat} values for the different hydrogeological layers and tested different initial GW heads ranging from 0-4 m below the surface as the start of the draining scenarios. We tested over 37 different combinations until a scenario modelled GW heads that were within the historically observed levels for most of the available shallow wells. We identified the output time where the simulated GW heads and the average observed heads were in closest agreement, giving preference to match shallow GW heads (< 10 m depth) located close to the streams which are known to potentially develop into gaining conditions (Appendix K). The porous media head from the selected scenario and output time was subsequently used as the initial conditions for the porous media in the subsequent simulations.

1.16.4.5 Boundary Conditions

Boundary conditions for the outflow in the surface domain were set as a critical-depth boundary at the catchment's outlet and as a no-flow boundary condition for the rest of the domain. For the subsurface domain, a fluid transfer boundary condition was set at the outlet faces. The hydraulic gradient for the fluid transfer was given by setting a hydraulic head ≈4 m below the surface elevation (the known deepest GW head near the outlet) and at 10 m from the outlet faces.

Sets of nodes comprising the stream cross-section were included at 32 locations distributed across the catchment as hydrograph nodes (Figure 3.2.a). Gauging data (flow) or river stage data

(water depth) were available at 6 of those hydrograph locations. Similarly, the network of observation wells previously described was included as observation wells in the model.

1.16.4.6 Simulation Implementation

The simulations were performed in HGS using the control-volume finite-element mode and the dual-node approach for surface-subsurface coupling. We used an adaptive time step with a computed under-relaxation factor scheme to aid the computational efforts. Adaptive time-stepping was applied by an initial step size of 0.001 days, a maximum step multiplier factor of 2.0, and a maximum time-step of 5 days. The simulations were run in parallel mode using 6 CPUs to partition the model domain. The HMC method was set up to track the flow generation mechanisms originating from the different soils in the overland areas (clay, loam, and sand hillslopes), directly in the river (in-stream), and from the porous media (Table 3.1).

We ran over 52 preliminary models testing different mesh discretizations, time resolutions for the model forcings (i.e. precipitation and ET), simulation controls values, and draining simulations to try to select the optimal model setup. From the final setup we developed a final set consisting of 8 scenarios to be tested; four corresponding to sets with different combinations for the shallow soils hydraulic properties (K_{sat} and their corresponding unsaturated storage parameters α, β, and θr); and four scenarios with different values for incising the river nodes (Table 3.3). Due to the computational burden, only one set of soil hydraulic properties was used to test the scenarios with the incised stream. Results from these two sets of scenarios were used to evaluate the need to modify and test further scenarios.

Table 0.3 Final set of tested model scenarios

Scenarios testing the shallow soils Ksat (m/d)[a]	
Scenario 1	Sand = 1.06 Loam = 0.108 Clay = 0.0009
Scenario 2	Sand = 0.314 Loam = 0.0624 Clay = 0.0009
Scenario 3	Sand = 1.06 Loam = 0.0624 Clay = 0.0009
Scenario 4	Sand =0.314 Loam = 0.108 Clay = 0.0009

Scenarios testing the stream incision values (m)[b]	
Scenario 5	4
Scenario 6	6
Scenario 7	8
Scenario 8	10

[a] For the corresponding values of the unsaturated storage parameters refer to Table 0.2
[b] Soil hydraulic properties for these scenarios correspond to scenario 4

1.17 Data Analysis of Model Results

To evaluate the differences among scenarios we compared the results from the water balance components, the hydrographs, the observation wells, and the information from the surface and subsurface domains.

1.17.1 Development of Active Areas and Flow Generation Processes Analysis

Model output for the surface domain (2D) was post-processed to identify and quantify the activation of areas (flow onset) by a given flow generation mechanism. The output files were processed in Python to determine the HMC fraction that contributed most of the flow (dominant fraction) at every single node and for each output time. Results of the dominant fraction were then included as a new variable to the overland output file to allow visualization. A water depth threshold equal to the rill storage height (0.01 m) was used to determine when an area was considered active (i.e. values of 0.01 m or less were considered as rill storage and not flow). Output for the porous media (3D) was used to explore any potential surface water-GW interactions to support the HMC dominant fractions findings.

The results from the HMC dominant fractions coupled with the PM output was used to contrast the simulated flow generation mechanisms with the hypothesized physical processes proposed in the conceptual model.

1.18 Results

The computational demands of modelling a large and variably saturated domain resulted in extremely slow model convergence which was exacerbated during the sudden state changes

from dry to wet. From the set of scenarios testing different values for incising the stream (Table 3.3), only scenario 8 (incision = 10 m) finished under a reasonable computation timeframe. Scenarios 5-7 showed less than 10% of progress after 20 days of computation time. Nevertheless, the comparable results between scenario 8 and 4 which shared the same soil hydraulic properties but had the two ends of the spectrum in respect to the river incision (the most vs. none) suggest that results from scenarios 5-7 would have likely shown similar results. Therefore, from here on we will only focus on the results from scenarios 1-4 and 8.

1.18.1 Water Balance Results

Among the scenarios with different sets of hydraulic properties (scenarios 1 through 4), the water balance breakdown was virtually identical for scenarios 2&3 (<0.1% difference) and 1&4 (≈0.1% difference) and only small differences (as a percentage of the overall water balance) were observed (≈0.1 - 4% difference) as shown in Figure 3.6. The results showed a higher PM and OLF and smaller FT values for scenarios 2&3 than for scenarios 1&4. Since the change in storage is the sum of the OLF and PM components, scenarios 2&3 also showed a larger change in storage than scenarios 1&4. The largest differences were simulated among the results from scenarios 1-4 (no incised stream) and scenario 8 (incised stream). Scenario 8 had the largest OLF and change in storage values and the smaller ET values.

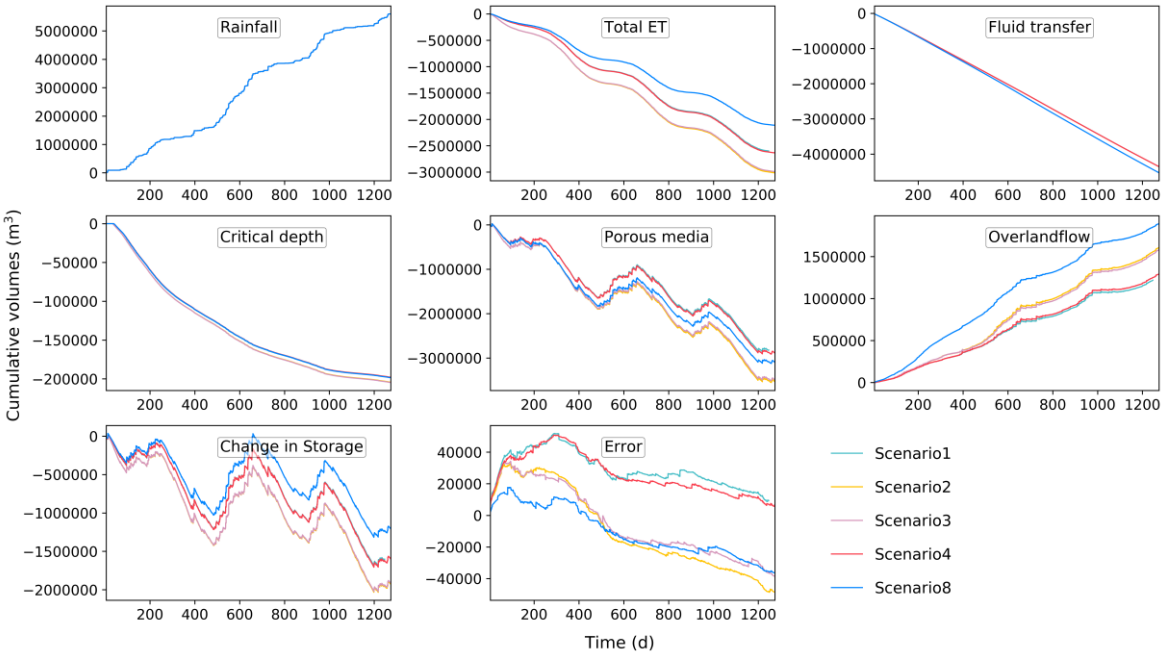

Figure 0.6 Cumulative values of the water balance components for scenarios 1-4 and 8

Across scenarios, the largest component of the water balance was the FT which accounted on average for over 35% with values ranging from 34-38% (Figure 3.7). The average PM and ET were ≈26 and 22% with values ranging from 25-28% and 18-24% respectively. The OLF component ranged from 11-16% and the critical depth (surface outflow at the model outlet) accounted roughly for <2%. Random errors were noted in all the simulations, however, the overall total error accounted for less than 0.5% of the total water balance in all the scenarios. Among the scenarios with different sets of hydraulic properties (scenarios 1 through 4), scenarios 2&3 showed practically the same results and scenarios 1&4 were in close agreement (1-3% differences for some components). The largest difference between scenarios 2&3 and 1&4 was reflected in the porous media component with an average difference of over 12%.

Another difference between the set of scenarios 1-4 and scenario 8 was observed in the partition of the total evapotranspiration components (Figure 3.8). Across all the scenarios the largest component was the PM evaporation with 41-42%. However, surface evaporation accounted for 36% and PM transpiration for 23% for scenarios 1-4, while for scenario 8 the second ET component was PM transpiration with 34% followed by surface evaporation with 25%.

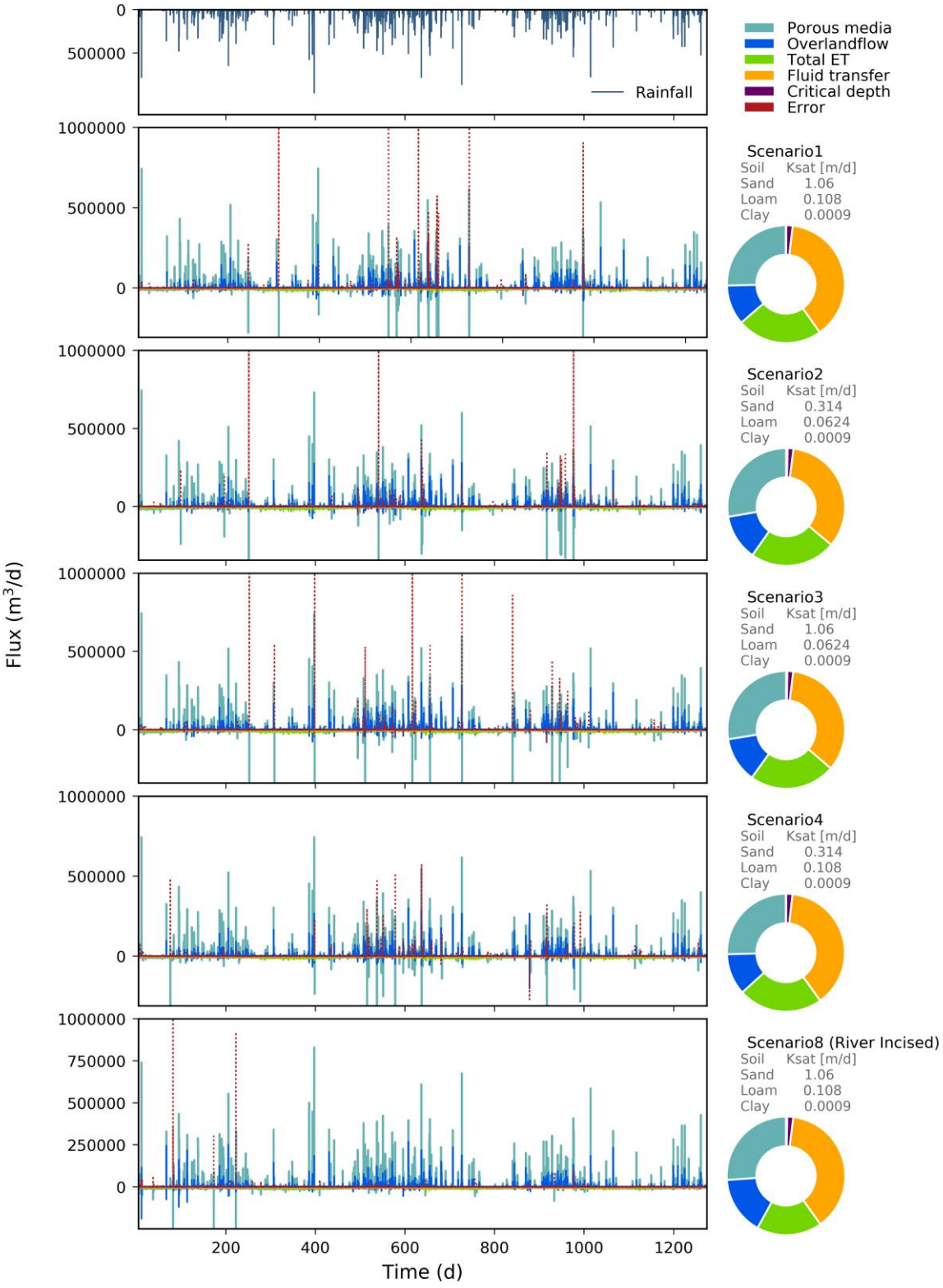

Figure 0.7 Water balance for each scenario and breakdown of the rainfall input. The pie chart shows the breakdown of the proportional contribution in percentage of each water balance component

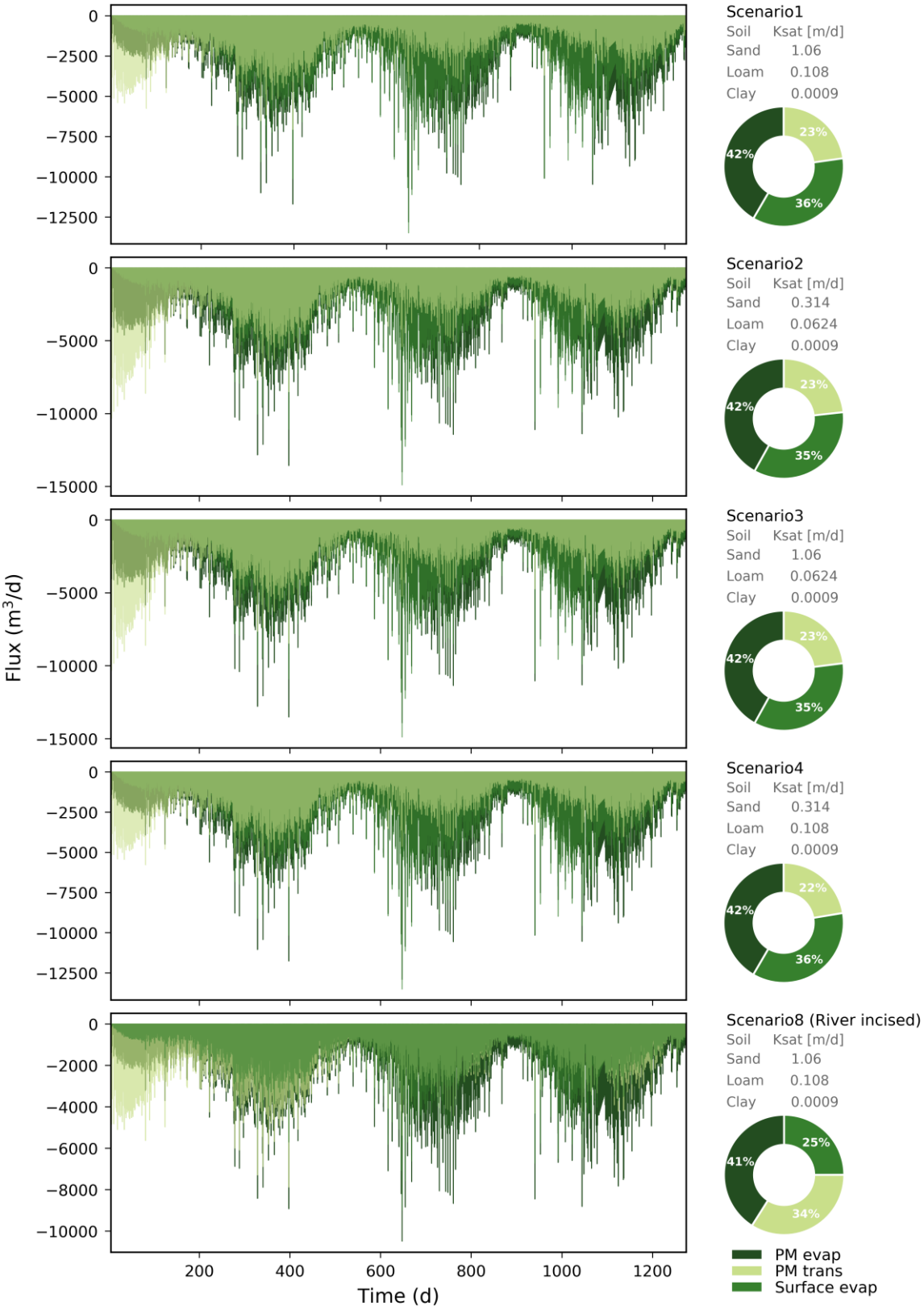

Figure 0.8 Simulated ET components for each scenario. The pie chart shows the breakdown of the proportional contribution in percentage of each ET component.

1.18.2 Hydrographs and Observation Well Results

From the 33 hydrograph nodes distributed across the catchment, streamflow was only simulated at the outlet nodes in all the scenarios (Figure 3.9). The simulated flow response was comparable across all scenarios with only slight differences mostly on the magnitude. Similarly to the water balance results, the hydrographs were practically identical among scenarios 1, 4 and 8, and between scenarios 2 and 3 (Figure 0.10). For scenarios 1, 4 and 8, flow started at simulation day 38 and for scenarios 2 and 3 at day 33. For neither of the scenarios, the transition to streamflow was explained by a rainfall event, since the preceding last precipitation occurred around simulation day 12 and the observed streamflow (at the closest stream gauge to the simulated outlet) occurred around day 195. Besides the wrong timing of the simulated flow versus the observed flow, the magnitude of the simulated flows was two orders of magnitude less than the observed flows. The simulated flows at the outlet were so small that they could be considered sheet flow rather than streamflow (max rates $\approx 0.0138 m^3/s$). Moreover, once flow was simulated at the outlet it continued to flow throughout the rest of the simulation in all the scenarios.

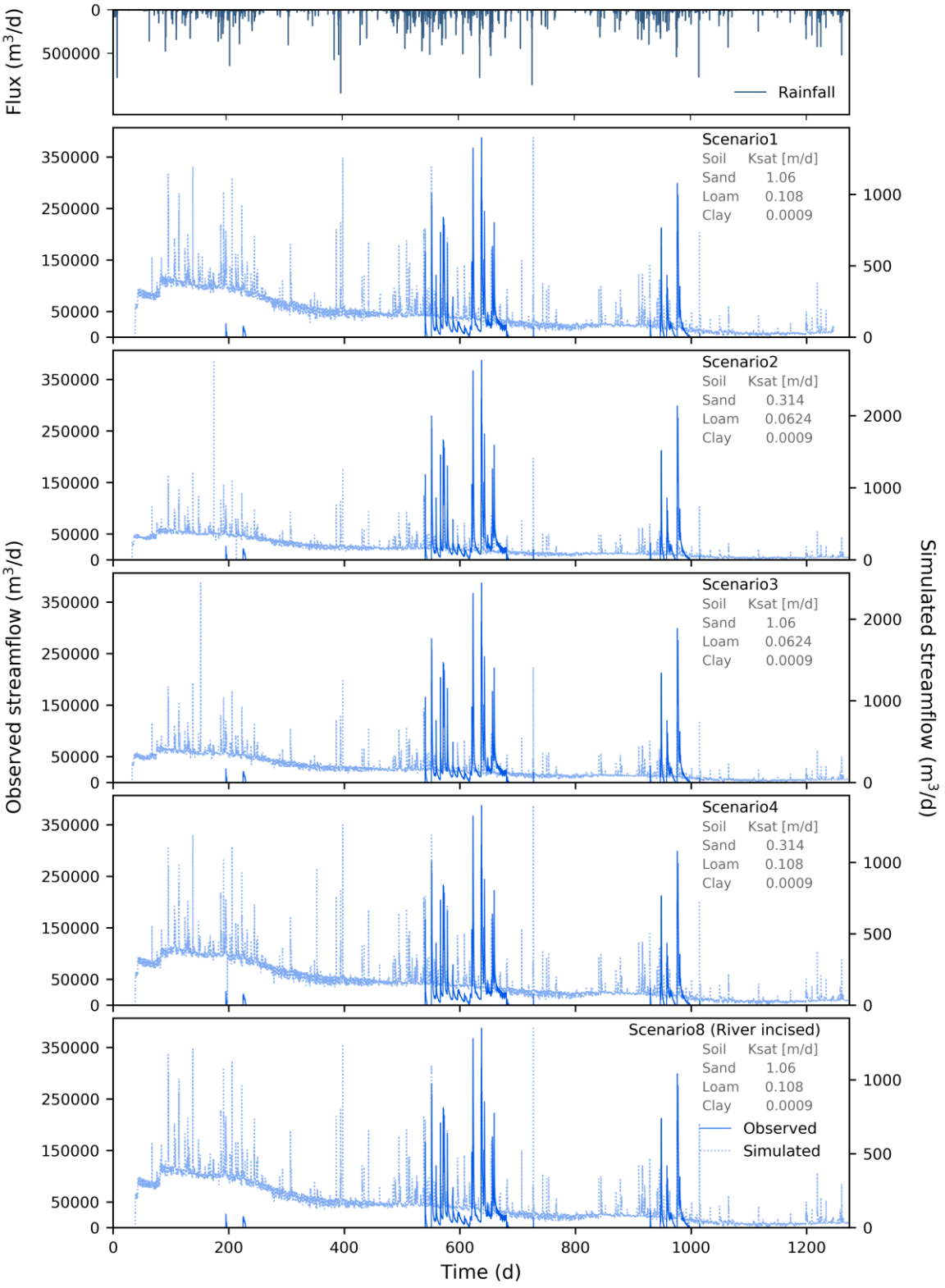

Figure 0.9 Catchment's outlet hydrograph for all scenarios showing the simulated flow versus the observed flow from the closest nearby gauging station.

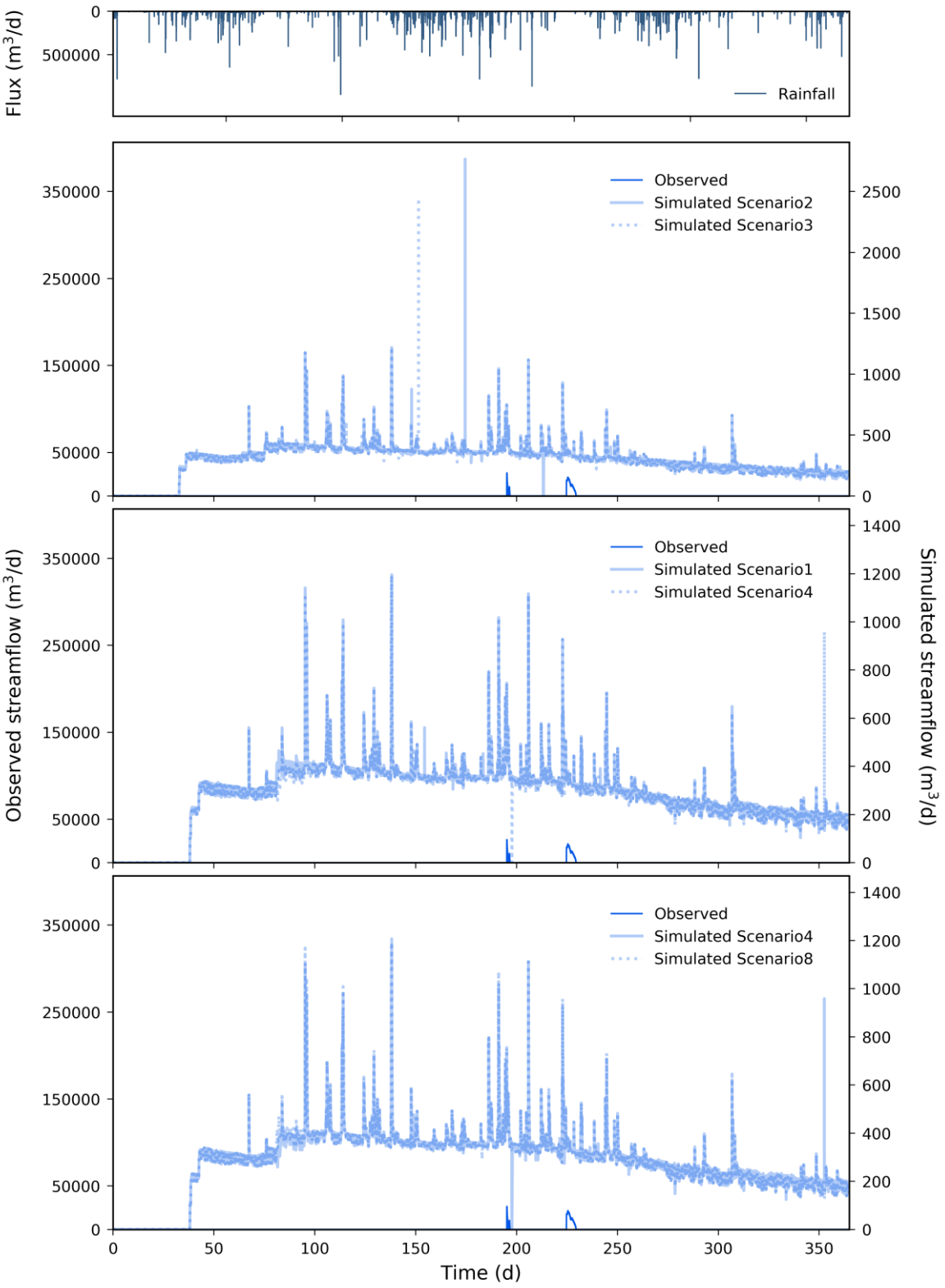

Figure 0.10 Catchment's outlet hydrograph zoomed to show the simulated flow similarities between the scenarios.

With the exception of wells 9, 11 and 12, all wells presented either a gradually-continuous upward or downward trend. Rising heads were simulated for wells 1, 2, 4, 5, 6, 7(scenario 8), 8, 9, 10, and 11 with head increases ranging from 7.3 to 0.33 m with an average of 2.5 m. Decreasing heads were simulated for wells 3 and 7 (scenarios 1-4) with an average head decrease of 0.7 m ranging from 0.2 to 5.9 m. A seasonal response to precipitation was simulated only on wells 9 and 11 and well 12 stayed constant during the simulation. In general, the response was similar among scenarios in most wells. Except for well 1, the simulated GW heads were practically identical for scenarios 1-4 (± 0.01-0.15 m) while heads for scenario 8 show larger differences for wells 1, 2, 3 and 7. GW heads were simulated to rise above the surface elevation only at the location of well 1.

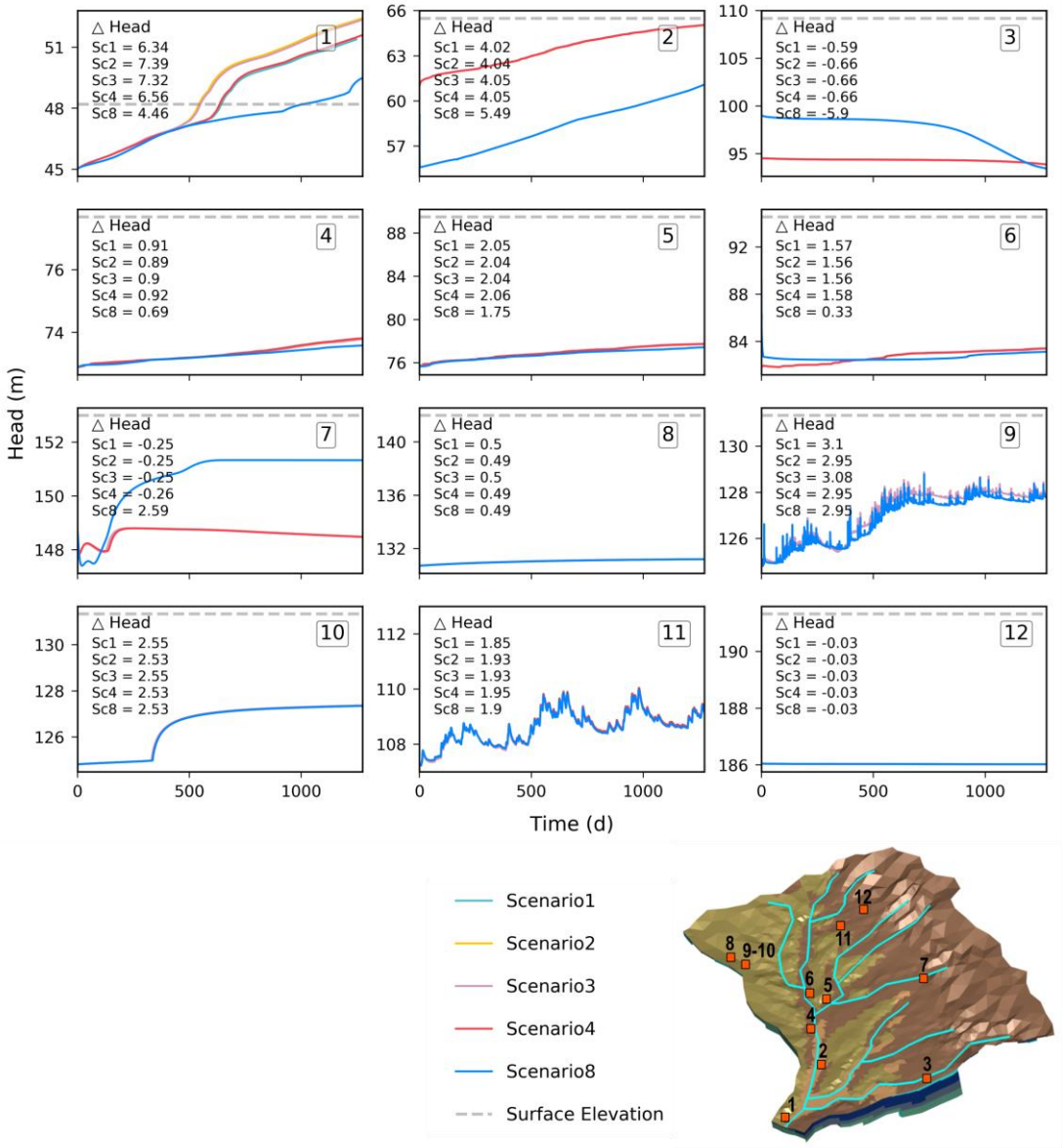

Figure 0.11 Simulated GW head elevations for all the different scenarios. The surface elevation for each location is depicted by the grey dashed line. Location of the observation wells is shown in the map insert.

1.18.3 Active Areas and Simulated Dominant Flow Generation Processes

The development of active areas (initiation of flow) in terms of the timing and extent was similar among scenarios 1-4, while for scenario 8 (scenario with the incised stream nodes) the aerial extent was consistently smaller. Across all scenarios, flow was generated first on areas from the steep hills and these areas expanded and contracted throughout the simulation. Fragmented active areas developed along the stream network for scenario 8 while for scenarios 1-4, the

active areas along the stream develop as a result of the flow from the hills connecting to stream network and expanding from there. Although the overall active areas along the river were larger for scenarios 1-4, a larger length of the stream network showed flow for scenario 8.

The development of active areas across scenarios matched the areas where the shallow soil profile reached saturation. The dominant flow generation mechanism on most of the steep hills shifted from IE-OF from the loam soil in the hill slopes during precipitation events to pre-event GW afterwards. A few small areas on the steep hills also showed unsat-IF as the dominant mechanism. In the area near the outlet the flow generation mechanisms during precipitation events included IE-OF from the clay hillslopes, in-stream unsat-IF, and pre-event GW. After precipitation events, pre-event GW was prevalent in the areas near the outlet. Flow was simulated mostly through unsat-IF in a few areas along the stream network in the mild-sandy hills.

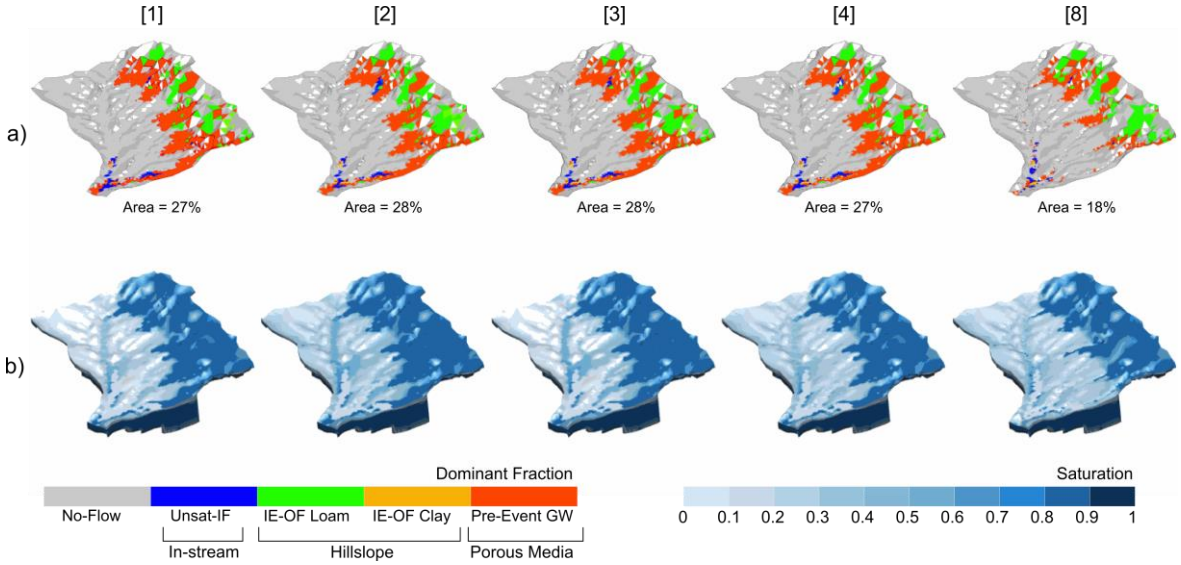

Figure 0.12 Snapshots of time step 960 during a rainfall event showing (a) the spatial extent of active areas by their dominant HMC component (flow generation mechanism) and (b) the porous media saturation for each scenario (1-4 and 8). The spatial extent of active areas as a percentage of the catchment area is shown below the snapshots. Colours for the HMC components show both the dominant process and the origin of the water contributing to the flow in each cell. For example, all red areas are from Pre-event GW some of which can contribute to active areas in both the stream and in the stream banks.

1.19 Discussion

The goals of this chapter were to provide insight into streamflow generation processes for an intermittent Mediterranean-climate catchment under a similar approach to prior theoretical models. The key consideration for this study, therefore, was to try to replicate the approach of small and simplified theoretical models for a real catchment, with the aim of understanding processes rather than matching observations and to evaluate how well previous findings translate to a larger and more complex model setup. For this, we developed a conceptual framework based on lessons learnt from previous studies (in particular from Gutierrez-Jurado et al. [2019]), on historical observations of streamflow and GW heads, and all the available information of the catchment characteristics such as slope, the spatial distribution and characteristics of shallow soils, and the local geohydrology. Overall, the conceptualization of the hydrological processes leading to distinct flow generation mechanisms across the catchment relied mostly on the vertical and longitudinal heterogeneity of the shallow soils, on the catchment topography and to a lesser degree on SW-GW interactions (for the area near the outlet). The conceptual model identified three distinct subregions within the catchment and proposed likely flow generation mechanisms within those subregions. The steep hills are characterised by permeable shallow loam soils, steep slopes and deep GW heads which would result in Sat-IF and SE-OF. The undulating hills are characterised by high permeable deep sandy soils, mild slopes and deep GW heads which would result in unsat-IF. The flat valley consisted of a mix of the previous soils with the addition of a clay area all located in low-gradient terrain and with areas of shallow GW heads towards the outlet which would result in a mix of flow generation processes.

Because of the lack of information of the soil hydraulic properties, and soil properties also tend to have high heterogeneity, we tested 4 scenarios with different values that are within the ranges found in the literature and which were validated by estimates from the ROSETTA model for each soil type. Additionally, we tested 4

A final set of 8 models comprising 4 scenarios testing different sets of soil hydraulic properties for the shallow soils and 4 scenarios testing different values for incising the stream nodes were tested. Results among the tested scenarios, however, showed only small disagreements which were driven by the hydraulic properties of the loam soil since the scenarios with identical

responses (2&3 and 1&4) shared the same loam but different sand hydraulic properties. The loam's smaller hydraulic conductivity for scenarios 2&3 (0.0624 m^3/d) limited infiltration which translated to more OLF while at the same time the higher water holding capacity in the loam areas, might have slow down subsurface flows to either exfiltrate to the surface or to contribute to the FT. In contrast, the tested values for the sand resulted in a low water holding capacity that allowed the incoming precipitation to drain past the root zone and move in the subsurface contributing to the FT. This is supported by the higher FT values shown for scenarios 1&4. Similarly, the development and extent of active areas and the dominant flow generation mechanisms were also practically identical for scenarios 1-4. This overall similar responses among scenarios 1-4 was unexpected, given that the role of soil heterogeneity on different streamflow generation processes has been documented in previous studies. For instance, studies have shown that vertical soil heterogeneity can result in the development of perched saturated zones that contribute to flow generation (Hathaway et al., 2002; Maxwell and Kollet, 2008). Other studies indicated that horizontal heterogeneity contributed to the spatio-temporal variability of flow generation under different mechanisms which overall resulted in longer flow durations due to delays in runoff occurring from areas with high infiltration capacities (Ebel et al., 2016; Luce & Cundy, 1994; Smith & Hebbert, 1979).

The major differences were simulated between the set of scenarios 1-4 (no incised stream) and scenario 8 (incised stream). The lack of stream definition resulted on larger OLF component, a smaller ET component and smaller active areas for scenario for scenario 8. The roles of a good channel representation in ISSHMs is extensively discussed by Käser et al. (2014). While their discussion of channel representation revolves on the ability of ISSHMs to quantify GW-stream interactions (which was not a major component for this model), the hydrological principles are relevant and transferable to explain the importance of channel representation to capture streamflow generation processes. An important consideration for the channel representation in streamflow generation studies for IRES is the relationship of flow and the wetted area. The larger the channel (both vertically and horizontally) the larger the area of exchange to the unsaturated zones during a flow event (Doble et al., 2012), which would be exacerbated under low flows (Käser et al., 2014). This is particularly significant when evaluating streamflow generation for IRES where high streambed infiltration and transmission losses are common (Gutierrez-Jurado et al., 2019; Levick et al., 2008; Shanafield & Cook, 2014; Snelder et al., 2013)

and often prevent flows from even reaching the catchment outlet as documented on the works of Keppel and Renard (1962) and Aldridge (1970). For the scenarios 1-4 (no incised stream), we observed that without a defined stream to 'channel' the water, the little overland flow that was simulated (water depth was barely larger than the rill storage) spread over a larger area than in scenario 8 which had the stream incised (Figure 3.11). The same was true for the patterns of increased saturation of the PM across the catchment. Results from the water balance reflected the effects of having both flows and PM saturation spread over larger areas by exacerbating ET and decreasing the overall amount of overland flow for scenarios 1-4. This is consistent with the remarks by Käser et al. (2014) regarding the likely impacts to the water flow budget by the spatio-temporal aspects linked to channel representation due to spatial exchange patterns.

Importantly however, our results support our conceptual understanding of the flow generating processes in Pedler Creek. Results from the active areas showed distinct mechanism developing in the three major areas supporting the idea that there is a spatial variation of flow generation processes in Pedler Creek. In the model, flow developed first at the steep hills areas (fast-flow) and the dominant mechanism was SE-OF with a few areas showing unsat-IF as hypothesized in our conceptual model (Figures 3.4b and 3.12). An unexpected development was the contribution of pre-event GW during flow recessions. In this area the pre-event GW was likely to be pre-event soil water since the wells located in the hills (7 and 12) had GW heads that did not rise to intersect land surface (Figure 3.11). The flows generated in the valley near the outlet were similarly simulated via the conceptualized mechanisms (Figures 3.4d and 3.12). We saw small areas with flow originating from IE-OF from the clay areas, and a combination of unsat-IF and pre-event GW for the rest of the active areas in this region. The GW heads rising above the surface elevation in well 1 supported the GW contribution to flow in this area. Finally, in the few small areas close to the sandy mild hills, flow was simulated through the unsat-IF mechanism as predicted in our conceptual framework.

These results support the findings by Gutierrez-Jurado et al. (2019) who suggested that soil properties largely dictate the dominant flow generation mechanisms. Yet, our lack of simulated streamflow from the different hydrograph node-sets did not allow us to evaluate the hypothesis that different mechanisms dominate different parts of the hydrograph response at different locations across the catchment. We attributed streamflow being simulated only at the outlet to

the loss of channel representation and the coarseness of the riverine elements. Without a defined channel the connection to the floodplain was lost and the shallow sheet-flow and most of the precipitation infiltrated and stayed within the porous media. The importance of the connection of the floodplain to the channel is discussed by Käser et al. (2014), as he argued that not only is the channel topography important but also its connection to the floodplain given that riverbank geometry is key for bank storage and overbank flooding. While overbank flooding is not considered important for this study (flows in Pedler only rarely will experience overbank flooding), the stream-floodplain connectivity and bank storage were key aspects under our model conceptualization. Namely, the predicted dominant mechanisms relied upon either the saturation to build up on along the riverine zone in the loamy areas which would lead to saturation excess overland flow; and we expected a perched groundwater developing on the sandy hillslopes which would, after intersecting the stream, contribute with interflow into the stream. While we observed these processes developed, they only occurred briefly as very shallow runoff.

1.19.1 Main Challenges

The large computational time to run the simulations was the major restraint we encountered since the early preliminary stages of this study. During the preliminary simulations, we started with an ambitious model setup consisting of a finer mesh and quarterly-hour model inputs. However, while trying to obtain the PM initial conditions by draining the model, we saw a very slow model convergence (simulations running for over 10 days only got to day ≈100 of the simulation). We decided to relax the mesh and we were able to get a set of initial conditions after testing over 37 scenarios.

During the first set of scenarios running for the full 4-year simulation, we observed that the simulation convergence consistently slowed down when the simulation encounter a precipitation input (Appendix L) and particularly during prolonged precipitation events (i.e. consecutive precipitation inputs). We tried implementing different input times (daily and hourly) and while we observed a slight improvement for the hourly time scale, the slow convergence prevailed (simulations times ranged between 17-30 days). We attributed the slow model convergence, particularly during precipitation inputs, to the model struggling to solve the highly non-linear equations for unsaturated flow in a complete unsaturated surface domain. Overall,

the slow model convergence had a significant impact on our ability to develop and test further model scenarios in the iterative processes of trial and error common for complex integrated models.

Furthermore, the importance of the topography, which was a major component on our model conceptualization, was largely affected after we were forced to relax the mesh discretization. Although the general characteristics of the elevation difference for the valley and the hills were preserved, the representation of the stream channel was completely lost and our attempt to lower the stream nodes probe ineffective given the coarseness of the stream elements. At the end, by completely losing the channel representation, we lost the ability for those processes to develop as streamflow which we believe was the major pitfall that explains our lack of streamflow results.

As stated before, GW-stream interactions were conceptualized to occur only near the catchment outlet (and likely only during certain 'wet' years) and therefore were not the focus of this study. However, as mentioned by Snelder et al. (2013) flow intermittence in many rivers can be attributed to a water table fluctuation relative to the stream channel elevation. In such catchments, a good representation of the stream and the initial GW heads would be paramount to capture flow intermittency (i.e. flow generation and flow recession). Estimating the initial GW heads for a multi-aquifer system proved to be an intensive and challenging task. Our first approach was to use all available information from shallow wells (0-30 m deep) in the area to create a GW elevation raster. While we found almost 50 wells suitable to use in our analysis (from analysing around 400 wells as shown in Appendix J), due to the spatial distribution of the observations (mostly skewed north of the catchment) we considered the resulting raster would not be reliable. In most transient ISSHMs the standard to obtain the initial conditions for both the porous media and the surface domain is to use the results from a steady-state model (Anderson et. al., 2015). Under this approach, the steady-state is achieved by matching observed base flows at the catchment outlet which is not possible when modelling IRES. In a variation of this approach, we tried to obtain the initial conditions by draining an initially saturated model until we could match the simulated GW heads with the average GW head elevation from the shallow observation wells. While at the end we were able to reasonably match most of the wells in the valley, the wells close to the hills were difficult to match. Moreover, it is important to

recognize that extensive shallow well information is not likely to exist in most IRES systems particularly at the catchment scale.

1.19.2 Future Work

From the lessons learnt in this study, we recognise several key points that would aid in future ISSHM modelling studies addressing streamflow generation modelling in IRES. Firstly, reducing the computational times should not be achieved by compromising the topography representation, particularly the channel representation. In our case, this could have been attempted in a few ways which are discussed below.

By rethinking our conceptual model, most of the streamflow generation processes were hypothesized to develop on the shallow soil profile and the GW contribution to streamflow was expected to be small and limited to a lesser portion of the catchment (near the outlet). We could, therefore, have model only the shallow soils using the clay layer as the no-flow boundary condition. Only including the shallow soils would have had a massive impact since it would eliminate over two-thirds of the PM layers on the sandy areas and almost three-quarters on the loam areas (leaving only 9 and 4 layers out of 28 respectively). This setup would have reduced the number of elements vertically, without compromising the 2D mesh discretization. Another possible modification to reduce the number of nodes without compromising the channel representation would have been to simplify the representation of the stream network (i.e. included fewer stream branches). While we wanted to capture streamflow generation processes across all stream orders, we could have simplified the stream network to include only a few strategic branches into the mesh discretization.

A different approach altogether could have been to model smaller representative sub-catchments for the three areas of our conceptual model (the steep hills, the undulating hill, and the valley). This would have allowed us to explore the processes contributing to flow in each area which was the core proposition on our conceptual model. The benefits of having smaller model domains not only relates to the ability to use a finer discretization but also by dramatically reducing the computational effort, more scenarios could have been tested. The ability to run more scenarios would have been particularly important to test a larger range of soil hydraulic properties. Although we have previously discussed the pitfalls of limiting IRES modelling to small plots or headwater catchments, we argue that we could use smaller sub-catchments to test

our parameterization and the principles of the proposed conceptual model. Results from this approach could inform the parameterization of a larger catchment and modifications to the conceptual model.

1.20 Conclusion

A physically-based ISSHM for a medium-size Mediterranean-climate catchment with IRES was developed to test how streamflow generation concepts and theories from smaller and simplified models would apply in a real catchment. The focus of this study was to develop a conceptual understanding of the processes and thresholds of streamflow generation rather than to match observations. We aim to unravel how different processes developed across the catchment and how their interaction could explain the integrated catchment response. A conceptual model for Pedler Creek was developed and used to inform the parameterization of the numerical model. The two core aspects of our conceptual model were the effects of soil heterogeneity (both vertically and horizontally) and the catchment topography to hypothesize streamflow generation processes. The simulated flow generation mechanisms were in overall agreement with our conceptual understanding of the spatial flow generating processes in Pedler Creek. However, the simulated flows did not translate into streamflow due to problems with the channel representation. From our results we have highlighted important insights into the pitfalls and challenges of using ISSHMs to model streamflow generation for IRES at the catchment scale. Overall, the large computational time was the main challenge for this study as we experienced very slow model convergence, particularly during the precipitation inputs. After exhausting all options to reduce improve convergence, we resorted to relax the 2D mesh which caused the loss of the channel topographic representation. The loss of channel representation led to a disconnection of the stream with the floodplain which resulted in only runoff and not streamflow being simulated. Our results highlight the importance of preserving channel representation to model streamflow generation on IRES. We propose that in future modelling efforts the nodal relaxation (to reduce the computation time) could be achieved by simplifying the vertical representation instead of the 2D mesh. However, this would only work for IRES were the GW is not a major contributor to streamflow generation. Another alternative to overcome slow convergence is to break down the catchment into smaller representative areas which can be informed by the catchment's conceptual model. The smaller models could be used

during the preliminary simulations to test the validity of the conceptual processes and to find optimal surface-subsurface parameters that could be later implemented to a catchment scale model. Results on capturing the dominant flow processes are promising and provide an important insight of flow in IRES. This study is an initial step towards understanding flow generation processes at the catchment scale and providing insight on the challenges of implementing ISSHMs for process understanding in IRES. Future work should build upon the lessons learned from this study.

.

Chapter 4

Testing and Advancing a New Methodology to Capture Intermittent Streamflow from Streambed Temperature Data.

1.21 Introduction

Non-perennial streams are defined as waterways that alternate between dry and wet states (Assendelft & van Meerveld, 2019). Although flow regimes classification can be complex (Costigan et al. 2017; Kennard et. al 2010), non-perennial streams are typically grouped into intermittent rivers and ephemeral streams (IRES). Intermittent streams are characterized by long (often seasonal) flowing phases, while ephemeral streams present sporadic flows that occur in direct response to extreme precipitation events. IRES constitute over half of the global river network, contribute with half of the total river discharge and are found across all landscapes and climates (Costigan et al. 2016; Datry et al. 2014; McDonough et al. 2011; Sheldon et al. 2010). For arid and semi-arid regions, including those in Mediterranean climates, IRES dominate the landscape and are often the only source of surface water. For instance, they account for over 70% of the streams in Australia (Sheldon et al., 2010), over 80% of the stream network in the Southwest USA (Levick et al., 2008), and they encompass a higher proportion of the river length in Mediterranean basins in Europe (Stubbington et al., 2018). Moreover, in the last 50 years, most of the formerly perennial rivers in arid and semiarid regions have become intermittent, including some major rivers such as the Nile in Africa, the Yellow in Asia, and the Rio Grande bordering the US and Mexico (Datry et al., 2014). With projected climate shifts and the increasing demand on water supply, more perennial rivers are likely to become intermittent (Costigan et al., 2016; Datry et al., 2014; Larned et al., 2010; McDonough et al., 2011). Besides their widespread distribution, IRES are important for biotic communities, the transport of nutrients and organic matter processing, groundwater replenishment, and in most arid and semi-arid regions they support the local population livelihood (Lange, 1998; Seely et al., 2003).

Increasing awareness of their importance and their vulnerability to climate change has been at the centre of a surge of research on IRES over the past decades (Assendelft & van Meerveld, 2019). However, the bulk of these studies have been done under the scope of ecological and biological research (Acuña et al., 2014; Bond & Cottingham, 2008; Costigan et al., 2016; Datry et al., 2016, 2014; Kennard et al., 2010; Larned et al., 2010; Skoulikidis et al., 2017; Steward et al., 2012; Stubbington et al., 2018) and important knowledge gaps of the hydrological functioning of IRES remain. Among the biggest limitations for hydrological studies in IRES is the unpredictable and variable nature of flow and the often-difficult access to the remote areas where they are found. Historically, these limitations have resulted on the lack of long-term-spatially-distributed streamflow observations for IRES as they are often located on ungauged basins (Fekete & Vörösmarty, 2002; Poff, Bledsoe, & Cuhaciyan, 2006; Tzoraki & Nikolaidis, 2007). As a result, many studies on IRES have derived from research of perennial streams which contain intermittent or ephemeral sections common in small mountainous headwater catchments in temperate-humid climates. The majority of these studies have therefore focused on understanding streamflow dynamics on IRES from the expansion and contraction of the drainage network (Durighetto et al., 2020; Goulsbra et al., 2014; Prancevic & Kirchner, 2019; Ward et al., 2018; Whiting & Godsey, 2016; Wigington et al., 2005; Zimmer & McGlynn, 2017). These studies have provided important insight to the role of geological attributes (Durighetto et al., 2020; Ward et al., 2018), topography (Prancevic & Kirchner, 2019) and water table depth (Goulsbra et al., 2014; Zimmer & McGlynn, 2017) on the unsaturated storage dynamics that affect streamflow/runoff generation and stream network dynamics (Gutierrez-Jurado et al., 2019; Mirus & Loague, 2013; Smith & Hebbert, 1983; Vanderkwaak & Loague, 2001; Whiting & Godsey, 2016). However, in many arid-semiarid- catchments, IRES do not originate from the expansion of an already flowing stream but rather develop from completely dry stream network sections. Under these conditions, the development of flow generating areas at the catchment scale occur fragmented across the stream network resulting in highly variable flow patterns. Arguably one of the most important gaps in the understanding of the hydrology of these arid-semiarid IRES is how they transition from dry to flowing and back to dry (i.e. onset and cessation of flow) and the streamflow processes associated with these transitions (Costigan et al., 2016, 2017; Gutiérrez-Jurado et al., 2019; Shanafield et al. [in prep]).

To study streamflow generation and stream network dynamics of IRES at the catchment scale, a dense and spatially distributed monitoring network is paramount. The flashy and erosive flows in most IRES, coupled with the need for a high spatiotemporal resolution, hinder the use of traditional streamflow monitoring approaches such as stream gauges or pressure transduces in IRES (Assendelft & van Meerveld, 2019; Blasch et al., 2002; Constantz et al., 2001). To overcome these challenges and limitations, researchers have continued to develop and test low-cost streamflow monitoring alternatives including temperature sensors (Blasch et al., 2004; Constantz et al., 2001), electrical resistance sensors (Blasch et al., 2002; Jensen et al., 2019; Peirce & Lindsay, 2015), float switch sensors, and multi-sensor approaches (Assendelft & van Meerveld, 2019). While the use of electrical resistance sensors and multi-sensors approaches have become more common in recent years, temperature sensors remain widely used as they present certain advantages. First, temperature sensors are relatively inexpensive, do not require special modifications, and are broadly available off the shelf (Partington et al. [in-prep]). More importantly, their ruggedness and small size makes them better suited to withstand erosive flows and flows with high sediment and debris loads which are ubiquitous in most IRES.

The concept used to infer flow using streambed temperature was tested in the pioneer study from Constantz et al. (2001). Put simply, the specific heat of water is significantly greater than the specific heat of air (4:1 ratio), therefore, the diurnal temperature variation of a dry stream (i.e. air temperature at the streambed) is significantly larger than that of a stream with water (i.e. temperature of water in the stream) (Arismendi et al., 2017; Assendelft & van Meerveld, 2019; Blasch et al., 2004; Constantz et al., 2001). The dry-wet transitions in a temporary stream can be determined accordingly by identifying these changes in the streambed temperature signal (Figure 4.1).

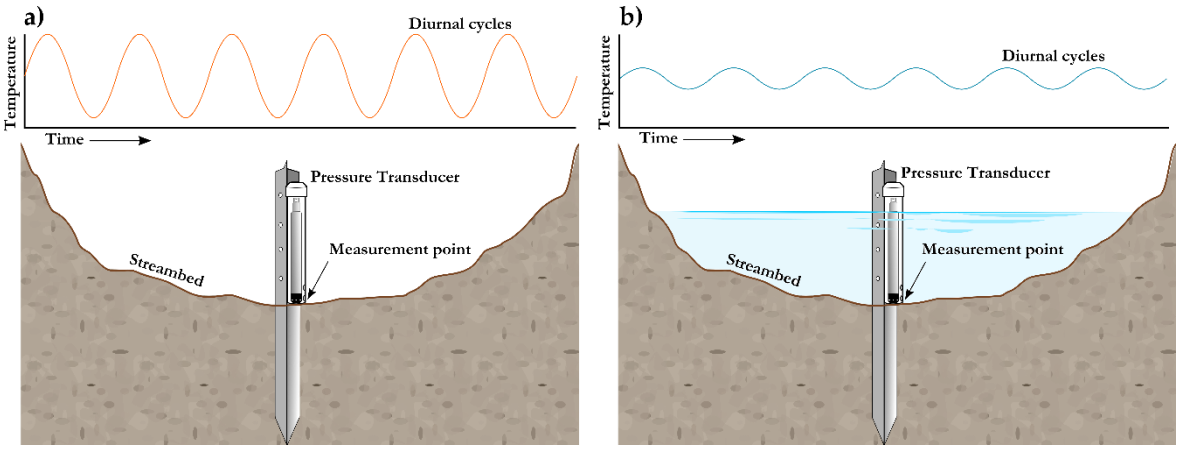

Figure 0.1 Conceptual model of the streambed diurnal temperature fluctuation for a dry (a) and a flowing stream (b)

While the concept is simple and has been successfully used in several studies to identify periods of flow on IRES, some challenges remain. For instance, most of the setups and data analysis methods require additional "benchmark" data/sensors (Arismendi et al., 2017; Assendelft & van Meerveld, 2019; Constantz et al., 2001), a calibration period (Assendelft & van Meerveld, 2019; Blasch et al., 2004; Gungle, 2006), the determination of subjective and site-specific (i.e. for each sensor) sets of parameters (Assendelft & van Meerveld, 2019; Blasch et al., 2004), and/or complicated installations that include burying the temperature sensors (Blasch et al., 2004; Constantz et al., 2001; Gungle, 2006). While in small-scale experiments these considerations might not be troublesome, they would hinder the implementation of such methods at the catchment scale.

In a recent study Partington et al. (in-prep) explored a series of alternative time series analysis methods that use only temperature time series data to predict flow. They compared six non-stationary time-frequency transforms methods and tested them in two synthetic and one field data example. The initial analysis showed good results for both the synthetic and field datasets with flow/no-flow matching predictions of over 90% for all methods. Although promising, it is common that temperature signals differ among sites due to stream micro-climates and/or setup conditions, and therefore the application of these methods to other field data sites are necessary to validate their performance results. More importantly, the application of any of these proposed new methods still requires guidelines to determine the flow/no-flow threshold (i.e. the change in the signal) which is necessary for identifying the flow/no-flow transitions.

In this chapter, we build on using signal processing to identify periods of flow in time series data (Partington et al., [in-prep]) by examining flow/no-flow thresholds at the catchment scale. The goal of this study is to test the applicability and performance of the method over a range of conditions typical of arid or semiarid, low-gradient catchments with IRES. Specifically, we use the continuous wavelet transform (CWT) method on a field dataset from a mid-size catchment with a temporary stream network. The dataset includes 27 monitoring sites with stream water level (SWL) and streambed temperature data, which span a three-year period and represent a variety of distinct flow conditions. The advantages of testing the method from a network of distinct sites across the catchment will allow us to expand the performance analysis from the individual overall matching metrics used by Partington et al. (in-prep) to include a spatial analysis of the performance of the method across the catchment. Additionally, we aim to develop a simple method to estimate the threshold needed to identify flow/no-flow periods which is possibly the most critical element missing for this method yet. The specific objectives of this study are to:

1. Test the performance of a manually selected flow threshold using the stream water level data.
2. Develop a repeatable, non-site specific technique to estimate an appropriate threshold using only the temperature data and evaluate how its performance compares with the best visually selected threshold from objective 1.
3. Expand the evaluation of the performance of the CWT method to include how well it can capture the spatiotemporal variability of flow across the catchment.

1.22 Methods

1.22.1 Study Site

Data from a sub-basin of Pedler Creek catchment, located within the larger Willunga basin roughly 30 km south of the city of Adelaide, South Australia (Figure 0.2) was chosen for this study. Pedler Creek has a catchment area of approximately 107 km^2 and a creek length of approximately 180 km, and the sub-basin encompass over 60% of the catchment (69 km^2) and over and 80% of the total length of the stream network. Although there are a few small, perennial reaches east of the Willunga fault, most of the creek behaves intermittently during the winter months and ephemerally during the rest of the year. The creek flows intermittently from

late-June/early-July throughout September in response to the winter rainy season and ephemeral flows are observed after extreme rainfall events during the rest of the year. Ephemeral events frequently precede the start of the intermittent flow across the catchment. For the context of this paper, we consider flows lasting 7 or more days as intermittent while events of less than 7 days were considered as ephemeral. The 7-day threshold was based on a rough estimate of the duration of spring and summer ephemeral flows from historical streamflow records in the catchment. Because the creek flows in response to the winter rains, streamflow permanence and stream discharge varies widely among seasons. The creek flows 33-199 days per year (on average 120 d yr^{-1}) and has a mean annual discharge of 3.88 x 10^6 m^3, with the higher flows occurring during the intermittent season (period of record 2000-2018 at gauge A5030543; AMLR, 2019). The catchment's mean annual precipitation is 550 mm, ranging widely from 300 to 800 mm and mean daily temperatures range from 37 to 5 °C (period of record 1900-2018 at station 232729; SILO - Australian Climate Data, 2019, Jeffrey et al., 2001).

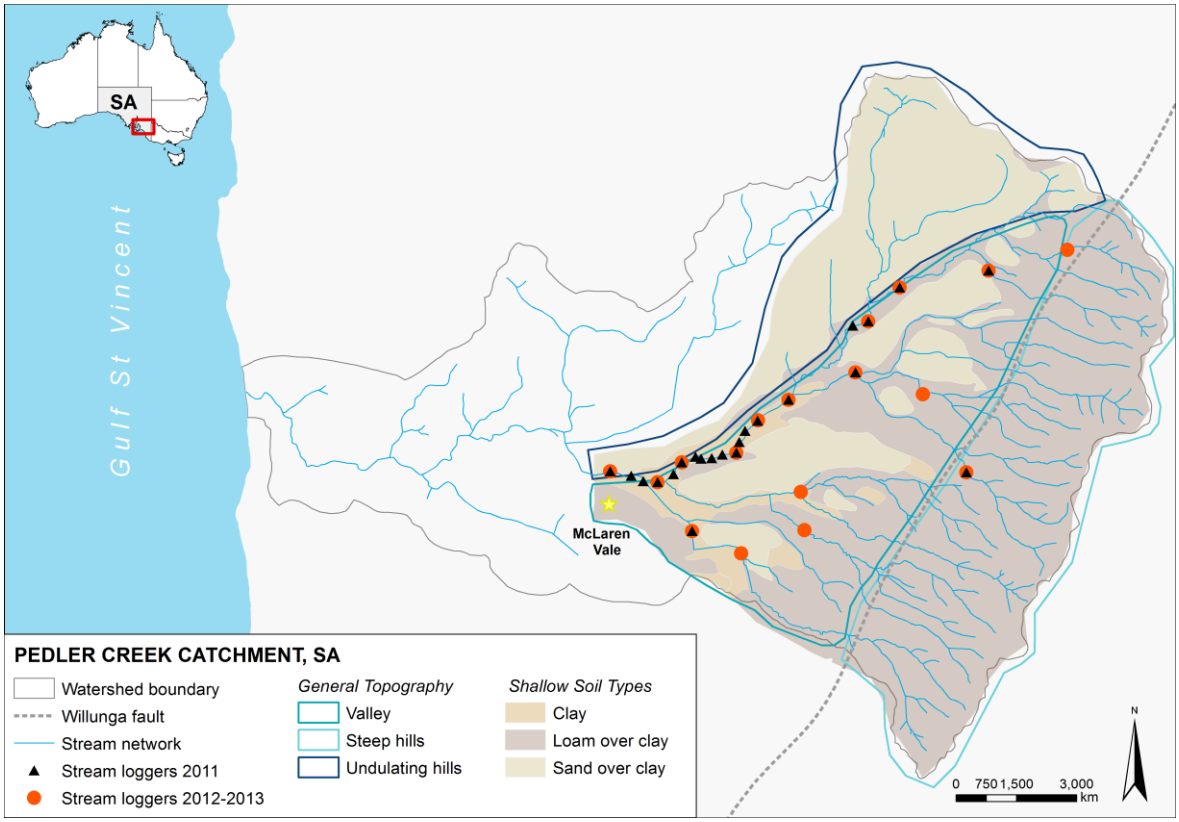

Figure 0.2 Location of the Pedler Creek Catchment showing the location of the stream loggers for 2011 and 2012-2013, the main topographic features, and the main shallow soil types within the subcatchment area.

The subcatchment has three main topographic characteristics: low-laying coastal plains which are surrounded by the mild, undulating hills to the north and the steep hills located east of the Willunga fault. The shallow soil types can be similarly grouped into three dominant soils: loam, sand, and clay. The loam soil is found in the coastal plains and throughout the steep hills which cover the majority of the catchment (≈62%). The sandy soils comprise roughly 30% of the catchment and are found throughout the mild, undulating hills, and on the coastal plains. The clay areas are found mostly in the downstream coastal plains where the three main stream branches converge. Vertically, the soils profiles also vary across the catchment, mostly along the lines of the topographic features. The hills east of the fracture are characterized by very shallow soils (≈0.5 m) underlain by bedrock, while the undulating hills have deep sandy profiles (≈1.5 m) underlain by heavy clay, and most of the coastal plain has a shallow profile (0.5 m) of either sand or loam underlain by a heavy clay layer. Towards the outlet a small area consists of clay soil profiles.

1.22.2 Field Methods

The Willunga Basin was designated in 2009 as one of the six long-term groundwater monitoring sites by the National Research Infrastructure for Australia (NCRIS) initiative. The infrastructure at the Willunga site was planned to tackle five main research areas, one of which was surface water-groundwater interactions between intermittent creeks and groundwater systems. As a result, a network of stream gauges, SWL monitoring sites and shallow piezometers were installed and instrumented across the Pedler Creek catchment. Due to the existence of a wastewater treatment plant in the town of McLaren Vale, the monitoring network was concentrated upstream from the town in the sub-basin area described in this chapter.

For this study, we used the data from the SWL monitoring sites from 2011-2013, which includes data of stream stage and streambed temperature (Figure 4.1). The stream stage (or water level) was used as a proxy of flow in this study. The number and distribution of the monitoring sites was determined by the research being conducted back during the early stages of the NCRIS Willunga monitoring site. A larger number of sensors were installed during 2011; however, they were mostly concentrated along a relatively short stretch of the main branch of Pedler Creek. In subsequent years (2012-2013), the density of sensors was reduced along the main branch, but new stream tributaries were instrumented to obtain a better spatial coverage of streamflow

across the catchment. In summary, we are using data for 22 sites from 2011, and for 17 sites from 2012-2013.

For each stream monitoring site a steel post was hammered into the streambed and a non-vented pressure transducer (In-Situ Level Troll 300) was secured to the post with the end of the logger (where the pressure and temperature are measured) at streambed level (Figure 4.1). The sensors measure pressure within a range of 30 psi (10.9 m) with an accuracy of ±0.2%, and temperature ranging from -20 to 80 °C with an accuracy of ±0.1° and a resolution of 0.01 C°. Two barometric loggers (In-Situ Baro TROLL) were installed at two nearby shallow piezometers to record the atmospheric pressure. The loggers (barometric and pressure transducers) were setup to record data at 30-min intervals. The pressure data from the stream loggers were corrected for atmospheric pressure fluctuations and a series of manual field measurements of water levels (≈10 per year) were used to validate the logger's SWL data. After an initial visual inspection, it was noted that some "noise" remained in the corrected signal as the readings did not go to 0 m (no water) for the times where the field observations recorded a dry stream. A correction factor was therefore calculated for each logger as the maximum value recorded during the day when the manual observation recorded no-flow. The SWL time series data was corrected by changing any value smaller than the correction factor to equal 0. Daily precipitation data (mm) for the McLaren Vale station 23876 for 2011-2013 were obtained from the SILO database (SILO- Australian Climate Data, 2019).

1.22.3 Continuous Wavelet Transform Method

Wavelet transforms are an alternative to Fourier transforms which allow for a range of basis functions to be used in wavelet analyses. The continuous wavelet transform (CWT) is a convolution of a data sequence (here, a time series of flow or temperature) with a set of functions generated by the mother wavelet, in this case a complex Morlet wavelet. CWT and similar wavelet methods allow for relatively easy analysis of time-localized oscillations, and have been used previously in hydrologic applications, where oscillations in time series data are commonly of interest (Partington et al., [in-prep]; Rhif et al., 2019; Sang et al., 2013). The CWT was selected from the signal processing methods tested by Partington et al. (in-prep) because it performed well among the signal processing methods examined, and holds significant advantages in terms of simplicity, low computational cost, and ease of implementation.

As observed by Partington et al. (in-prep), the scaleogram from the CWT showed distinct decreases in energy in the signal at the one cycle per day (1-cpd) frequency that matched the streamflow events. However, there was still some noise present in the transformed signal and therefore, the amplitude of the transformed temperature signal at 1-cpd was convoluted using a triangle function (hat function) with an integrand of 1 as the kernel and with a window of 500 samples. The resulting convoluted amplitude signal was subsequently used to infer streamflow occurrences. Assuming that all points within the time series were independent, points where the convoluted temperature amplitude (CTA) dropped below a given threshold were considered indicative of streamflow, whereas periods when the amplitude signal was above the threshold represented no-flow conditions. The procedures to determine the threshold are provided in the subsequent sections.

1.22.4 Flow/No-Flow Thresholds

The threshold determination process was split into two parts: (1) selecting a visual threshold using the SWL data, and (2) developing a procedure to estimate the threshold without knowledge of SWL. By taking advantage of the SWL data to select visual thresholds we expected to be able to detect repeating trends on the data to develop a systematic process to estimate the thresholds with only the input data and CWT results.

During the first attempt at selecting a visual threshold we observed that a single value for a number of multi-year datasets would match flow/no-flow periods for a given year but would over/under-estimate the matches for other years. Consequently, we decided to continue the remainder of the analysis (threshold selection/estimation and flow/no-flow prediction) for yearly datasets for each monitoring site. By analysing the time series datasets by year, we increased our sample size by more than double (from 27 time series to 56) which made our analysis and the evaluation of the method more robust.

1.22.4.1 Visually Selected Thresholds

The basic concept to select the threshold was to estimate a value that was consistently smaller than the CTA signal during periods of no-flow and that was greater during flow periods. Visually, this meant selecting a line where the CTA signal above the threshold captured no-flow periods and CTA signal below the line corresponded to flow periods.

Although the concept to visually select the threshold is straightforward, deciding on the "best" threshold was often subjective because improvements to match flow periods frequently resulted in some false positives (detecting no-flow times as flow) and vice versa. Similarly, matching the time of flow initiation was often mutually exclusive to matching the time of flow cessation, choosing values that favour one translated to match decreases for the other.

To try to minimize subjectivity in selecting the "best" threshold value we followed a simple series of steps. First, we identified and tested an initial threshold that basically captured most of the flow and no-flow periods. Subsequently, we tested the performance of thresholds 0.1 less and greater than the initial value (Tables 8-10). The performance of the all tested thresholds was evaluated using a set of flow/no-flow matching metrics that evaluated the total number of observations that were rightly classified as either flow or no-flow. The matching metrics are overall match percentage (OM), flow match percentage (FM), and no-flow match percentage (NFM). The matching metrics were calculated as follows:

$$OM = \left(\frac{matched\ flow\ observations + matched\ no\text{-}flow\ observations}{total\ number\ of\ observations}\right) \times 100 \quad \textbf{(4.1)}$$

$$FM = \left(\frac{matched\ flow\ observations}{total\ number\ of\ flow\ observations}\right) \times 100 \quad \textbf{(4.2)}$$

$$NFM = \left(\frac{matched\ no\text{-}flow\ observations}{total\ number\ of\ no\text{-}flow\ observations}\right) \times 100 \quad \textbf{(4.3)}$$

While these metrics allowed us to quantitatively evaluate the performance of each threshold, the challenge remained to select the "best" one. Knowing that frequently matching flows and no-flows were mutually exclusive, we could not use the FM or NFM. Moreover, because the number of no-flow observations is disproportionally larger than the number of flow observations using the OM would be biased towards matching no-flows. To overcome this we calculated a weighted matching metric as $WM = (FM \times 0.75) + (NFM \times 0.25)$ and followed a simple two-step final selection process. [1] We discarded the threshold that presented the worst overall performance (>OM) and [2] from the two remaining threshold values, we selected the one that had the best weighted performance (<WM). By following this simple two-step selection we were able to objectively select a threshold that would give preference to match flow observations (by choosing the best WM), while trying to minimize errors for the no-flow observations (by choosing from the two best OM).

Table 0.1 Visually selected thresholds and their corresponding flow/no-flow matching metric for 2011

2011 Sensor ID	------ Tested Visual Thresholds -----			---------- Flow/no-flow matching metrics for each Threshold ----------												Selected Threshold
	Threshold (- 0.1)	Threshold Initial	Threshold (+ 0.1)	Overall (- 0.1)	Overall Initial	Overall (+ 0.1)	Flow (- 0.1)	Flow Initial	Flow (+ 0.1)	NoFlow (- 0.1)	NoFlow Initial	NoFlow (+ 0.1)	Weighted (- 0.1)	Weighted Initial	Weighted (+0.1)	
1	0.6	0.7	0.8	71.83	75.77	70.96	48.30	58.75	67.99	96.92	93.91	74.12	60.45	67.54	69.53	0.7
2	2.9	3.0	3.1	75.84	74.61	73.37	39.65	41.29	42.48	92.07	89.56	87.22	52.76	53.36	53.66	3.0
3	1.0	1.1	1.2	73.19	70.66	66.48	16.47	26.35	31.51	87.58	81.90	75.35	34.25	40.24	42.47	1.1
5	0.97	1.07	1.17	97.42	96.34	92.25	94.03	95.12	96.43	97.74	96.45	91.85	94.96	95.45	95.29	1.07
6	0.7	0.8	0.9	75.56	74.87	71.32	49.94	55.42	61.36	92.89	88.03	78.05	60.68	63.57	65.54	0.8
7	1.1	1.2	1.3	74.97	71.94	66.40	27.29	30.42	32.42	90.71	85.64	77.61	43.15	44.22	43.72	1.2
8	1.9	2.0	2.1	80.06	79.63	78.63	37.62	39.39	41.00	91.29	90.28	88.59	51.03	52.11	52.90	2.0
9	1.4	1.5	1.6	64.41	67.09	68.52	47.85	55.33	61.65	95.57	89.22	81.45	59.78	63.80	66.60	1.6
10	0.9	1.0	1.1	80.38	80.54	77.83	53.66	56.43	58.88	97.43	95.92	89.93	64.60	66.31	66.64	1.0
11	0.8	0.9	1.0	80.54	80.61	79.39	28.39	30.10	34.56	96.70	96.26	93.28	45.46	46.64	49.24	0.9
12	1.2	1.3	1.4	97.81	97.34	96.52	97.93	99.31	99.88	97.69	95.59	93.52	97.87	98.38	98.29	1.3
13	2.5	2.6	2.7	89.52	89.46	89.15	91.11	92.34	93.01	86.74	84.39	82.36	90.01	90.36	90.35	2.6
14	1.0	1.1	1.2	99.55	99.24	98.96	58.17	59.48	59.48	100.00	99.67	99.39	68.63	69.53	69.46	1.1
15	1.0	1.1	1.2	91.29	89.94	84.47	65.08	78.58	80.29	93.52	90.91	84.83	72.19	81.66	81.42	1.1
17	1.0	1.1	1.2	85.75	87.24	81.79	49.08	62.79	66.42	97.05	94.77	86.53	61.07	70.79	71.45	1.1
19	1.3	1.4	1.5	91.38	91.57	91.60	52.94	58.72	63.91	98.23	97.42	96.53	64.26	68.40	72.07	1.5
20	3.2	3.3	3.4	63.26	64.06	64.32	53.77	55.40	57.07	78.97	78.39	76.31	60.07	61.15	61.88	3.4
21	0.9	1.0	1.1	95.12	94.75	94.30	94.54	95.00	95.35	96.09	94.35	92.58	94.93	94.83	94.66	0.9
23	0.9	1.0	1.1	93.27	92.37	89.85	87.18	88.70	90.22	94.23	92.95	89.79	88.94	89.76	90.11	1.0
24	2.3	2.4	2.5	84.64	86.13	85.63	69.71	74.63	76.34	95.49	94.49	92.38	76.16	79.60	80.35	2.5
26	0.8	0.9	1.0	94.60	95.05	94.91	73.31	78.84	82.67	98.59	98.09	97.20	79.63	83.66	86.30	1.0
27	0.8	0.9	1.0	89.30	87.39	85.19	79.78	85.52	87.33	93.65	88.25	84.22	83.25	86.20	86.55	0.9
mean	1.40	1.45	1.57	82.89	82.89	81.10	58.41	62.56	64.58	92.89	90.91	86.80	67.02	69.65	70.18	1.46
max	3.3	3.3	3.4	99.55	99.24	99.55	99.31	99.31	99.88	100.00	99.67	100.00	98.38	98.38	98.38	3.4
min	0.6	0.7	0.6	63.26	64.06	63.26	16.47	26.35	16.47	78.39	78.39	74.12	34.25	40.24	34.25	0.7

Note: The two best performances from the overall matching metric are highlighted in blue and the selection is mirrored for the weighted matching metric. The greater performance from the highlighted weighted values is underlined and represents the final selected threshold.

Table 0.2 Visually selected thresholds and their corresponding flow/no-flow matching metrics for 2012

2012 Sensor ID	------ Tested Visual Thresholds ------			---------- Flow/no-flow matching metrics for each Threshold ----------												Selected Threshold
	Threshold (- 0.1)	Threshold Initial	Threshold (+ 0.1)	Overall (- 0.1)	Overall Initial	Overall (+ 0.1)	Flow (- 0.1)	Flow Initial	Flow (+ 0.1)	NoFlow (- 0.1)	NoFlow Initial	NoFlow (+ 0.1)	Weighted (- 0.1)	Weighted Initial	Weighted (+0.1)	
2	0.9	1.0	1.1	93.47	90.07	82.48	94.75	97.00	99.03	93.17	88.48	78.67	94.36	94.87	93.94	1.0
3	0.9	1.0	1.1	96.86	94.68	91.15	92.75	97.56	99.34	97.83	94.00	89.21	94.02	96.67	96.81	1.0
4	0.9	1.0	1.1	94.62	93.98	91.84	83.70	84.65	86.11	99.04	97.76	94.17	87.53	87.92	88.12	1.0
5	0.98	1.08	1.18	98.10	98.89	98.84	93.50	97.11	97.98	99.71	99.51	99.14	95.05	97.71	98.27	1.18
6	0.7	0.8	0.9	95.35	92.50	85.20	90.10	96.42	98.34	98.10	90.46	78.33	92.10	94.93	93.34	0.8
7	1.2	1.3	1.4	87.22	83.55	77.87	58.47	65.42	68.90	92.56	86.92	79.54	66.99	70.80	71.56	1.3
8	1.6	1.7	1.8	96.94	96.98	96.41	91.78	93.74	93.95	98.81	98.15	97.30	93.54	94.84	94.79	1.7
9	2.0	2.1	2.2	91.60	93.01	92.55	91.25	94.91	94.94	91.89	91.46	90.62	91.41	94.05	93.86	2.1
10	0.9	1.0	1.1	98.13	97.96	96.52	94.89	98.25	98.83	99.89	97.80	95.27	96.14	98.14	97.94	1.0
11	0.6	0.7	0.8	96.87	97.44	97.29	87.76	90.66	91.86	100.00	99.77	99.16	90.82	92.94	93.69	0.8
12	1.3	1.4	1.5	99.07	98.54	97.72	98.19	98.67	98.90	99.69	98.45	96.87	98.56	98.61	98.39	1.4
17	1.0	1.1	1.2	98.27	98.21	97.26	94.57	96.10	96.73	99.51	98.92	97.43	95.81	96.80	96.91	1.1
20	1.9	2.0	2.1	96.25	96.31	96.17	91.22	91.86	92.87	98.83	98.59	97.86	93.12	93.54	94.12	2.0
28	1.2	1.3	1.4	94.17	93.12	90.32	94.03	94.03	97.75	94.20	92.93	88.78	94.07	93.76	95.51	1.2
29	1.1	1.2	1.3	96.86	96.42	95.13	94.73	96.03	97.93	97.69	96.57	94.04	95.47	96.16	96.96	1.2
30	1.1	1.2	1.3	86.01	85.80	85.58	76.64	81.75	85.57	91.48	88.16	85.59	80.35	83.35	85.57	1.2
31	1.3	1.4	1.5	97.98	96.87	94.09	95.58	97.72	99.17	98.60	96.65	92.77	96.33	97.45	97.57	1.4
mean	1.18	1.28	1.38	94.88	93.97	91.70	88.93	91.64	93.25	97.13	94.82	91.20	90.98	92.44	92.74	1.27
max	2.0	2.1	2.2	99.07	98.54	97.72	98.19	98.67	99.34	100.00	99.77	99.16	98.56	98.61	98.39	2.1
min	0.6	0.7	0.8	86.01	83.55	77.87	58.47	65.42	68.90	91.48	86.92	78.33	66.99	70.80	71.56	0.7

Note: The two best performances from the overall matching metric are highlighted in blue and the selection is mirrored for the weighted matching metric. The greater performance from the highlighted weighted values is underlined and represents the final selected threshold.

Table 0.3. Visually selected thresholds and their corresponding flow/no-flow matching metrics for 2013

2013 Sensor ID	------ Tested Visual Thresholds ------			---------- Flow/no-flow matching metrics for each Threshold ----------												Selected Threshold
	Threshold (- 0.1)	Threshold Initial	Threshold (+ 0.1)	Overall (- 0.1)	Overall Initial	Overall (+ 0.1)	Flow (- 0.1)	Flow Initial	Flow (+ 0.1)	NoFlow (- 0.1)	NoFlow Initial	NoFlow (+ 0.1)	Weighted (- 0.1)	Weighted Initial	Weighted (+0.1)	
2	2.4	2.5	2.6	94.07	94.05	93.70	87.74	90.32	90.95	96.58	95.54	94.80	89.95	91.62	91.91	2.5
3	0.8	0.9	1.0	92.29	88.92	85.73	81.35	87.65	92.01	93.63	89.08	84.96	84.42	88.01	90.25	0.9
4	0.9	1.0	1.1	88.36	82.63	78.89	94.08	95.16	96.50	86.68	78.95	73.71	92.23	91.11	90.81	0.9
5	1.0	1.1	1.2	96.54	95.84	94.82	94.80	98.30	98.62	97.42	94.59	92.88	95.45	97.38	97.19	1.1
6	0.5	0.6	0.7	93.23	90.22	84.41	86.21	88.68	90.74	96.10	90.85	81.82	88.68	89.23	88.51	0.6
7	1.1	1.2	1.3	88.26	86.18	84.15	67.50	82.40	92.30	90.84	86.65	83.13	73.34	83.47	90.01	1.2
8	1.3	1.4	1.5	94.01	94.60	93.33	89.72	93.75	94.20	95.51	94.89	93.02	91.17	94.03	93.90	1.4
9	2.1	2.2	2.3	89.25	90.48	91.86	88.06	92.37	97.34	89.99	89.30	88.43	88.54	91.60	95.12	2.3
10	0.8	0.9	1.0	96.21	95.73	93.52	88.55	89.58	90.94	99.45	98.33	94.61	91.27	91.76	91.86	0.9
11	0.7	0.8	0.9	98.40	97.69	95.04	96.76	97.32	97.80	98.93	97.81	94.16	97.30	97.44	96.89	0.8
12	0.9	1.0	1.1	97.28	92.96	92.60	98.08	98.82	99.37	96.70	88.74	87.75	97.73	96.30	96.47	0.9
17	1.1	1.2	1.3	96.93	95.29	93.23	94.71	95.76	96.77	97.76	95.12	91.91	95.47	95.60	95.55	1.2
20	1.9	2.0	2.1	93.22	92.56	92.07	97.27	97.78	98.21	90.34	88.86	87.70	95.54	95.55	95.58	2.0
28	1.2	1.3	1.4	86.42	86.43	86.06	87.05	92.04	99.00	86.26	85.02	82.82	86.85	90.29	94.96	1.3
29	0.85	0.95	1.05	84.09	82.89	84.34	71.52	73.45	77.96	93.81	90.20	89.28	77.09	77.64	80.79	1.05
30	0.75	0.85	0.95	87.07	89.97	88.32	66.60	79.07	85.06	99.72	96.71	90.33	74.88	83.48	86.38	0.95
31	1.0	1.1	1.2	92.41	92.29	92.39	88.13	91.22	95.15	93.77	92.63	91.51	89.54	91.57	94.24	1.2
Mean	1.24	1.34	1.44	91.94	90.87	89.52	86.65	90.38	93.34	94.19	91.32	88.34	88.53	90.61	92.09	1.35
Max	2.7	2.8	2.9	98.40	97.69	95.04	98.08	98.82	99.37	99.72	98.33	94.80	97.73	97.44	96.89	2.9
Min	0.5	0.6	0.7	84.09	82.63	78.89	66.60	73.45	77.96	86.26	78.95	73.71	73.34	77.64	80.79	0.6

Note: The two best performances from the overall matching metric are highlighted in blue and the selection is mirrored for the weighted matching metric. The greater performance from the highlighted weighted values is underlined and represents the final selected threshold.

Table 0.4. Selected thresholds for each site and year.

Sensor ID	Selected Threshold by year		
	2011	2012	2013
1	0.70	NA	NA
2	3.00	1.00	2.50
3	1.10	1.00	0.90
4	NA	1.00	0.90
5	1.07	1.18	1.1
6	0.80	0.80	0.60
7	1.20	1.30	1.20
8	2.00	1.70	1.40
9	1.60	2.10	2.30
10	1.00	1.00	0.90
11	0.90	0.70	0.80
12	1.30	1.40	0.90
13	2.60	NA	NA
14	1.10	NA	NA
15	1.10	NA	NA
17	1.10	1.10	1.20
19	1.50	NA	NA
20	3.40	2.00	2.00
21	0.90	NA	NA
23	1.00	NA	NA
24	2.50	NA	NA
26	1.00	NA	NA
27	0.90	NA	NA
28	NA	1.20	1.30
29	NA	1.20	1.05
30	NA	1.20	0.95
31	NA	1.40	1.20
Mean	1.46	1.27	1.35
Max	3.40	2.10	2.90
Min	0.70	0.70	0.60

Note: Sites where inter-annual threshold differences were higher than 0.1 are highlighted in blue

1.22.4.2 Repeatable and Non-Site Specific Guidelines to Estimate the Threshold

Following the lessons learned by analysing and visually selecting a threshold for each of the 56 datasets we developed and tested a procedure to estimate the threshold using the daily precipitation, the streambed temperature, the scaleogram from the CWT analysis, and the convoluted temperature amplitude at one cycle per day (1-cpd). The systematic guidelines are discussed below and illustrated in Figure 4.3.

1. First, we created a similar figure to the one used in the previous analysis, but this time without the SWL data. The figure contained subplots for the precipitation, the stream temperature signal, the scaleogram from the CWT analysis, and the convoluted temperature amplitude at one cycle per day.
2. All the "clear breaks" in the scaleogram at the 1 cycle per day area (the dark blue areas) were tagged for further consideration by drawing a line throughout the whole figure (a line across all the subplots).
3. Each line was subsequently analysed to determine if the "break" in the frequency concurred with a noticeable decrease in the stream temperature signal for a day where rain was recorded. If all three considerations were met, we assumed flow was likely and the line was aligned with the "break" in the scaleogram, the decrease in the temperature signal and the precipitation. If the considerations were not met, we presumed the frequency change was likely caused by a climatic event and the line was discarded.
4. The value of the intersection of each line with the CTA were noted (4a) and averaged to obtain an initial estimated threshold (4b).
5. The initial estimated threshold was subsequently evaluated to ponder a final correction by either raising or lowering the threshold accordingly to the following criteria:
    a) If the initial estimated threshold captured additional CTA dips that after a visual evaluation were considered as no-flows, then the threshold was lowered. The criteria to lower the threshold was to exclude as much as possible the no-flow sections (1), while trying to maximise capturing the flow areas (2).
    b) If the initial estimated threshold did not capture all the CTA dips previously tagged as likely flows the threshold was raised. The criteria to raise the threshold was to include all the tagged flow events (1), while excluding sections of no-flow (2).

When match improvements were mutually exclusive with match decreases of flow/no-flows by lowering/raising the threshold, and the trade-off was estimated to be similar, we favour the threshold that would match the most flows. The values used to estimate the initial threshold, the information of any corrections to the initial estimates, and the comparison between the final estimated and the visually selected thresholds are provided in Table 0.5 – 4.7

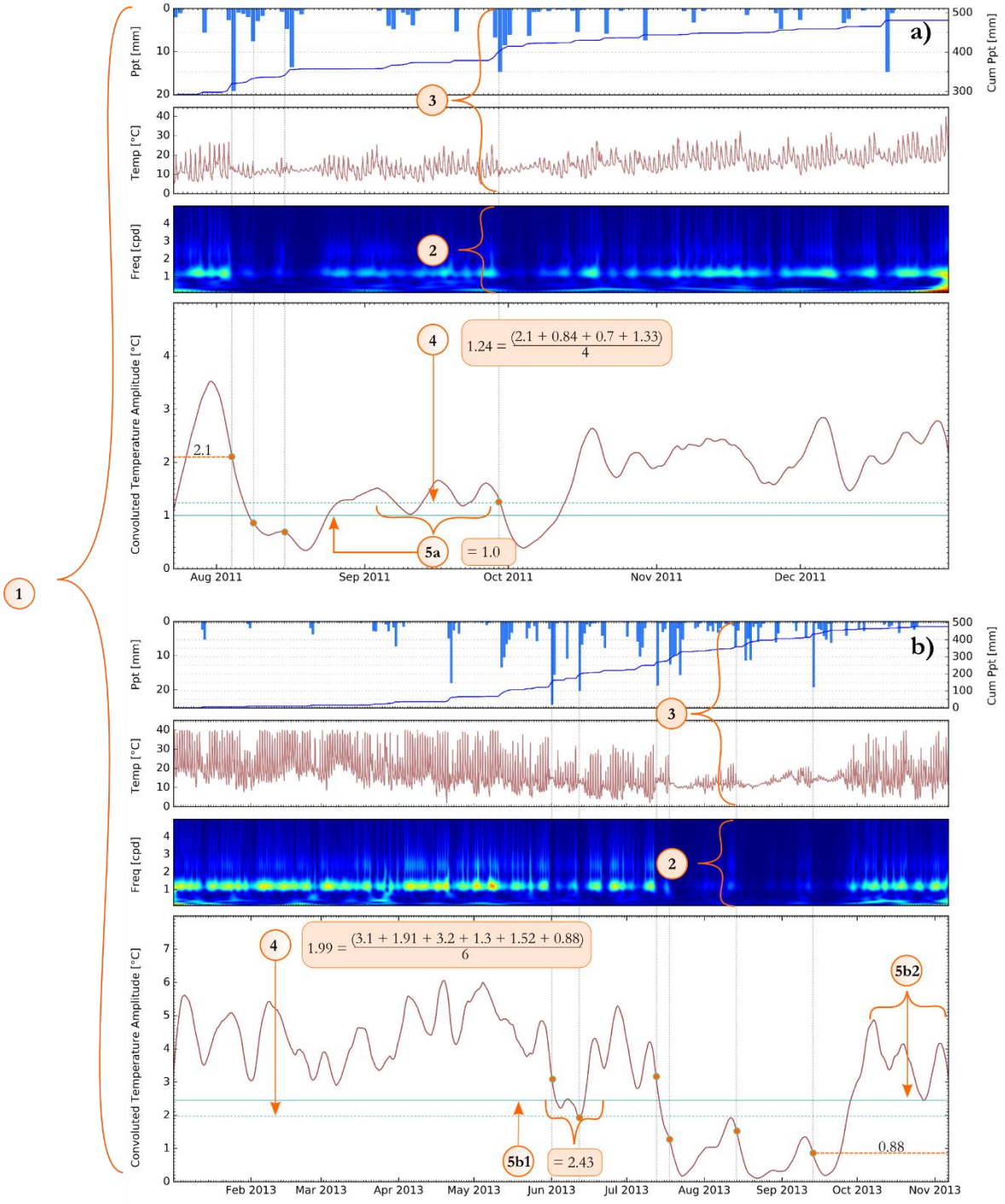

Figure 0.3. Illustration of the guidelines presented in section to estimate the threshold at two locations (a and b). Steps 1-4 are used to estimate the initial threshold (green dotted line) and are the same for subplots a) and b). Steps 2, 3 and 4a are repeated for each grey-dotted line but for clarity they are shown once in each subplot. Step 5 (a, b1, b2) showed the criteria for the corrected final threshold (green solid line).

Table 0.5 Table with the values used to estimate the threshold, and a comparison among the initial and final estimated thresholds and the visually selected threshold for the 2011 datasets.

2011 Sensor ID	---------- Identified Amplitude Intersections ---------						Thresholds			Abs Difference (Sel - Est)	
							Estimated Initial	Estimated Final *	Visually Selected	Est Ini	Est Fin
1	0.55	0.7	0.72	0.82	0.43	0.41	0.61	0.71	0.7	0.09	0.01
2	2.70	3.10	3.42	2.80	2.40	1.90	2.65	2.70	3.0	0.35	0.30
	1.21	3.00	3.30								
3	1.13	2.15	0.90	2.07	1.40	1.20	1.16	1.16	1.1	0.06	0.06
	1.10	0.93	0.80	0.80	1.10	1.28					
5	1.30	1.40	0.90	0.80			1.10	1.10	1.07	0.03	0.03
6	0.65	0.83	1.10	0.85	0.75	0.75	0.82	0.82	0.8	0.02	0.02
7	1.30	0.95	1.15	1.50	1.00	1.40	1.22	1.22	1.2	0.02	0.02
8	3.40	2.20	1.50	1.90	3.80		2.56	2.10	2.0	0.56	0.10
9	2.70	1.30	1.55	1.10	1.15		1.56	1.50	1.6	0.04	0.10
10	0.70	1.50	1.02	0.70			0.98	1.02	1.0	0.02	0.02
11	0.90	0.90	1.30				1.03	0.90	0.9	0.13	0.00
12	1.60	1.60	1.25	1.40			1.46	1.40	1.3	0.16	0.10
13	2.15	1.30	0.60	1.90			1.49	1.49	2.6	1.11	1.11
14	1.45	1.10					1.28	1.28	1.1	0.18	0.18
15	1.05	1.55	0.80	0.70	1.45		1.11	1.11	1.1	0.01	0.01
17	1.72	0.95	0.65	1.54			1.22	1.09	1.1	0.12	0.01
19	2.00	1.20	2.82				2.01	1.90	1.5	0.51	0.40
20	2.00	0.90	2.88				1.93	2.00	3.4	1.47	1.40
21	1.00						1.00	1.00	0.9	0.10	0.10
23	2.10	0.70	0.84	1.33			1.24	1.00	1.0	0.24	0.00
24	3.22	0.73	0.80	2.72	2.78		2.05	2.15	2.5	0.45	0.35
26	2.20	0.98	0.65	1.50			1.33	1.20	1.0	0.33	0.20
27	0.81	0.81	1.05	1.92	1.55		1.23	1.65	0.9	0.33	0.75
Average							1.41	1.39	1.46	0.30	0.26
Max							2.65	2.70	3.40	1.47	1.40
Min							0.61	0.71	0.70	0.01	0.00

*The Values highlighted in blue on the estimated final column indicate that for that site the initial threshold was corrected. If the value is higher the correction was to improve matching flows if it was lower was to improve matching no-flows

Table 0.6. Table with the values used to estimate the threshold, and a comparison among the initial and final estimated thresholds and the visually selected threshold for the 2011 datasets.

2012 Sensor ID	--- Identified Amplitude Intersections ---						Thresholds			Abs Difference (Sel - Est)	
							Estimated Initial	Estimated Final *	Visually Selected	Est Ini	Est Fin
2	0.95	0.53	0.75	0.68	0.47	0.70	0.68	0.95	1.0	0.32	0.05
3	1.00	0.55	0.48	0.69	1.02		0.75	0.98	1.0	0.25	0.02
4	1.00	0.55					0.78	1.00	1.0	0.23	0.00
5	1.00	0.88	0.78				0.89	1.00	1.18	0.29	0.18
6	0.70	0.70					0.70	0.70	0.8	0.10	0.10
7	1.00	1.12	1.10	1.02			1.06	1.06	1.3	0.24	0.24
8	1.10	0.85	1.00				0.98	0.98	1.7	0.72	0.72
9	0.92	1.08	1.12	1.12			1.06	1.06	2.1	1.04	1.04
10	0.87	0.35	0.35	0.51	0.60		0.54	0.90	1.0	0.46	0.10
11	0.78	0.73	0.60				0.70	0.70	0.8	0.10	0.10
12	1.10						1.10	1.10	1.4	0.30	0.30
17	0.90	0.90	0.87				0.89	0.90	1.1	0.21	0.20
20	0.85	1.35	1.42				1.21	1.50	2.0	0.79	0.50
28	1.15	0.70	0.90	0.80	1.35		0.98	1.31	1.2	0.22	0.11
29	1.07	0.57					0.82	1.07	1.2	0.38	0.13
30	0.60	0.40	0.92	0.65			0.64	0.66	1.2	0.56	0.54
31	1.30	0.80	0.82				0.97	1.35	1.4	0.43	0.05
Average							0.87	1.01	1.27	0.41	0.28
Max							1.21	1.50	2.10	1.04	1.04
Min							0.54	0.66	0.70	0.00	0.00

*The Values highlighted in blue on the estimated final column indicate that for that site the initial threshold was corrected. If the value is higher the correction was to improve matching flows if it was lower was to improve matching no-flows

Table 0.7 Table with the values used to estimate the threshold, and a comparison among the initial and final estimated thresholds and the visually selected threshold for the 2011 datasets.

2013 Sensor ID	-------- Identified Amplitude Intersections --------							Thresholds			Abs Difference (Sel - Est)	
								Estimated Initial	Estimated Final *	Visually Selected	Est Ini	Est Fin
2	3.10	1.95	3.20	1.30	1.52	0.88		1.99	2.43	2.50	0.51	0.07
3	0.98	0.85	0.80	0.92				0.89	0.89	0.90	0.01	0.01
4	1.20	0.88	0.85	0.70	0.54	0.62		0.80	0.95	0.90	0.10	0.05
5	1.13	0.51	0.70	0.68				0.76	1.13	1.10	0.35	0.03
6	0.91	0.60	0.57	0.47				0.64	0.70	0.60	0.04	0.10
7	1.40	1.58	1.08	0.92	0.98	1.20	0.75	1.13	1.22	1.20	0.07	0.02
8	1.52	1.48	1.45	0.99				1.36	1.48	1.40	0.04	0.08
9	2.10	1.20	0.98	1.67				1.49	1.77	2.30	0.81	0.53
10	1.86	1.20	0.66					1.24	1.07	0.90	0.34	0.17
11	1.01	0.86	1.00	0.93	0.52			0.86	1.01	0.80	0.06	0.21
12	1.18	0.82	0.92	0.54				0.87	0.90	0.90	0.04	0.00
17	1.78	1.12	1.25	0.55				1.18	1.18	1.10	0.08	0.08
20	1.90	1.35	1.95	0.70				1.48	1.81	2.00	0.53	0.19
28	1.45	0.88	0.81	0.53	0.50			0.83	0.90	1.30	0.47	0.40
29	1.05	0.40	0.92	0.55				0.73	0.99	1.05	0.32	0.06
30	1.00	1.14	0.84	0.78				0.94	0.94	0.95	0.01	0.01
31	1.05	0.60	0.38	0.58	0.80			0.68	1.09	1.20	0.52	0.11
Average								1.04	1.20	1.35	0.36	0.23
Max								1.87	2.43	2.90	2.15	1.77
Min								0.64	0.70	0.60	0.01	0.00

*The Values highlighted in blue on the estimated final column indicate that for that site the initial threshold was corrected. If the value is higher the correction was to improve matching flows if it was lower was to improve matching no-flows

A regression analysis to explore the relationship between the selected threshold values (the best performing value) and the temperature variance, the temperature amplitude at 1cpd variance, and the convolved temperature amplitude variance did not show good fits (Figure 0.4).

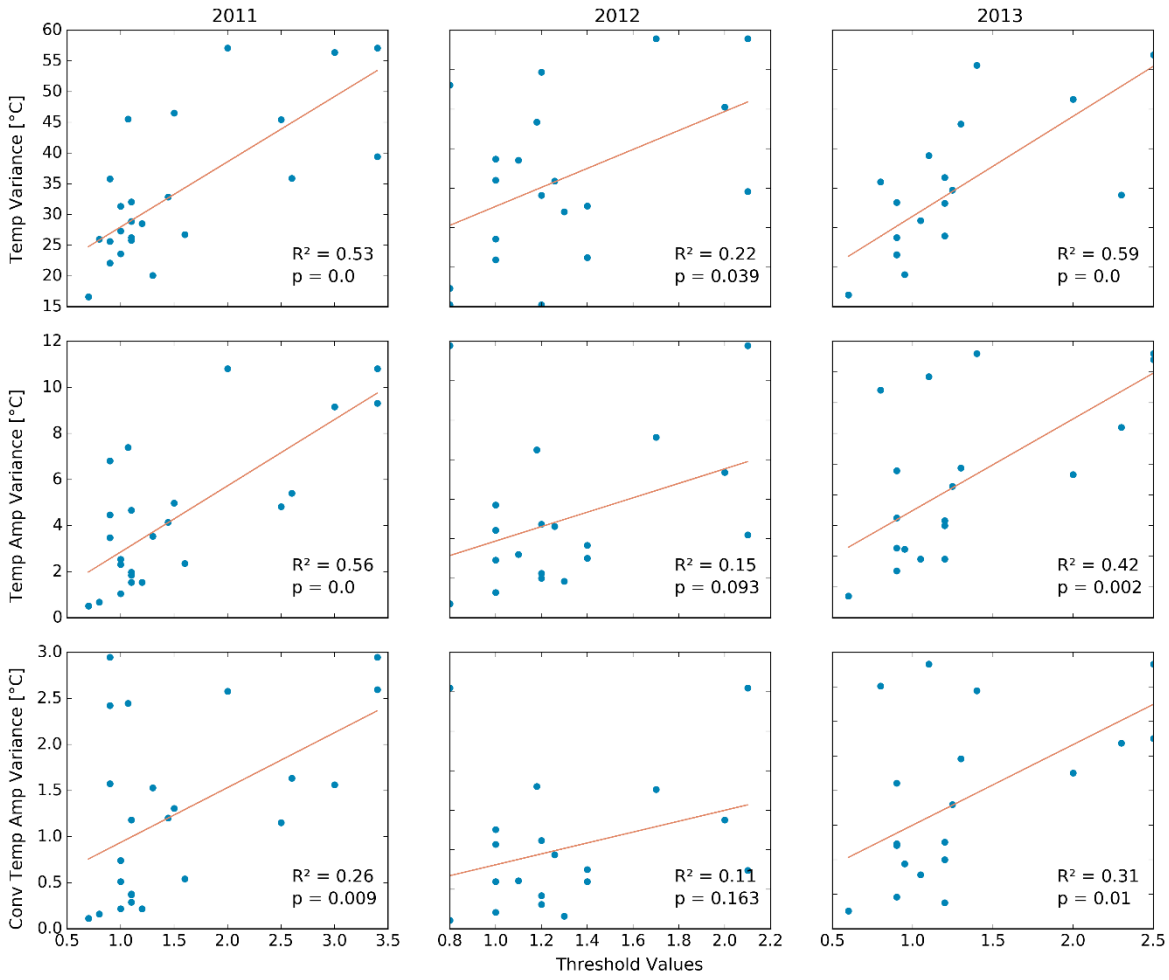

Figure 0.4 Variability of the selected thresholds versus the daily temperature variance (top row), the temperature amplitude variance (middle row), and the convolved temperature amplitude variance (bottom row) for each yearly dataset (2011, 2012, and 2013). The fitted linear regression is shown in red and the R^2 and p-values are reported in each subplot.

1.22.5 Comparison of the Spatiotemporal Variability of Flow from the SWL Data and the CWT Estimated Flow

For the spatiotemporal variability analysis we used the datasets from 2012 and 2013 which had a better spatial coverage. The analysis consisted of comparing how well the predicted flows from

the CWT method captured the spatiotemporal variability of flow across the catchment. For the comparison we used the SWL (real flow) data and the predicted flows from the estimated threshold. We created a python script to extract the onset and cessation of all flow events for each year for both the SWL data and the estimated flows. From the onset and cessation information we calculated each flow duration and we categorized each event as either intermittent or ephemeral for flow durations of ≥7 or <7 days, respectively.

We determined the order in which the start of the intermittent flow season occurred across the catchment by using the information of the first intermittent event at each site, and also calculated the total flow duration for each year as the sum of all intermittent and ephemeral flows. We used the information of the total flow duration, the average flow duration for ephemeral and intermittent events for each site, and the order of flow for the first intermittent event to evaluate the stream network dynamics in the catchment.

1.23 Results

1.23.1 CWT Flow/No-flow Performance for the Visually Selected and the Estimated Thresholds

The average OM performance for the visually selected threshold ranged from 86-94%, and from 83-93% for the estimated thresholds (Figure 0.5). Average FM performance ranged from 69-93% for the selected threshold and from 66-88% for the estimated ones. Average NFM ranged from 92-95% and from 92-98% for the selected and estimated thresholds respectively. The average performance of the selected and estimated thresholds was generally closer in agreement for the OM and the NFM with 1-3% differences. The greater divergence in the average performance was observed for the FM with differences of up to 8% among the two set of thresholds.

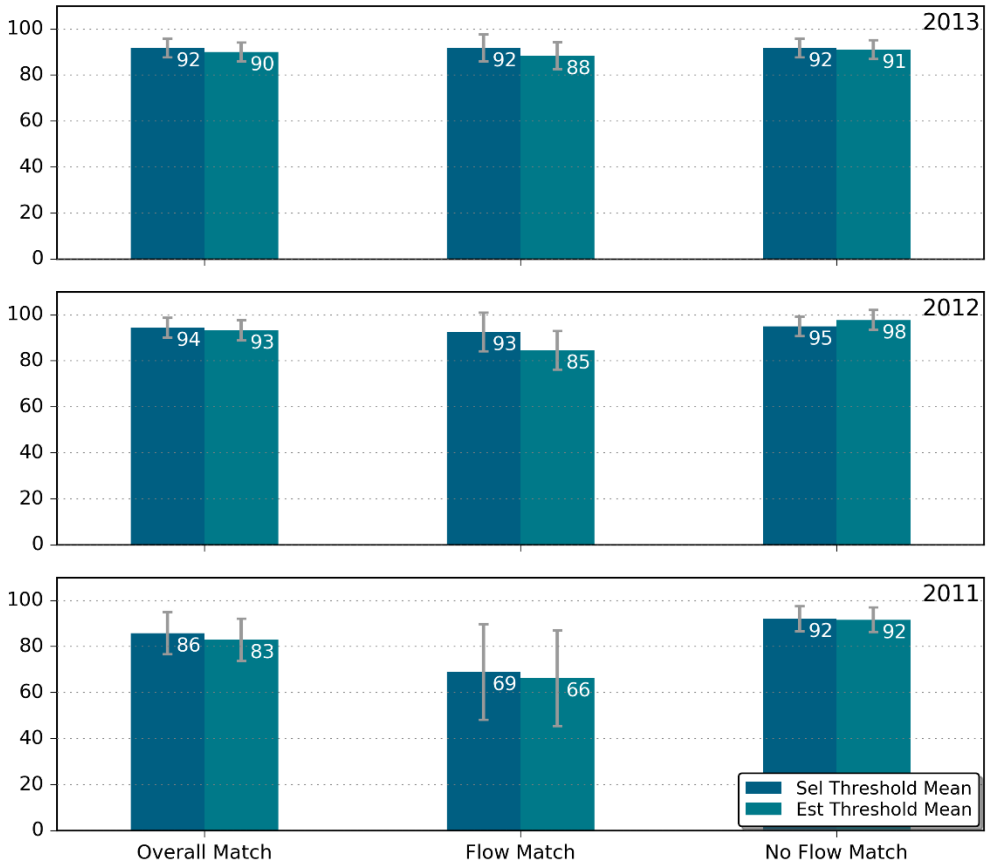

Figure 0.5 Mean matching performance for each year and matching metric for the visually selected and estimated thresholds. The error bars show the standard deviation for each metric.

We observed the worst matching performance for the 2011 dataset whereas the performances for the 2012 and 2013 datasets were similar. Although 2011 and 2013 had very similar total yearly precipitation with 480 and 499 mm respectively (Figure 0.6), the catchment's flow response was markedly different. The 2011 datasets recorded more ephemeral events and many sites had a broken up intermittent season that consisted of multiple shorter events instead of a single continuous flow (15 out of 22 sites). In contrast, the 2013 datasets had fewer ephemeral events and most sites presented a continuous intermittent flow season (13 out of the 17 sites).

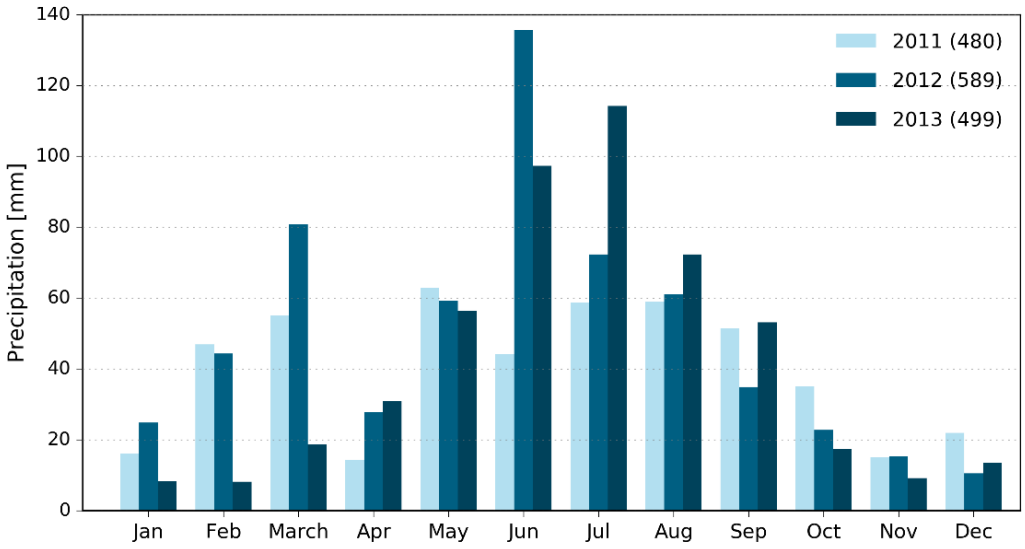

Figure 0.6 Monthly precipitation for 2011, 2012, and 2013. The total yearly precipitation in millimetres is shown in parenthesis for each year.

The bad performing datasets for 2011 corresponded to sites that had multiple ephemeral events that led to periods of prolonged ponding in the stream which were not captured by the CWT method (Figure 4.7a). Similar performance issues for FM were observed for datasets that presented shallow recession curves between events during the intermittent season and/or long recession periods preceding flow cessation, which were most likely indicative of ponding water (Figure 4.7b). At large, the CWT method did not performed well for predicting neither flows nor the presence of ponding water for sites that presented shallow water levels of approximately ≤ 0.05 m (Figure 4.7c-d). The greatest divergence in the performance of the visually selected (best) and estimated thresholds (worst) occurred also for these datasets (Figure 4.7b-d). While the performance of both thresholds (selected and estimated) for some datasets were equally bad, the greatest divergence in the performance between the two set of thresholds was noted on for these datasets (Figure 4.7b-d). The best performances were contrastingly observed for datasets that presented mostly long intermittent events and a few or no ephemeral flows (Figure 4.8). We observed that the closer an ephemeral event was from the start of the intermittent season, the more likely we were able to identify them, and vice versa, the furthest the least likely (Figure 4.8 b-d). Shorter and sharper recession curves leading to flow cessation were generally better captured (Figure 4.8c vs. Figure 4.8a) while short interflow periods (periods of no-flow between flows) were often miscategorised as flow (Figure 4.8 b&d).

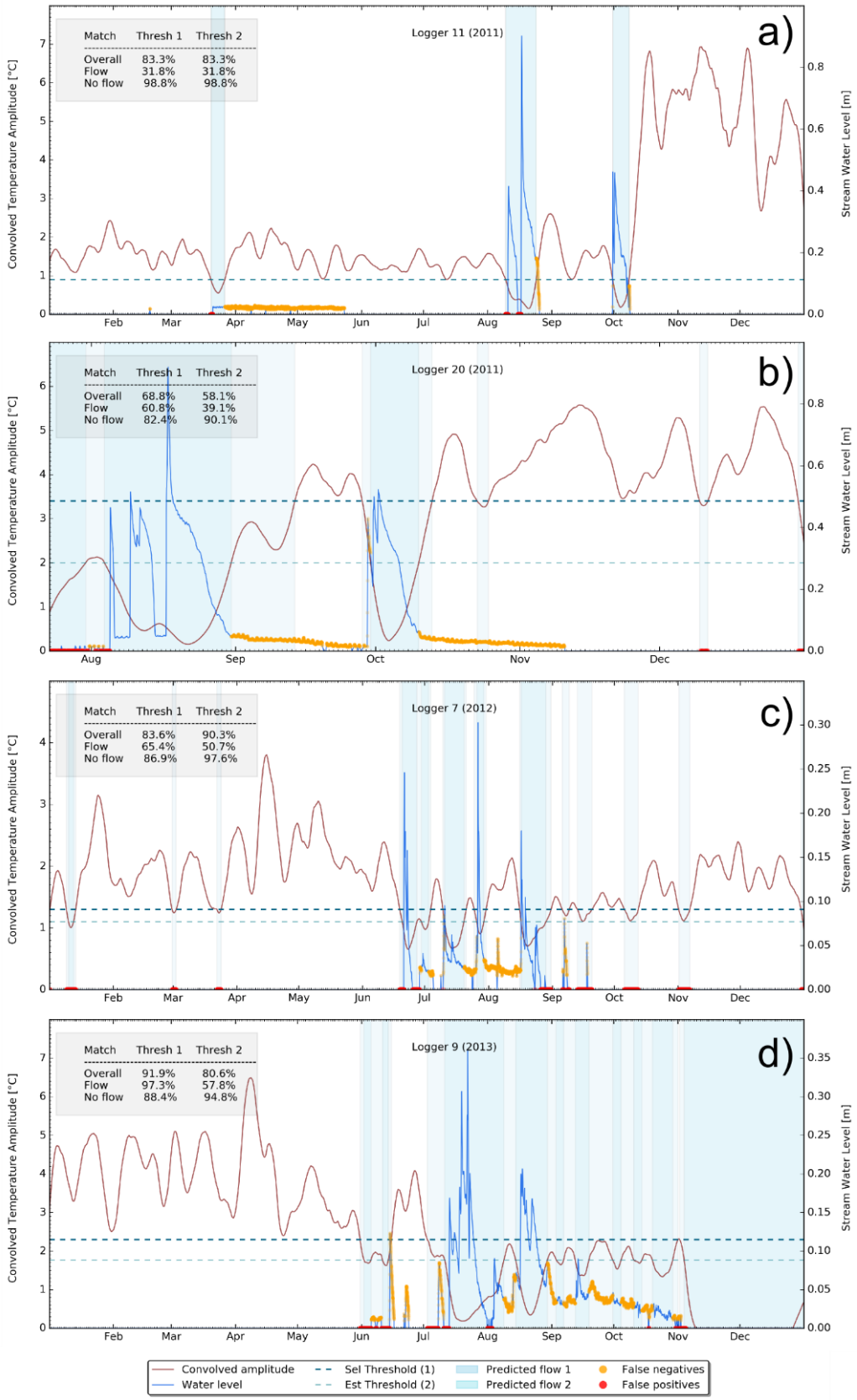

Figure 0.7 Example of sites showcasing the type of flows where the CWT had the worst matching metrics for both the selected and estimated threshold. A summary of the matching metrics is provided for each subplot.

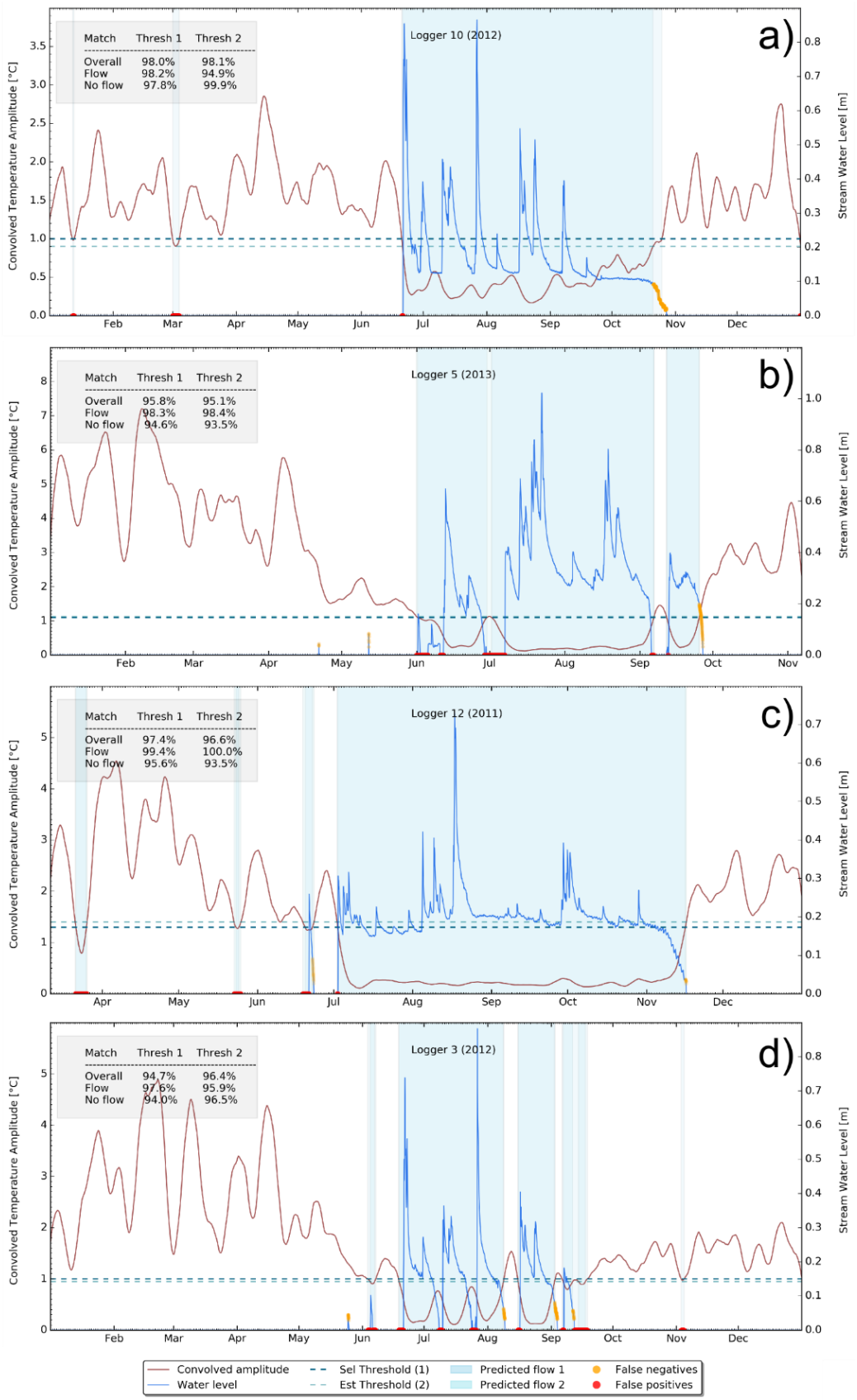

Figure 0.8 Example of sites showcasing the type of flows where the CWT had the best matching metrics for both the selected and estimated threshold. A summary of the matching metrics is provided for each subplot.

1.23.2 CWT Spatiotemporal Variability of Flow Performance

We observed that the poor performance of the CWT method for predicting the ephemeral flows failed to spatially capture ephemeral flows altogether for a number of sites while over predicting the average flow duration for most of the rest (Figure 0.9a&d and Figure 0.10a&d). The intermittent events were better captured by the method with all sites becoming active (showing intermittent flows) across the catchment for both 2012 and 2013 (Figure 0.9b&e and Figure 0.10b&e). However, the average intermittent flow duration for sites across the catchment was underestimated at 10 sites in 2012 and 11 in 2013; and overestimated at 7 sites in 2012, and at 5 sites in 2013. Only at one site the estimated and observed duration had the same length during 2013. The average absolute difference was 32 days for 2012 and 37 days for 2013. The estimated total flow durations were generally in closer agreement to the observed SWL data with roughly 70% of the monitoring sites for 2012 and 60% for 2013 showing differences of 10 days or less (Figure 0.9c&f and Figure 0.10c&f). The average time difference for the onset of the intermittent season (the first intermittent event at each site) was 2.5 days for 2012 and 39 days for 2013. The order in which flow originated across the catchment varied between the two years and it was not well captured by the estimated flows from the CWT method.

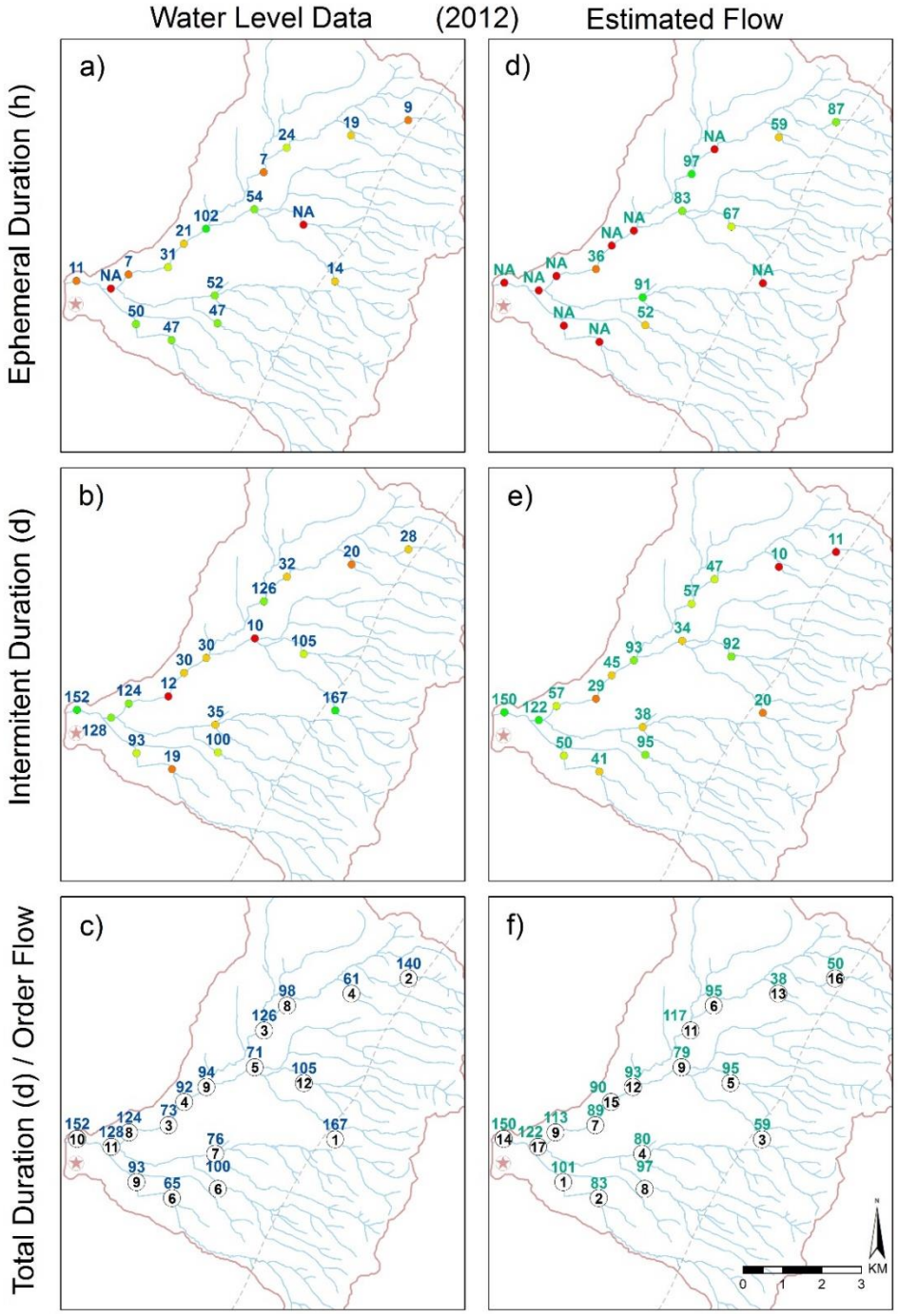

Figure 0.9. Average flow duration for ephemeral (a & d) and intermittent (b & e) events in hours and days respectively, for each site in 2012. Subplots c & f show the total flow duration in days (colour notation) of the first intermittent event and the order in which the event occurred across the catchment (black circles). Subplots a-c (blue notation) correspond to the values from the stream level data and subplots d-f (green notation) refer to the results from the CWT method with the estimated threshold.

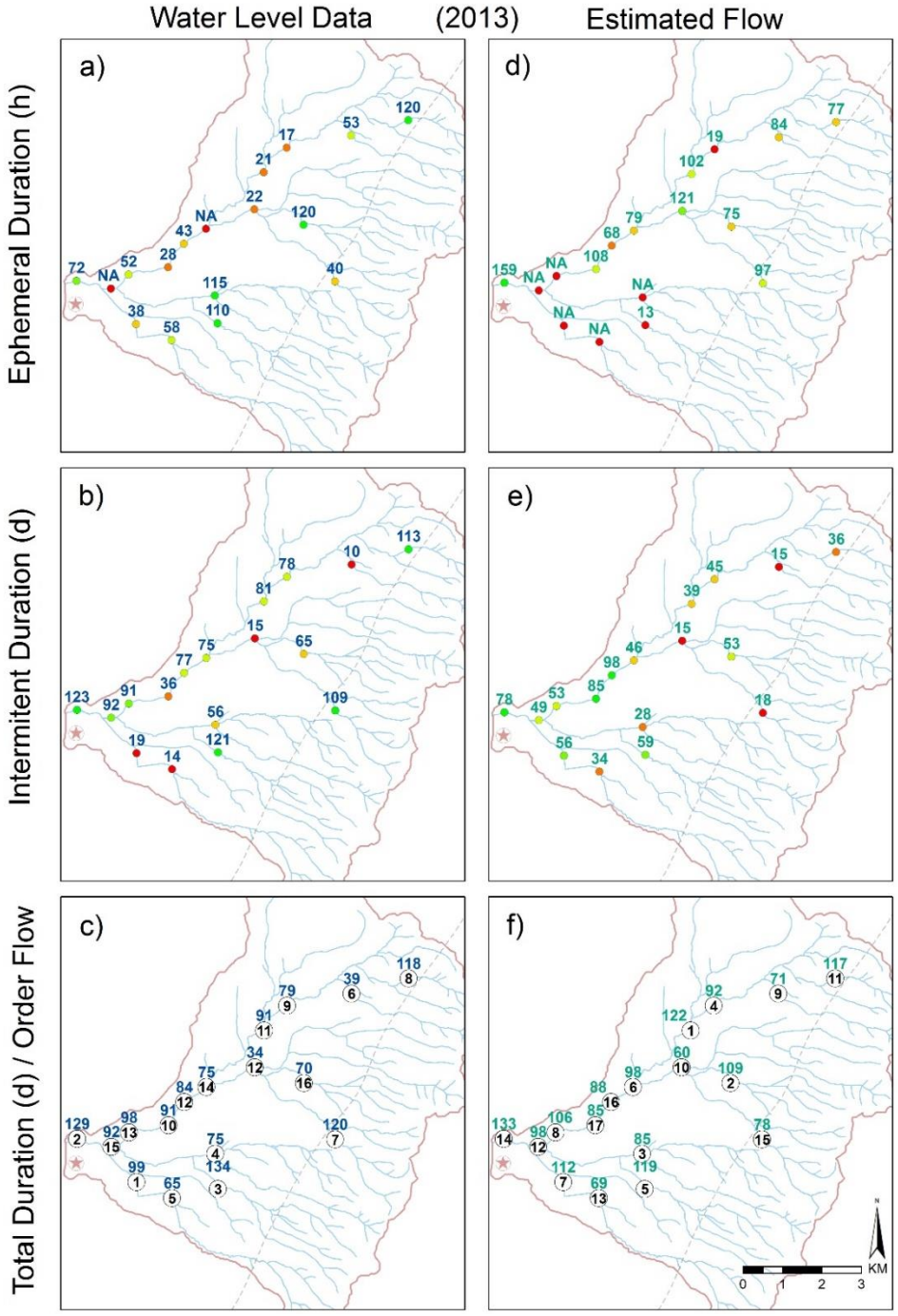

Figure 0.10. Average flow duration for ephemeral (a & d) and intermittent (b & e) events in hours and days respectively, for each site in 2013. Subplots c & f show the total flow duration in days (colour notation) of the first intermittent event and the order in which the event occurred across the catchment (black circles). Subplots a-c (blue notation) correspond to the values from the stream level data and subplots d-f (green notation) refer to the results from the CWT method with the estimated threshold.

1.24 Discussion

The goals of this chapter were to implement the CWT method to a field dataset with a variety of distinct flow conditions to evaluate its performance and to develop a procedure to estimate the threshold needed for the method to detect flow from streambed temperature measurements. The method was first evaluated by taking advantage of measurements of SWL that were used as proxies of flow to select a threshold that would produce the best flow/no-flow matches. After visually analysing all 56 datasets we noted that intermittent flows (flow duration ≥ 7 days) could be roughly identified for most datasets by the CTA signal dipping below 0.5 °C. However, neither the start/cessation of the intermittent flows nor the ephemeral events were easy to infer from the CTA signal alone. Under further inspection, we observed that the start of flow events matched reasonably well with the "breaks" in the frequency signal at 1-cpd, and flows always coincided with a precipitation event and the observable "dampening" of the streambed temperature signal. The combined information from the break in the frequency, the dampening of the temperature signal, and confirmation of a precipitation also allowed us to detect some of the ephemeral events. Finally, we could not identify a way to infer flow cessation particularly after intermittent events and/or when the SWL was likely to represent ponding water. The lessons learned from the visual analysis allowed us to develop a series of simple guidelines to estimate the thresholds. The results from the selected and estimated thresholds were compared to assess how well the new guidelines to estimate the threshold performed. Finally, we evaluated how well the predicted flows from the estimated threshold captured the spatiotemporal dynamics of flows across the catchment.

1.24.1 CWT Method Application and Threshold Determination (Selected and Estimated)

The application of the CWT method was straight forward, simple, and easily automated using code. We found that the scaleogram and the convoluted temperature amplitude were a good visual aid to help identify possible flow events that would otherwise be overlooked by only using the temperature signal. However, the selection of an 'optimal' threshold was challenging and a time consuming task as anticipated by Partington et al. (in-prep). Similar to what has been suggested in other similar studies (Assendelft & van Meerveld, 2019; Blasch et al., 2004; Gungle, 2006), we observed large variability in the selected thresholds among sites which suggests that

it is unlikely to find a "universal" threshold value that would yield good results across sites. Differently than the estimated parameters used for the methods proposed by Assendelft & van Meerveld (2019), Blasch et al. (2004), and Gungle (2006) we saw that a single threshold value did not perform well for over 60% of the sites with multi-year datasets. The inter-annual variability in the threshold values indicates that the threshold isn't site specific but rather might depend on the yearly temperature variability. Including a function of time for the temperature variability in our threshold selection was outside of the scope of this paper, but our results indicate that there is indeed a temporal variability that needs to be considered. These results are consistent with the remarks by Partington et al. (in-prep) who mentioned that threshold estimation might need to include a function of time to account for the seasonal variability of temperature amplitudes. Similarly, Gungle (2006) hypothesized that the seasonal variance in diurnal temperatures and daylight length would impact his threshold values and therefore analysed the thermographs in three separate periods with similar temperature amplitudes. The results from regression analysis exploring the relationship between the selected threshold values and the yearly temperature variance were however inconclusive. Further work on understanding the threshold variability would be valuable.

The proposed empirical guidelines to estimate the threshold are simple, easy to replicate and different from other temperature-based methods, it does not require the determination of a site-specific subjective set of parameters (Assendelft & van Meerveld, 2019; Blasch et al., 2004), a calibration period (Assendelft & van Meerveld, 2019; Blasch et al., 2004; Gungle, 2006), or having to bury the temperature sensors at depths up to 75 cm (Blasch et al., 2004; Gungle, 2006). The process, however, still required detailed visual inspection which was time consuming, and was prone to subjectivity for datasets that presented multiple ephemeral and intermittent events. Similar to Blasch et al. (2004) we use available precipitation records to improve accuracy. The precipitation records were most important when evaluating the likelihood of ephemeral events from short breaks in the frequency signal, which were overall the hardest to assess. The lessons learned from developing the guidelines could be used in future studies to automate the threshold estimation process, which could aid overcome the subjectivity and time-consuming challenges.

1.24.2 CWT Method Performance with Selected and Estimated Thresholds

The overall performance of the CWT method was comparable for the selected and estimated thresholds for most datasets. We saw the best performances for the datasets where most of the flow occurred during a single intermittent flow (matches >95%) and the worst performances for datasets that presented several short ephemeral and intermittent events, and for datasets which had periods that most likely represented ponding conditions. Similar to what was noted by Partington et al. (in-prep), the method generally struggled to capture ephemeral events of one day or less but was successful in capturing all intermittent events in all the tested datasets. These results are also consistent with the findings by Blasch et al. (2004) who stated that some of the parameters needed for his method were less critical for long duration events and by Assendelft & van Meerveld (2019) who concluded that the method showed the worst performance in sites with short episodic flows. It must be noted that possibly some of the categorized short and shallow flow events from the SWL data might have been ponding water after extreme rainfall events.

In terms of capturing the flow timing, we observed that detecting flows with a single threshold tends to over predict the start and under predict the end of the flow events. Therefore, improvements on the threshold position to capture the start of a flow event had a direct impact on capturing the recession of the hydrograph and vice versa. This offset in the timing of strreamflow onset and cessation is a recurring issue encountered in previous studies (Assendelft & van Meerveld, 2019; Blasch et al., 2004) and it was noted in the initial CWT work by Partington et al. (in-prep). In particular, we saw that flow cessation was generally more difficult to capture. During the visual analysis to develop the guidelines to estimate the threshold, we noticed that in most datasets the changes in the diurnal temperature fluctuations were more pronounced in the transition from dry to wet than from wet to dry states, particularly for intermittent events. While the clear break in the 1-cpd frequency signal aligned closely to the start of flow, an equivalent signal change was not clear to infer flow cessation. These findings are consistent with the remarks by Blasch et al. (2004) who stated that flow cessation was more difficult to identify and attributed it to shifts on the dominant heat transport mechanism affecting the temperature signal. In our study, the difficulties arose from the recession periods containing periods with shallow flows and and/or ponding water.

Within datasets, we observed that different events had different thresholds as reflected in the values of the identified amplitude intersections (Table 4.5 - 4.7). This is logical since the convoluted temperature amplitude is dependent on the surrounding observation points. Therefore, a flow preceded by a long dry period with large amplitudes would have a larger threshold value than a flow that included the dampened amplitude signals from a preceding flow. This insight allowed us to understand the reason for the misclassification of flow/no-flows around flows events and reaffirmed our notion that yearly and possibly seasonal thresholds are needed to account for temperature variability.

Partington et al. (in-prep) suggest in their discussion that it might be possible to evaluate flow magnitude during intermittent flow events using the amplitude signals. Although testing this theory was out of the scope of this study, our visual analysis uncovered certain patterns that support this idea. We noted that in most of the datasets, the convoluted signal allowed us to roughly speculate the shape/behaviour of the hydrograph mostly for the intermittent flows. For both short intermittent and some ephemeral flows, characterized by sharp recessions, the convoluted signal decreases and takes a "V" shape, where the dip roughly mirrors to the hydrograph peak. The wider the "V" shape, the longer peak flow levels were maintained and the narrower, indicated a fast recession. During longer intermittent events that consisted of multiple-consecutive large flows (peaks), the convoluted amplitude drops and plateaus. During long recession periods, the signal creates a hump that raises until the next peak occurs, and the signal drops again. These "humps" during the recessions were noticeably smoother for deeper water levels and more pronounced for shallow ones. The bad performances capturing ponding/shallow flows similarly suggest that with further analysis an additional threshold could be developed to capture and differentiate ponding/shallow flows from larger flows.

Since we have established that our application (using a single threshold) of the CWT method under or over-estimated the timing of the onset and cessation of flow and did not perform well capturing ephemeral events, the spatiotemporal performance was limited in its ability to reliably capture the occurrence and approximate duration of intermittent flows. Nevertheless, the capability to capture the behaviour and patterns of intermittent flows for a mostly intermittent stream network is decidedly valuable. From the estimated flows from the CWT, for example, we were able to recognize differences in the catchment's response corresponding to the annual

precipitation distribution. Although 2011 and 2013 had practically the same annual precipitation (a difference of only 19 mm), it was evident by simply looking at the scaleogram, that in 2011 most sites had multiple and shorter flows in contrast to the longer intermittent flows observed throughout the 2013 season. Similar observations could be made when comparing the responses from 2012 and 2013. With roughly 100 mm more rain, the 2012 flow season presented longer intermittent flows than 2013, which was captured for over 70% of the sites. For both 2012 and 2013, we were also able to capture the overall pattern of flow duration for sites across the catchment. Moreover, the differences in the start of the intermittent season between both years can be inferred clearly from the CWT results when focusing only on the intermittent flows. The intermittent flow season for 2012 started around mid-late June, whereas for 2013, it started about a month later during mid-late July. The start of the intermittent season for both years occurred coincidentally during the months that recorded the greatest monthly precipitation. These observations are consistent with other studies that have found that changes in the precipitation input have a direct impact on the streamflow response on IRES (Gutierrez-Jurado et al., 2019; Park et al., 2011; Thomas et al., 2016). These results from this chapter show the potential of the CWT method to provide insight into intermittent flow dynamics for IRES. At the catchment scale.

1.24.3 Study Limitations, CWT Potential and Future Work

Our findings debunk the idea that a single universal threshold could be used across datasets, and not even across years for multiyear datasets. The variability of the thresholds by site and year, suggest that the thresholds are affected not only by seasonal temperature variability but possibly by other factors. These results are consistent with findings by Gungle (2006) who observed noisy datasets from sites where physical structures generated intermittent shading above the logger. Further studies that analyse the threshold variability using the temperature variability and site characteristics would most valuable.

Our detailed visual analysis and performance tests for the CWT method exposed some important limitations and some promising potentials. It is important to note that this discussion is constrained by our implementation of the CWT method which used a single threshold to identify flows in a yearly dataset, and without exploring other parameter values with the CWT analysis.

The limitations can be summarized into the bad performances of the method to capture short ephemeral flows, periods of ponding water, and to accurately capture the timing of flow onset and cessation. There are a few considerations worth exploring in future applications of the CWT method to overcome some of these limitations. Partington et al. (in-prep) mention the possibility of incorporating a function of time to include the higher temperature variation during the summer to capture the ephemeral flows during that period. Likewise, the yearly datasets could be analysed by periods of similar temperature amplitudes like Gungle's (2006) approach. While accounting for seasonal temperature variability would likely improve the overall performance of the CWT method, single thresholds for multiple events even within a season are not likely to improve getting the timing of the onset of flow. From our analysis we suggest that the best results would be obtained by developing a procedure to identify and treat every single "break" in the frequency signal (i.e. possible flow) as an individual occurrence with its specific threshold, similar to how we identified the amplitude intersections for each signal break when estimating the threshold. Treating every signal break separately has the potential to enhance the ability of the method to predict shorter events as well as to improve capturing the onset of flow. Nonetheless, some of these shorter events are not easy to identify accurately and additional information such as benchmark temperature sensors would likely be needed to assist the identification process. Moreover, unless such approach is automated the process would be extremely time consuming and unfeasible for large datasets.

Overall, our results show that the CWT has great potential for analysing intermittent flow seasons if the short ephemeral events are considered negligible in the big scheme. Since for most datasets the signal break for an intermittent event is quite clear, the estimated flow duration and timing of onset and cessation would likely be improved. This would improve our capacity to understand the spatiotemporal dynamics of flow onset and cessation across the catchment. Our analysis further suggests that the convoluted amplitude signal contains some important information to infer where hydrograph peaks and recessions occur. At this point our observations provide only a qualitative understanding of the hydrograph characteristics, however, future work could evaluate a way to perform a quantitative analysis. While preliminary, these findings are promising and unique from any of the other methods that have been used in previous studies to infer flow occurrence that have been used in previous studies.

Finally, while our proposed guidelines are easy to implement, at this point, visual analysis of all the individual datasets is required. Even if this process is simplified by excluding the hardest events to asses (i.e. ephemeral), the method remains time consuming. Finding a way to automate the threshold selection would, therefore, be necessary if this method is to be used in a large-scale catchment with a dense network of temperature sensors and/or for a long record period.

1.25 Conclusion

A novel temperature-based method was applied to a field dataset to develop guidelines to estimate a flow/no-flow threshold and to evaluate its application and performance capturing streamflow in an intermittent Mediterranean-climate catchment. The CWT method was tested on over 56 datasets that spread over three years which included a variety of flow conditions. After a detailed analysis of the 56 datasets, a set of simple guidelines was developed that allowed us to estimate the flow threshold. The results from the CWT with the estimated threshold show that the method performs well to capture periods of intermittent flow and struggles to capture short ephemeral events and ponding water. Our results suggest that for intermittent flows, the CWT method would be able to capture relatively well the onset, cessation and duration of the intermittent season. Our detailed analysis additionally showed that it might be possible to infer the hydrograph peaks and recessions, as well as ponding conditions, from the temperature amplitude signals. This is an important development which, if developed in further studies, could set apart the use of temperature with the CWT analysis as a proxy to detect flow from other methods. With intermittent streams being some of the most vulnerable freshwater systems to the impacts of climate change and other human-driven impacts, understanding the seasonal flow variability is critical. Our results suggest that the CWT method can be used to generate a better understanding of the seasonal flow variability as it was observed by our ability to detect differences in the seasonal flows in response to different yearly precipitation patterns. The application of the CWT method is simple and does not require other benchmark data, calibration periods, the calculation of complicated and site-specific set of parameters, or complicated installations. The simple guidelines developed in this study showed to be effective in selecting a threshold that performs well at capturing flow/no-flow periods. Future work should attempt to automate the threshold selection and test different applications that could improve the method performance for capturing shorter ephemeral events.

Chapter 5

Conclusions

The literature review provided in Chapter 1 highlighted some of the most important knowledge gaps and challenges to understand streamflow generation in IRES from semi-arid catchments with Mediterranean climates. Among the most important gaps and challenges were [1] the need of research with a focus on understanding the hydrological processes leading and contributing to streamflow generation in IRES, and [2] the difficulty to monitor flow in these systems and the need of long-term and spatially distributed streamflow data. Three main research questions were posed in section 1.3 with the aim to provide insight into the processes that contribute to streamflow generation in IRES (Chapters 2-3) and to provide new solutions to overcome some of the challenges of monitoring streamflow in these systems (Chapter4). The contributions of this thesis are summarized in the key findings from each question (contained in Chapters 2-4) and are presented in the sections below.

1.26 Summary of Findings

1.26.1 Question 1. *What triggers streamflow for Intermittent Rivers and Ephemeral Streams in Low-Gradient Catchments in Mediterranean Climates?*

To answer this, we followed a concept-development approach using ISSHM's to explore the effect of a range of catchment and climatic controls representative of low-gradient Mediterranean-climate IRES on the threshold of flow. We focused on understanding the dominant flow generation mechanisms and the development and spatial extent of active areas at the threshold of flow generation.

Key findings from this study are:

1. Soil type exerts the greatest overall influence on streamflow generation and is the main factor determining the spatiotemporal development of active areas by a given flow generation mechanism and threshold contributing processes. The dominant flow

generation mechanism is Dunne overland flow for sandy soils, Horton overland flow for sandy loam soils, and interflow for sandy gravel soils.

2. The identified dominant mechanism for each soil demonstrated the effect of the initial groundwater head and rainfall scenarios on the timing and processes that trigger streamflow onset.
3. The tested catchment characteristics highlighted the important role of the unsaturated storage dynamics in explaining the thresholds and pathways of flow generation, which were visible from the development of active areas by a given flow generation mechanism.

1.26.2 Question 2. *Can an integrated model be used to capture the conceptualized streamflow generation processes of an intermittent stream at the catchment scale?*

An ISSHM for a medium-size Mediterranean-climate catchment in South Australia was developed to test how streamflow generation concepts and theories from smaller and simplified models would apply in a real catchment. To inform the parameterization of the numerical model and evaluate the model results, we developed a conceptual model of the catchment. The conceptual model was based on field data combined with the lessons learned from the previous question and our understanding of the geology, topography, and GW levels across the catchment.

Key findings from this study are:

1. The active areas (flow generating areas) showed distinct mechanisms developing in the three major conceptualized areas in the catchment with distinct soils and topographic characteristics. These results support the findings from the previous study, about the key roles of soil, topography, and the saturated storage dynamics as the drivers of flow generation in IRES.
2. Results provide insight on the spatiotemporal dynamics of flow generation processes at the catchment scale.
3. The spatiotemporal variability of flow generation at the catchment scale occurs in response to the different flow pathways resulting from the distinct dominant flow generation mechanisms across the catchment.

In a broader sense, the findings presented in 5.1.1 and 5.1.2 can aid management decisions when evaluating the vulnerability of a catchment dominated by a given mechanism to impacts from factors such as GW level declines, land use changes, soil erosion, and shifts on precipitation patterns. Additionally, flow generation mechanisms are key to understand flow pathways which highly influence ecosystems functions, water quality, and land surface processes (Alexander et al., 2007; Freeze, 1974; Haria & Shand, 2004; Liu et al., 2008; Zimmer & McGlynn, 2018). The insights gained from these findings highlight the importance of studying streamflow generation in IRES with a focus on understanding processes and the potential of using ISSHM as a tool to achieve this understanding.

1.26.3 Question 3. *Can we use only streambed temperature data to monitor intermittent streamflow in an intermittent Mediterranean-climate catchment?*

A novel temperature-based method based on a CWT analysis was applied to a field dataset to develop guidelines to estimate a flow/no-flow threshold and to evaluate its application and performance capturing streamflow in an intermittent Mediterranean-climate catchment in South Australia.

Key findings and developments from this study are:

1. A set of simple, repeatable, and non-site guidelines was developed to estimate the flow/no-flow threshold.
2. The CWT method with the estimated threshold showed an overall good performance capturing intermittent flow.
3. Detailed visual analysis of over 56 datasets show trends that indicate the CWT results contain information with the potential to infer ponding conditions and hydrograph peaks and recession periods.

With intermittent streams being some of the most vulnerable freshwater systems to the impacts of climate change and other human-driven impacts, understanding their seasonal flow variability is critical. Our results suggest that the CWT method can be used to generate a better understanding of the seasonal flow variability as it was observed by our ability to detect differences in the seasonal flows in response to different yearly precipitation patterns. Different

than previous similar methods, the application of the CWT analysis is simple and does not require other benchmark data, calibration periods, the calculation of complicated and site-specific set of parameters, or complicated installations. These advantages combined with the ruggedness and low cost of temperature sensors provide a valuable alternative in the use of temperature data with the CWT method to monitor intermittent streamflow in IRES.

1.27 Limitations and Future work

IRES occur all around the world, from humid and temperate, to arid and Mediterranean climates; and from small headwater streams to major rivers. In this PhD, we have focused on IRES from semi-arid catchments in Mediterranean climates with weathered geology. Therefore, some of our specific findings might not be appropriate for IRES in humid climates or alpine systems, where flow intermittency occurs in response to snowmelt and for arid catchments with summer rains. Future work should consider exploring streamflow generation in the other type of IRES with a similar focus on understanding processes and thresholds of flow generation. For instance, for areas where rainfall occurs during the summer months such as the Sonoran and Chihuahuan Deserts in North America (Pierini et al., 2014) future research should investigate the impact of ET on streamflow generation in IRES. Further considerations about the importance of considering ET in streamflow generation in IRES is discussed in section 2.7.4.

Chapters 2 and 3 highlighted important insights into the pitfalls and challenges of using ISSHM's to model streamflow generation in IRES. The large computational time to run the simulations was the major restraint we encountered from the early preliminary stages. The slow model convergence was observed particularly during the sudden state changes from dry to wet, and we attributed to the model struggling to solve the highly non-linear equations for unsaturated flow in a mostly unsaturated surface domain. While in Chapter 2 the slow convergence constrained us to use a small model domain with no further impacts, in Chapter 3 we had to relax the 2D mesh discretisation which had further implications. By relaxing the mesh, we lost the channel representation which led to a disconnection of the stream with the floodplain. As a result, we lost the ability to capture flow in the stream network (i.e. streamflow) which was the major pitfall that explains our lack of hydrograph results. These results highlight the importance of preserving channel representation to model streamflow generation on IRES. Specific advice to overcome this challenge is discuss at length in section 3.5.2.

Another challenge experienced in Chapter 3, was the determination of the initial conditions for the PM. The multi-aquifer system in our catchment made the estimation of initial GW heads an intensive and challenging task. The skewed distribution of the available shallow wells in the catchment kept us from being able to estimate a reasonable GW head raster. In our study, we tried to overcome this challenge by draining an initially saturated model until we could match the simulated GW heads with the average GW head elevation from the shallow observation wells. However, the lack of shallow wells information is likely to be a common issue that would be faced for any catchment-scale simulations of IRES elsewhere. While the GW-stream interactions were not considered critical and were outside of the scope of our study, flow intermittence in many rivers can be attributed to a water table fluctuation relative to the stream channel elevation (Snelder et al., 2013).

The main limitations of the CWT method (Chapter 4) are summarized in the bad performance of the method to capture short ephemeral events and the inability to recognize ponding water conditions. However, these limitations are comparable to those of the current existing methods as discussed in section **Error! Reference source not found.**. Additionally, the proposed guidelines still require a visual inspection to estimate the flow/no-flow threshold. Future work should attempt to automate the threshold selection and test different applications that could improve the method performance for capturing shorter ephemeral events. A further discussion into possible modifications to the method are discussed in section 4.4.3. Finally, the preliminary observations about the potential to infer ponding conditions and hydrograph peaks and recession periods should be explored in future studies.

The results from Chapters 2 and 3 on capturing the dominant flow processes are promising and provide an important insight of flow in IRES. These studies are an initial step towards understanding the thresholds and pathways of flow generation and providing insight on the challenges of implementing ISSHMs for process understanding in IRES. The results from Chapter 4 showed the potential of the CWT method to capture streamflow and generate a better understanding of the seasonal flow variability in IRES. Future work should build upon the lessons learned from this PhD to continue advancing our understanding of streamflow generation in IRES.

Appendix A

Field parameterization to determine trigger mechanisms of streamflow generation in an ephemeral-intermittent system, South Australia

American Geophysical Union, Fall Meeting, 2016

Karina Gutiérrez[1], Margaret Shanafield[2], Okke Batelaan[1], Peter Cook [2].
School of the Environment, Flinders University[1]
National Centre for Groundwater Research and Training, School of the Environment, Flinders University, Adelaide, South Australia, Australia[2]

For non-perennial streams (intermittent and ephemeral streams) the processes that control streamflow generation remain poorly understood and represent one of the greatest challenges to better understand the dynamic behavior from one of earth's most widespread water systems. This study examines an intermittent-ephemeral catchment in South Australia where little is scientifically known about the relative contributions of overland flow, soil saturation, and groundwater inflow to creek flow, although there are many well-developed hypotheses among the local vineyard owners. Detailed field data were used to characterize the hydrologic links between precipitation, antecedent soil moisture, groundwater levels, and resulting streamflow to identify triggers at the threshold to flow in the creek. A previous study in the catchment documented a complex interaction between the creek and the shallow aquifer outlining the spatially and temporally variability between losing and gaining conditions along the creek. Monitoring sites were distributed across the catchment to capture the hydrologic processes under gaining, losing and variably loosing-gaining stream conditions. Results from this study will provide of a better understanding on the controlling mechanisms of stream flow generation on non-perennial streams under varying stream conditions. Furthermore, the results are expected to be used for the development of an analytical equation to predict streamflow that will be used in development of an integrated surface water-groundwater model of the basin.

Appendix B

Streamflow generation in fully integrated surface-subsurface hydrological models for IRES with varying catchment and environmental characteristics

EGU General Assembly 2018

Karina Gutierrez (1), Margaret Shanafield (1), Daniel Partington (2), Okke Batelaan (1), and Peter Cook (2)
(1) College of Science and engineering, Flinders University, Adelaide, Australia
(2) National Centre for Groundwater Research and Training, Flinders University, Adelaide, Australia

For IRES (intermittent and ephemeral streams) the processes that control streamflow generation remain poorly understood, challenging our ability to characterize the dynamic behaviour of one of earth's most widespread water systems. With complex temporal and spatial interactions between surface water and groundwater, variable flow regimes, flashy and erosive flows, and unpredictable timing, field-based research is challenging and often not feasible in such systems. Integrated Surface-Subsurface Hydrological Models (ISSHM) can serve as a proxy to overcome these challenges. ISSHMs have been widely used in recent years for their ability to fully integrate the surface and subsurface flow domains and produce physically consistent simulations; however, most models are still limited to large scale spatial and temporal variability of the hydrological processes controlling streamflow generation The previous is particularly relevant for IRES, where streamflow generated at the catchment scale is often segmented. With losing, gaining and variably losing-gaining stream sections commonly present in IRES, it is necessary to be able to interrogate the models at any point within the catchment. ISSHMs combined with the Hydraulic Mixing-Cell method overcome this issue by allowing the identification and quantification of the contribution of all streamflow generation mechanisms to the hydrograph at any chosen point along the stream. This study implements an ISSHM coupled with the Hydraulic Mixing-Cell method to determine the main processes involved in runoff and streamflow generation for a range of synthetic catchments. A simple configuration

of a symmetrical catchment with one river crossing in the middle was used to develop the synthetic scenarios. Contrasting catchment characteristics and environmental inputs were tested to examine their influence in model results with a total of 1080 unique model combinations. Varying catchment characteristics included a round and an elongated catchment shape with Form Factors of 0.44 and 0.82 respectively, a mild (0.02) and steep (0.05) hill slope, and soil hydraulic properties for a sandy and sandy loam soil. Similarly, a total of 27 rainfall and 5 potential evapotranspiration (ET_0) inputs were developed using maximum, minimum and average values typical of a South Australian catchment with Mediterranean climate. Rainfall datasets were developed by combining three total rainfall amounts (min, max and average) with event durations of 1, 2, and 3 days and inter-event lapses of 2, 5, and 8 days. ET_0 was varied from min to max values in even increments. Additionally, hydrograph nodes were distributed every kilometer along the stream to determine the partitioning of contributing flow generation mechanisms into infiltration-saturation excess overland flow, stream interception, and groundwater discharge. The goal of this study is to understand the influences of catchment and environmental parameters and to identify the main drivers controlling streamflow generation and their spatiotemporal variability, in particular the threshold behaviour that results in IRES at the catchment scale.

Appendix C

Understanding the drivers and timing of streamflow for IRES

American Geophysical Union, Fall Meeting, 2018

Karina Gutiérrez[12], Margaret Shanafield[12], Daniel Partington[12], Okke Batelaan[12]
College of Science and Engineering, Flinders University, Adelaide, Australia[1]
National Centre for Groundwater Research and Training, Flinders University, Adelaide, Australia[2]

IRES (intermittent and ephemeral streams) make up 50% of the world's river network and are expected to increase due to projected climate shifts and the increasing demand on water resources. Understanding the timing and processes controlling streamflow generation in IRES remain the greatest challenge to manage these systems. The goal of this study is to understand the influence of groundwater depth, soil hydraulic properties, and rainfall to identify the main drivers controlling the threshold behaviour of streamflow generation in IRES. Therefore, we implement a concept development approach using an ISSHM coupled with the Hydraulic Mixing-Cell (HMC) method to provide insight into the generation mechanisms in a theoretical catchment with a temporary stream.

We tested a range of initial groundwater depths, three soil types (sand, sandy gravel and a sandy loam) and 9 rainfall applications based on the average annual exceedance probability records for arid and semiarid regions in the US and Australia. Hydrograph nodes were distributed along the river to determine the effect of contributing area and the partitioning of contributing flow generation mechanisms into infiltration-saturation excess overland flow at the hillslope and riverbed, and groundwater discharge.

Results show that soil type highly regulates streamflow generation with the sandy loam soil producing the most flow events and the sandy gravel producing the least. Rainfall influenced the generation of flow across soils. Long duration low intensity precipitation accounted for 50% of the flows generated for sandy gravel soil and 39% for sandy soil; whereas short duration high intensity rainfall accounted for 50% of generated flows for sandy loam. Depth to groundwater

had a greater effect on the timing of the first flow for sandy gravel and sandy soils than for sandy loam. Dominant mechanisms are mainly influenced by the soil type. For the sandy loam soil flow generation is dominated by infiltration excess overland flow; the sandy gravel dominant mechanism is saturation excess infiltration discharging as interflow to the river; and for sand the dominant mechanism is saturation excess overland flow on the river channel. This study is a first step to advance our understanding on controls of flow generation for IRES.

Appendix D

Streamflow generation mechanisms for an intermittent-ephemeral catchment in South Australia: a modelling approach

Australasian Groundwater Conference, 2019

Karina Y. Gutierrez-Jurado [1], Margaret Shanafield [1], Daniel Partington [1]
Flinders University, Bedford Park, SA, Australia

In Australia, Intermittent Rivers and Ephemeral Streams (IRES) are the common features that dominate the landscape. Contributing with roughly 70% of the stream network, IRES are key for ecosystems health, are important for farming and agriculture and represent a main source of groundwater recharge. However, the understanding of streamflow generation mechanisms for IRES remains a challenge. This study examines an intermittent-ephemeral catchment in South Australia where little is scientifically known about the processes leading to streamflow generation and the contributing mechanisms, although there are many well-developed hypotheses among the local vineyard owners. Previous research in the catchment has shown complex spatiotemporal interactions between the creek and the shallow aquifer, outlining changes in losing and gaining conditions along the creek during the intermittent flow season. We used a fully integrated surface-subsurface hydrological model coupled with the Hydraulic Mixing-Cell method to investigate the processes leading to the onset of flow for the intermittent season and to determine the spatiotemporal variability of the streamflow generation mechanisms. For this, we analyzed the development of flow generating areas and the dominant contributing flow generation mechanisms at different locations along the catchment at the onset of flow, and during the transition from ephemeral to intermittent flow. The expected results from this study will allow us to better understand streamflow generation at the threshold of flow and at the transition from ephemeral to intermittent flow for an intermittent-ephemeral creek in South Australia. This will be useful to aid IRES management decisions such as those pertaining to ecosystems health monitoring, the vulnerability of the catchment to the effects of droughts, and potential impacts of declines to the shallow groundwater system.

Appendix E

Chronological summary of relevant literature on runoff-streamflow generation studies using ISSHMs

Study	Aims	Model	Catchment regime	Catchment Size	Major outcomes
Vanderkwaak & Loague, 2001	Rainfall-runoff for streamflow generation processes	InHM	Intermittent	0.1 km^2	Both Horton and Dunne overland flow mechanisms contribute to the rainfall-runoff response
Ivanov et al., 2004	Test the use of irregular spatial discretization for large scale basins	tRIBS	Perennial	800-1600 km^2	Spatially variable hydrologic response due to rainfall, topography, soils, and land use/vegetation which suggest that distributed information on such parameters has potential for large scale hydrologic forecasting
Jones 2006	Study the hydrodynamic mixing processes to understand pre-event water contributions to streamflow generation	InHM	Ephemeral	0.001 km^2	Hydrodynamic mixing processes influence pre-event water estimates which might be problematic in quantifying groundwater contributions to streamflow by tracer-based separation techniques.

Vivoni et al., 2007	Transient runoff response in a catchment with heterogeneous properties and a varying range of initial conditions and rainfall forcing.	tRIBS	Perennial	65-808 km^2	Partition of runoff generation mechanisms affect the non-linear and scale-dependent basin response.
Jones et al., 2008	Reproduce surface-subsurface hydrodynamic processes at the catchment scale with a rainfall-runoff approach	InHM	Perennial	75 km^2	Model reproduced relatively well the rainfall-runoff response for both transient flow simulations.
Sudicky et al., 2008	Evaluate model performance to reproduce surface-subsurface flow characteristics and transport processes in transient and steady state simulations	HGS	Perennial	17 km^2	Simulated hydraulic head distribution and rainfall-runoff response agreed well with observed values demonstrating the capability of the model to reproduce fully integrated hydrodynamic processes at the catchment scale
Frei et al., 2010	Evaluate the effects of micro-topography on surface-subsurface interactions and runoff generation	HGS	Perennial	0.002 km^2	Micro-topography induce complex threshold processes and a dynamic surface flow network that by expansion and contraction governs streamflow generation and determines the surface or subsurface flow dominance

Park et al., 2011	Quantify and identify the sources of the hydrologic response to precipitation as overland and groundwater flow and to identify temporal and spatial variations of these processes	HGS	Perennial	0.002 km^2	Precipitation intensity greatly influences the contribution proportion of subsurface mechanical flow and mixing processes can be useful to enhance tracer signals used to identify streamflow source.
Mirus & League, 2013	To quantitatively characterize the environmental controls on runoff generation mechanisms	InHM	Ephemeral?	0.001-0.1 km^2	Runoff generation is highly influenced by relative rates of rainfall, infiltration, lateral flow convergence and storage dynamics in the soil.
Weill et al., 2013	Characterize links between runoff generation processes and saturated area dynamics	CATHY	Ephemeral	1.5 km^2	Surface topography is an important control on the evolution of saturated area patterns which determines dominant streamflow generation processes
Partington et al., 2013	Quantify in-stream and overland flow generation mechanisms at the catchment scale	HGS	Perennial	0.2-4.2 km^2	Improved Hydraulic Mixing-Cell method was developed to enable the distinction between active and contributing processes to quantify the streamflow generation mechanisms at the catchment scale.

Frei & Fleckenstein, 2014	Evaluate the use spatially distributed rill/depression storage zones to represent the effects of micro-topography on runoff generation.	HGS	Wetland	0.002 km^2	Rill/depression storage zones effectively represent the effect of micro-topography and adequately mimic runoff generation processes.
Pierini et al., 2014	Study the effects of mesquite encroachment on runoff thresholds	tRIBS	Ephemeral	0.01 km^2	The fraction of grass/bare soil is the main determining factor explaining the runoff response to different rainfall events
Ala-aho et al., 2017	Understand groundwater role in streamflow generation	HGS	Perennial	3.2 km^2	Groundwater contributions to streamflow occur mainly by saturation excess overland flow.

Appendix F

Map of Pedler Creek showing the full stream network extent and the discretized streams for the ISSHM

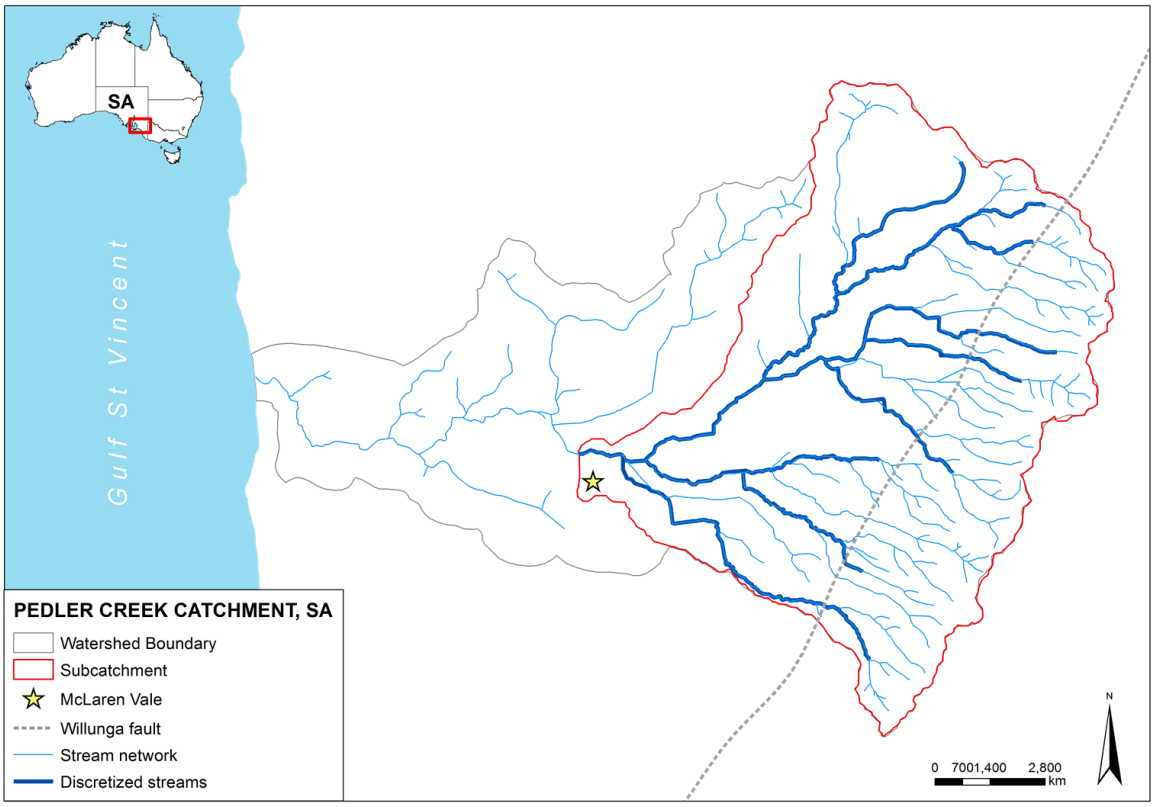

Appendix G

Different representations of the surface topography showing the original DEM and the post-processed DEM with the different incision values.

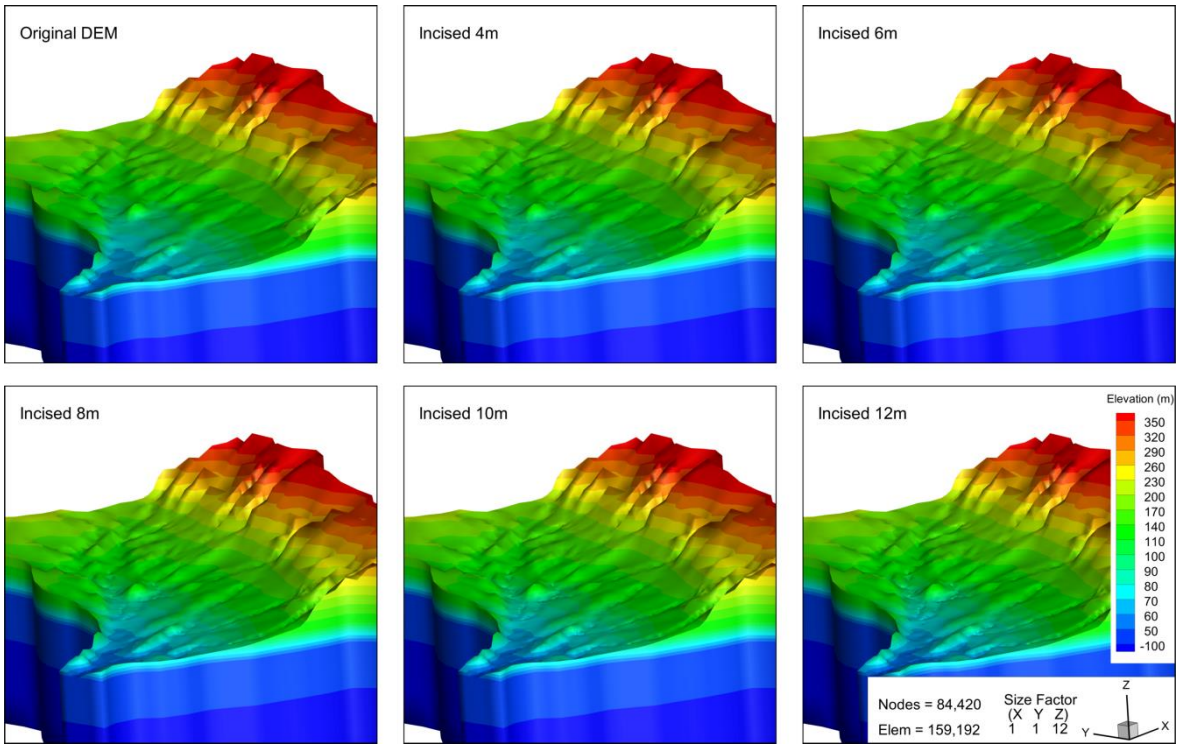

Appendix H

Sites containing soil information used for the conceptual model and for the ISSM parameterization.

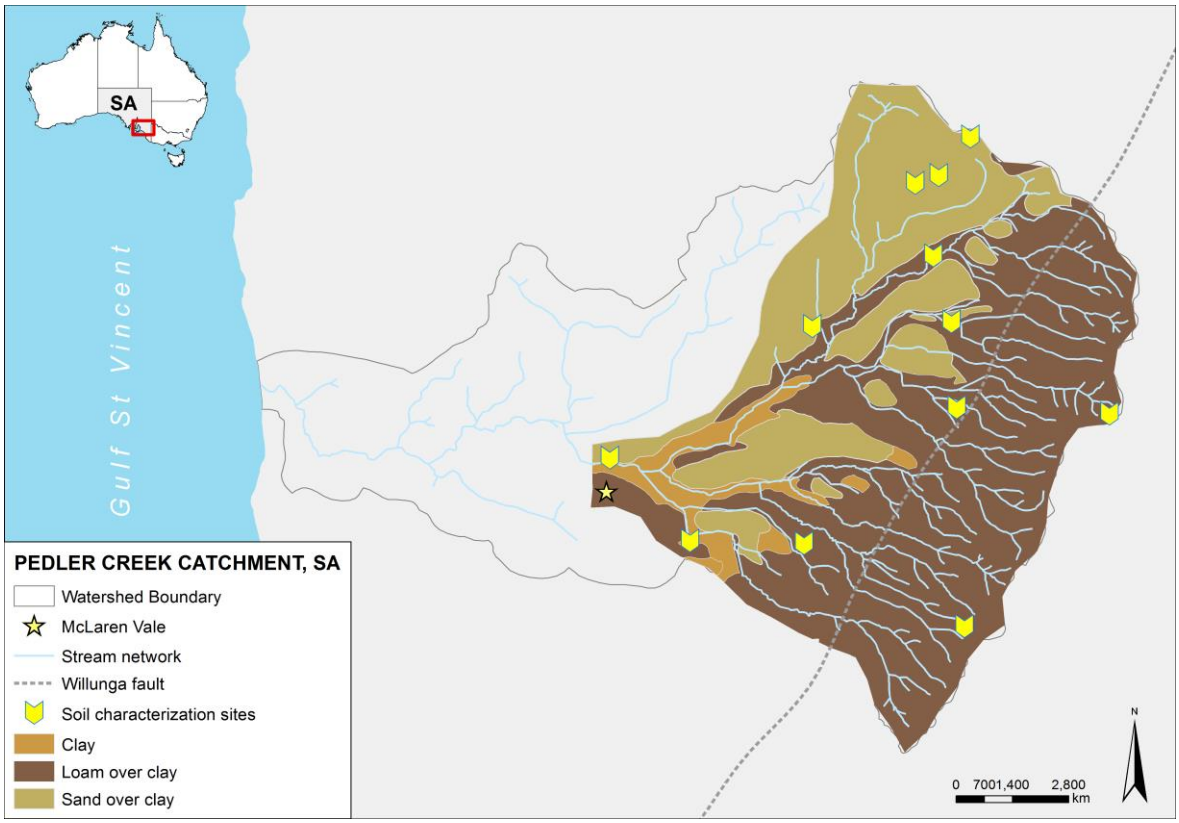

Site number	Soil name	Model Category	Clay layer Depth (cm)
CH066	Sand over acidic clay	Sand	75
CH079	Thick sand over wet sandy clay loam	Sand	110
CH082	Sand over acidic clay	Sand	90
CH092	Sandy loam over poorly structured brown clay	Sand	0.65
CH093	Loamy sand over poorly structured red clay	Sand	40
CH146	Deep bleached sand	Sand	105
CH147	Deep bleached sand	Sand	100
CH081	Silty loam over brown clay	Loam	28
CH091	Acidic loam over red clay on weathered rock	Loam	28
CH140	Ironstone loamy sand over red mottled clay	Loam	42
CH145	Loam over coarsely structured brown clay	Loam	32
CH155	Loam over red clay on rock	Loam	25
CH148	Black clay over buried clay loamy duplex soil	Clay	-NA

Appendix I

Soil sheet ID & Title	Soil Characterisation description	Depth cm	Textural Class	Sand %	Silt %	Clay %	θr	θs	α 1/m	β --	Ks m/d
CH77 Black Cracking Clay	Black well-structured highly calcareous clay (cracks when dry)	0-10	Clay	24	19	57	0.096	0.475	2.202	1.208	0.166
	Black and greyish brown finely structured highly calcareous heavy clay	0-35	Clay	20	17	63	0.098	0.486	2.203	1.190	0.163
CH078 Gradational Red Clay Loam	Dark brown clay loam with strong granular structure	0-11	SaCL	48	19	33	0.077	0.407	2.326	1.295	0.077
	Dark reddish brown friable medium clay	20-50	Clay	17	6	77	0.100	0.488	2.169	1.146	0.153
	Olive brown and orange sandy medium clay with blocky structure, 10-20% soft carbonate, and 2-10% shale and quartz gravel.	120-170	SaCL	59	12	29	0.071	0.387	2.682	1.285	0.121
Ch079 Thick sand over wet Sandy Clay Loam	Black soft loamy sand	0-10	Sand	95	2	3	0.054	0.375	3.224	3.331	7.227
	Grey and green mottled sandy clay loam with coarse blocky structure (buried soil)	135-150	SaCL	75	3	22	0.065	0.369	2.496	1.365	0.191
CH80 Sandy Loam over poorly structured red clay	Firm dark brown fine sandy loam with moderate granular structure and up to 10% ironstone gravel	0-15	Sandy Loam	63	19	17	0.055	0.383	2.764	1.369	0.251
	Hard massive dark reddish brown clay loam with up to 10% ironstone gravel	15-30	Clay Loam	44	22	33	0.078	0.411	2.062	1.314	0.065
	Firm dark reddish brown medium clay with coarse prismatic breaking to polyhedral structured medium clay	30-60	Clay	15	9	75	0.100	0.492	2.152	1.156	0.158
CH81 Silty Loam over Brown Clay	Dark grey weakly structured silty loam	0-15	Loam	51	37	12	0.046	0.391	1.466	1.453	0.225
	Grey and dark brown mottled medium clay with strong blocky structure	28-55	Clay Loam	38	25	37	0.083	0.429	1.900	1.312	0.052
CH82 Sand over Acidic Clay	Dark grey loose sand	0-10	Sand	96	1	3	0.055	0.374	3.142	3.488	8.241
	Orange and brown sandy light clay with blocky structure	90-120	Sandy Clay	54	1	45	0.084	0.399	2.850	1.184	0.187

Appendix J

Initial Groundwater Head Approximation

Preliminary analysis of GW levels to obtain the initial conditions of the porous media. We selected wells that range in depth from 0-30 m from the water connect portal for the McLaren Vale prescribed well area. From a total of 393 wells in the area (Subplot a&c) we filtered wells with at least 3 observations from the year 2000 onwards (Subplot b&d). A total of 47 wells meet the selection criteria and were used to create an average GW elevation head. The raster was created using the "multiquadric" radial basis function approximation/interpolation for scatter data from the Scipy library on Python (Subplot e). A final GW raster was created (subplot g)by correcting the interpolated raster with the surface elevation (subplot f).

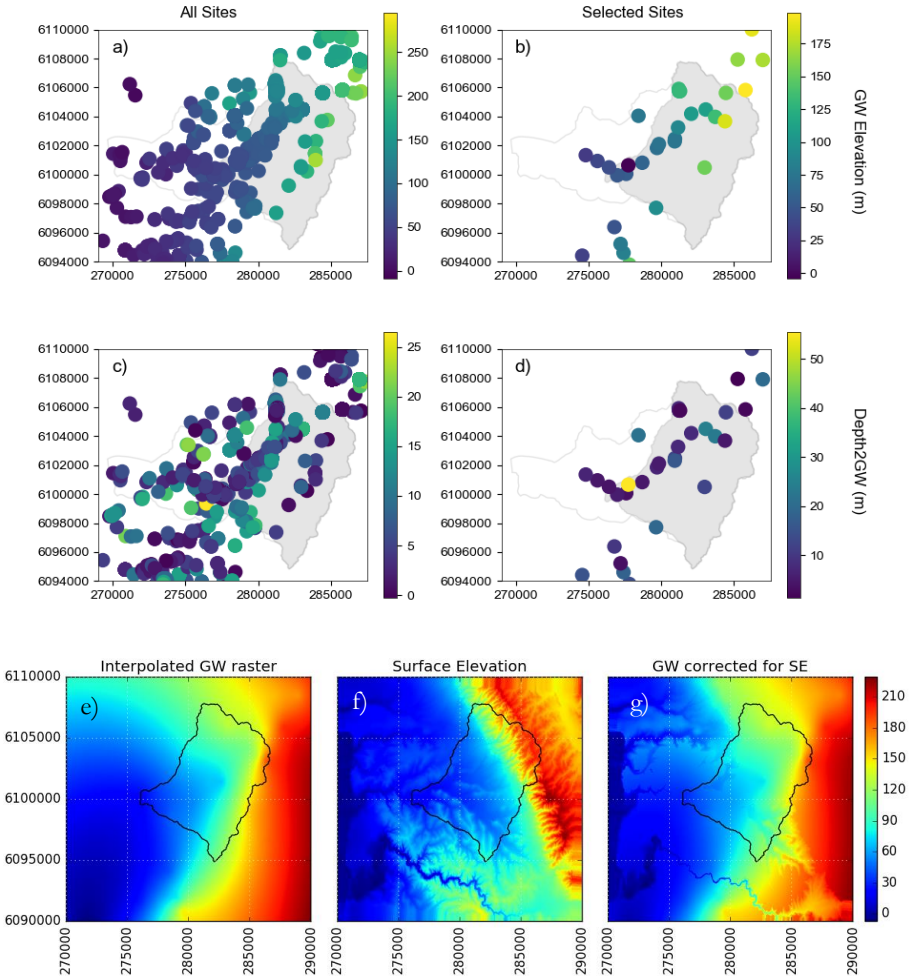

Appendix K

Comparison of observed versus simulated GW elevations from the final selected model output time.

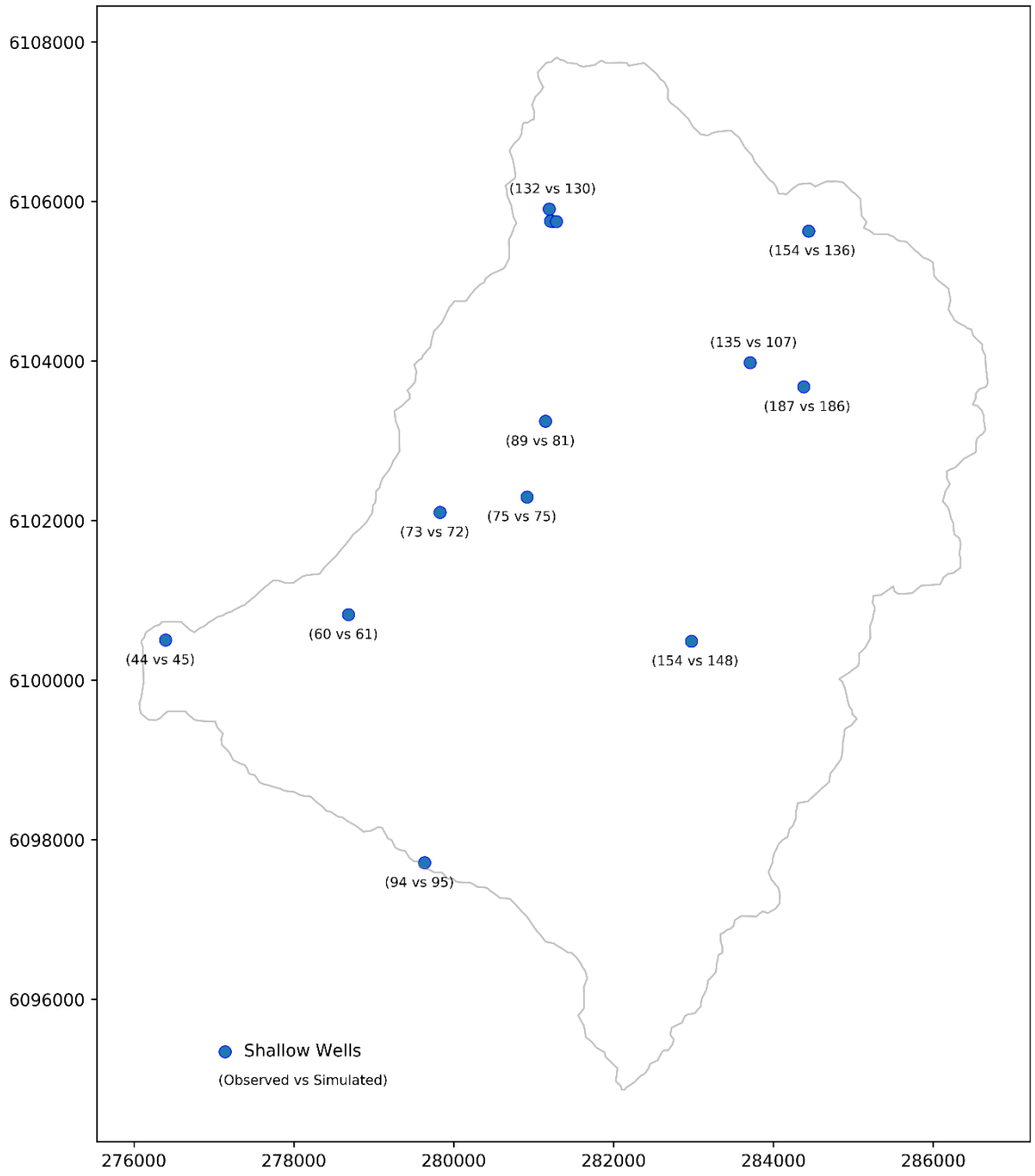

Appendix L

Comparison of the observed versus the simulated GW elevations from the selected model output time.

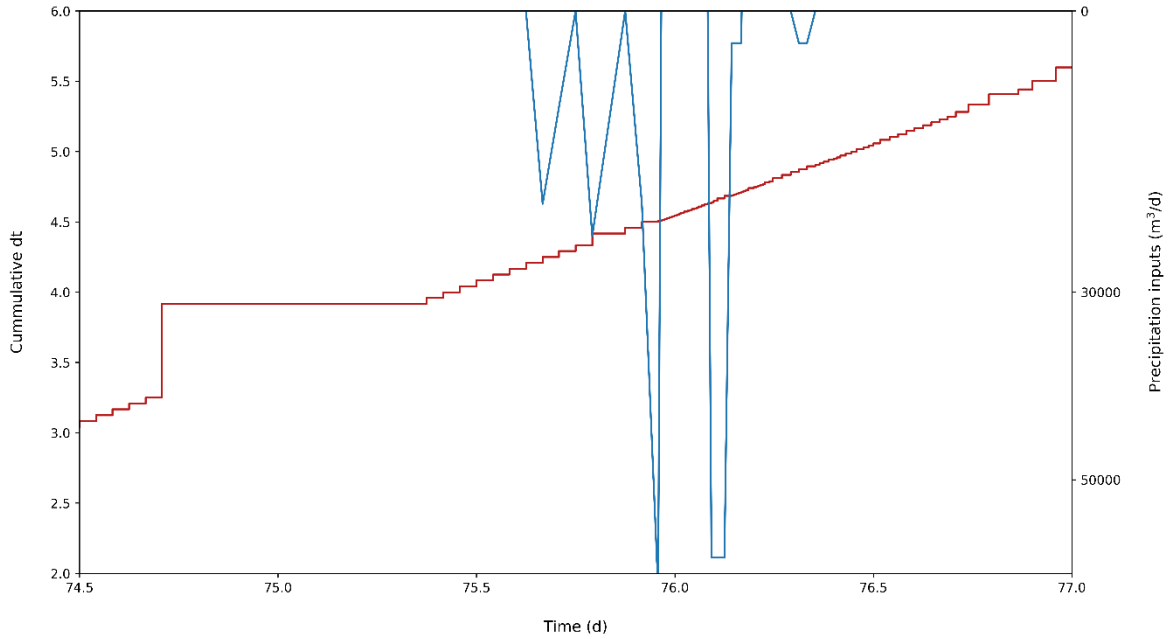

Appendix M

Comparison of the performance of the CWT with the Selected and Estimated Thresholds for each site and year.

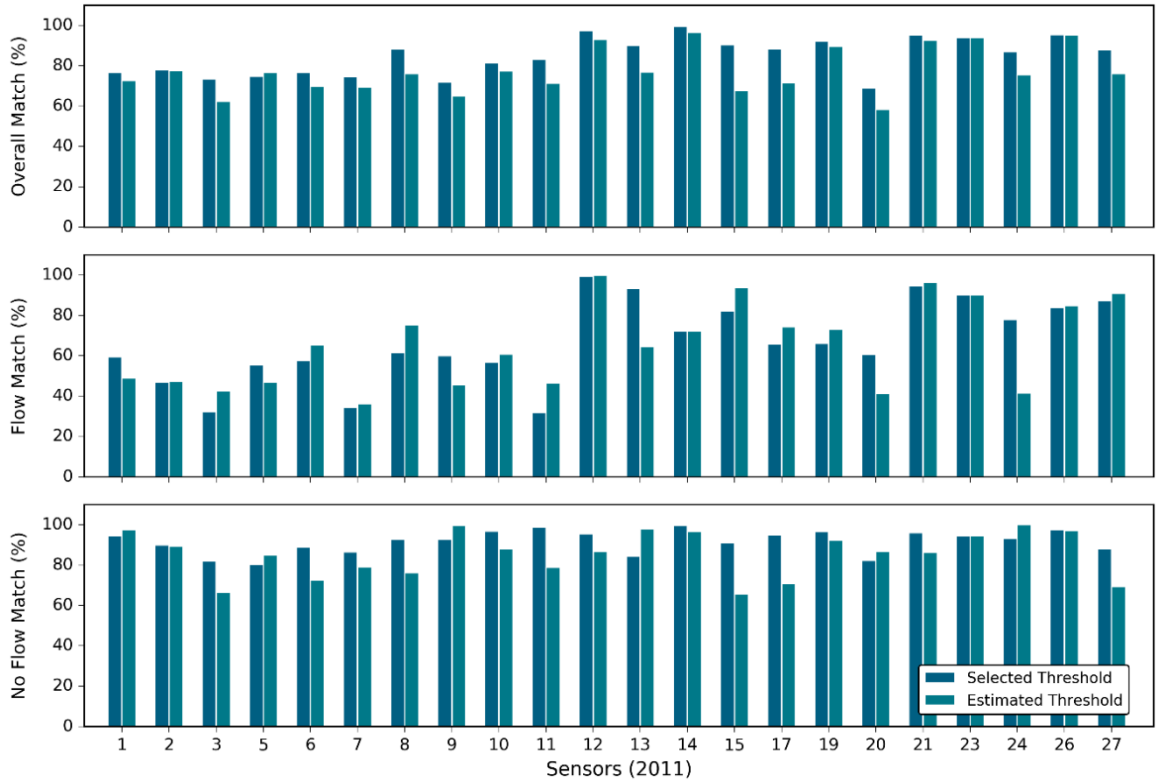

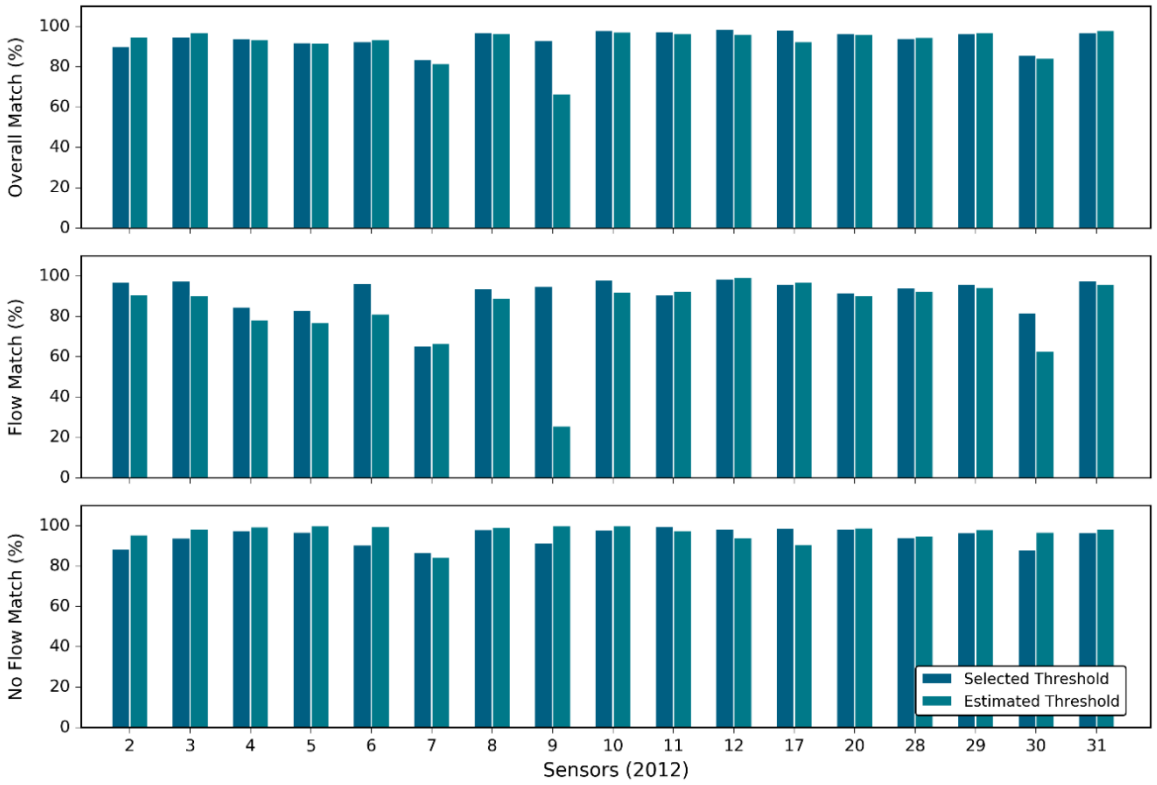
Overall Match (%)
Flow Match (%)
No Flow Match (%)
0
20
40
60
80
100
Selected Threshold
Estimated Threshold
2
3
4
5
6
7
8
9
10
11
12
17
20
28
29
30
31
Sensors (2012)

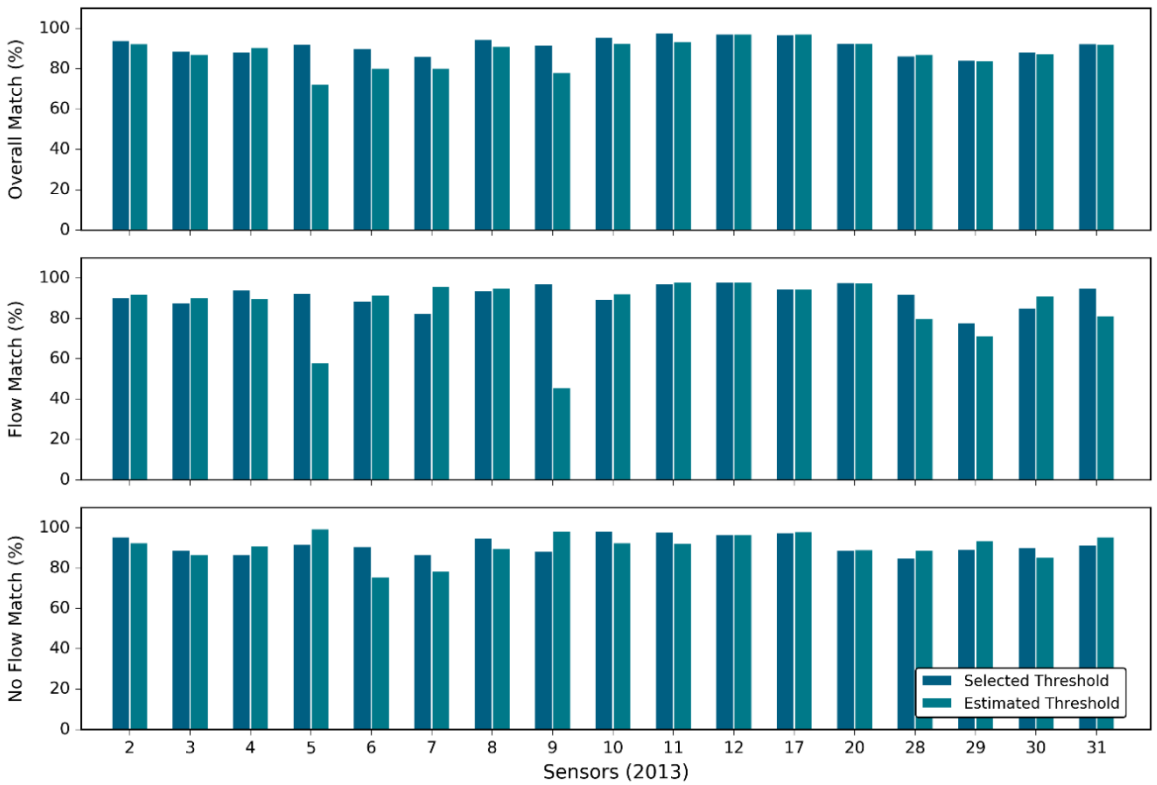
Overall Match (%)
Flow Match (%)
No Flow Match (%)
0
20
40
60
80
100
Selected Threshold
Estimated Threshold
2
3
4
5
6
7
8
9
10
11
12
17
20
28
29
30
31
Sensors (2013)

Bibliography

Abdul, A. S. (1985). Experimental and numerical studies of the effect of the capillary fringe on streamflow generation. Ph. D Thesis, 210 pp., University of Waterloo, Ontario, Canada.

Abdul, A. S., & Gillham, R. W. (1984). Laboratory studies of the effects of the capillary fringe on streamflow generation. Water Resources Research, 20(6), 691‐698. https://doi.org/ 10.1016/0022-1694(89)90177-7

Acuña, V., Datry, T., Marshall, J., Barceló, D., Dahm, C. N., Ginebreda, A., et al. (2014). Why should we care about temporary waterways? Science, 343(6175), 1080‐1081. https://doi.org/ 10.1126/science.1246666

Ala-aho, P., Soulsby, C., Wang, H., & Tetzlaff, D. (2017). Integrated surface-subsurface model to investigate the role of groundwater in headwater catchment runoff generation: A minimalist approach to parameterisation. Journal of Hydrology, 547, 664‐677. https://doi.org/10.1016/ j.jhydrol.2017.02.023

Alexander, R. B., Boyer, E. W., Smith, R. A., Schwarz, G. E., & Moore, R. B. (2007). The role of headwater streams in downstream water quality. Journal of the American Water Resources Association, 43(1), 41‐59. https://doi.org/10.1111/j.1752-1688.2007.00005.x

Aldam, R.G. (1989). Willunga Basin hydrogeological investigations 1986/88. South Australia Department of Mines and Energy. Report Book, 89/22.

Aldam, R. G. (1990). Willunga Basin Groundwater Investigation Summary Report. Groundwater and Engineering, Department of Mines and Energy, Government of South Australia. Report Book, 90/71

Aldridge, B. N. (1970). Floods of November 1965 to January 1966 in the Gila River basin, Arizona and New Mexico, and adjacent basins in Arizona. US Geological Survey Water-Supply Paper 1850-C, 176 p. https://doi.org/10.3133/wsp1850C

Ambroise, B. (2004). Variable 'active' versus 'contributing' areas or periods: A necessary distinction. Hydrological Processes, 18, 1149‐1155. https://doi.org/10.1002/hyp.5536

Anders, L. (2012). Surface - Water and Groundwater Interactions Along Pedler Creek, (December). M.Sc Thesis, 117 pp., Flinders University, SA, Australia.

Anderson, M. P., Woessner, W. W., & Hunt, R. J. (2015). Applied groundwater modeling:

simulation of flow and advective transport. Academic press (second edition).

Aquanty (2016). HydroGeoSPhere user manual, Release 1.0. Waterloo, Ontario, Canada: Aquanty Inc.

Arismendi, I., Dunham, J. B., Heck, M. P., Schultz, L. D., & Hockman-Wert, D. (2017). A statistical method to predict flow permanence in dryland streams from time series of stream Temperature. Water (Switzerland), 9(12). https://doi.org/10.3390/w9120946

Assendelft, R. S., & van Meerveld, H. J. I. (2019). A low-cost, multi-sensor system to monitor temporary stream dynamics in mountainous headwater catchments. Sensors (Switzerland), 19(21). https://doi.org/10.3390/s19214645

Australian Government Bureau of Meteorology. (2018). 2016 Rainfall IFD data system. Retrieved August 31, 2018, from http://www.bom.gov.au/water/designRainfalls/revised-ifd/

Batlle-Aguilar, J., Xie, Y., & Cook, P. G. (2015). Importance of stream infiltration data for modelling surface water–groundwater interactions. Journal of Hydrology, 528(July 2015), 683–693. https://doi.org/10.1016/j.jhydrol.2015.07.012

Betson, R. P. (1964). What is watershed runoff? Journal of Geophysical Research, 69(8), 1541-1552. https://doi.org/10.1029/JZ069i008p01541

Blasch, K. W., Ferré, T. P. A., Christensen, A. H., & Hoffmann, J. P. (2002). New field method to determine streamflow timing using electrical resistance sensors. Vadose Zone Journal, 1(2), 289-299. https://doi.org/10.2113/1.2.289

Blasch, K. W., Ferré, T. P. A., & Hoffmann, J. P. (2004). A statistical technique for interpreting streamflow timing using streambed sediment thermographs. Vadose Zone Journal, 3, 936-946. https://doi.org/10.2136/vzj2004.0936

Bond, N., & Cottingham, P. (2008). Ecology and hydrology of temporary streams: Implications for sustainable water management. eWater Technical Report. eWater Cooperative Research Centre, Canberra. Retrieved from https://ewater.org.au/uploads/files/Bond_Cottingham-2008-Temporary_Streams.pdf

Boulton, A. J., Rolls, R. J., Jaeger, K. L., & Datry, T. (2017). Hydrological connectivity in intermittent rivers and ephemeral streams. In Intermittent rivers and ephemeral streams (pp. 79-108). Academic Press.

Brown, K. G. (2004). Groundwater contributions to streamflow along Willunga Fault, McLaren

Vale, South Australia.

Brunner, P., & Simmons, C. T. (2012). HydroGeoSphere: A fully integrated, physically based hydrological model. Ground Water, 50(2), 170‐176. https://doi.org/10.1111/j.17456584. 2011. 00882.x

Campana, M. E., & Simpson, E. S. (1984). Groundwater residence times and recharge rates using a discrete-state compartment model and 14C data. Journal of Hydrology, 72, 171‐185. https://doi.org/10.1016 /0022-1694(84)90190-2

Cappus, P. (1960). Bassin expérimental d'Alrance–Étude des lois de l'Écoulement–Application au calcul et à la prévision des débits. La Houille Blanche. A., 493‐514. https://doi.org/10.1051/ lhb/1960007

Carr, A. E., Loague, K., & VanderKwaak, J. E. (2014). Hydrologic-response simulations for the North Fork of Caspar Creek: Second-growth, clear-cut, new-growth, and cumulative watershed effect scenarios. Hydrological Processes, 28(3), 1476‐1494. https://doi.org/ 10.1002/hyp.9697Use the "Insert Citation" button to add citations to this document.

Chiu, M., Leigh, C., Mazor, R., Cid, N., & Resh, V. (2017). Chapter 5.1 Anthropogenic threats to intermittent rivers and ephemeral streams. In T. Datry, N. Bonada, & A. Boulton (Eds.), Intermittent Rivers and Ephemeral Streams, (pp. 433‐454). Academic Press. https://doi.org/ 10.1016/b978-0-12-803835-2.00017-6

Chow, V. T. (1959). Open channel hydraulics (p. 680). New York: McGraw-Hill.

Constantz, J., Stonestrom, D., Stewart, A. E., Niswonger, R., & Smith, T. R. (2001). Analysis of streambed temperatures in ephemeral channels to determine streamflow frequency and duration. Water Resources Research, 37(2), 317‐328. https://doi.org/10.1029/ 2000WR900271

Costa, A. C., Foerster, S., de Araújo, J. C., & Bronstert, A. (2013). Analysis of channel transmission losses in a dryland river reach in north-eastern Brazil using streamflow series, groundwater level series and multi-temporal satellite data. Hydrological Processes, 27(7), 1046–1060. https://doi.org/10.1002/hyp.9243

Costigan, K. H., Jaeger, K. L., Goss, C. W., Fritz, K. M., & Goebel, P. C. (2016). Understanding controls on flow permanence in intermittent rivers to aid ecological research: integrating meteorology, geology and land cover. Ecohydrology, 9(7), 1141‐1153. https://doi.org/

10.1002/eco.1712

Costigan, K. H., Kennard, M. J., Leigh, C., Sauquet, E., Datry, T., & Boulton, A. J. (2017). Flow regimes in intermittent rivers and ephemeral streams. In Intermittent rivers and ephemeral streams (pp. 51-78). Academic Press

Datry, T., Corti, R., Foulquier, A., von Schiller, D., & Tockner, K. (2016). One for all, all for one: A global river research network. Eos, 97(15), 12‐15. https://doi.org/10.1029/2016EO053587

Datry, T., Larned, S. T., & Tockner, K. (2014). Intermittent rivers: A challenge for freshwater ecology. BioScience, 64(3), 229–235. https://doi.org/10.1093/biosci/bit027

Davies, B. R., O'keeffe, J. H., Snaddon, C. D., & Water Research Commission. (1993). A synthesis of the ecological functioning, conservation and management of South African river ecosystems.

DEWNR, Soil and Land Program (2016). Soil Characterisation Sites. Retrieved on: 10 June 2018 from: https://data.sa.gov.au/data/dataset/soil-characterisation-sites

Di Giammarco, P., Todini, E., & Lamberti, P. (1996). A conservative finite elements approach to overland flow: The control volume finite element formulation. Journal of Hydrology, 175(1‐4), 267‐291. https://doi.org/10.1016/S0022-1694(96)80014-X

Doble, R., Brunner, P., McCallum, J., & Cook, P. G. (2012). An analysis of river bank slope and unsaturated flow effects on bank storage. Groundwater, 50(1), 77-86. https://doi:10.1111 j.1745-6584.2011.00821.x

Dore, M. H. I. (2005). Climate change and changes in global precipitation patterns: What do we know? Environment International, 31(8), 1167‐1181. https://doi.org/10.1016/j.envint.2005. 03.004

Dunne, T., & Black, R. D. (1970). An experimental investigation of runoff production in permeable soils. Water Resources Research, 6(2), 478‐490. https://doi.org/10.1029/WR006i002p00478

Durighetto, N., Vingiani, F., Bertassello, L. E., Camporese, M., & Botter, G. (2020). Intraseasonal Drainage Network Dynamics in a Headwater Catchment of the Italian Alps. Water Resources Research, 56(4). https://doi.org/10.1029/2019WR025563

DWLBC. (2016). Soils (soil type). Department for Environment and Water. Retrieved on: 10 June 2018 from: https://data.sa.gov.au/data/dataset/soil-type

Ebel, B. A., Loague, K., Montgomery, D. R., & Dietrich, W. E. (2008). Physics-based continuous simulation of long-term near-surface hydrologic response for the Coos Bay experimental catchment. Water Resources Research, 44, W07417. https://doi.org/10.1029/ 2007WR006442

Ebel, B. A, Loague, K., VanderKwaak, J. E., Dietrich, W. E., Montgomery, D. R., Torres, R, & Anderson, S. P. (2007). Near-surface hydrologic response for a steep, unchanneled catchment near Coos Bay, Oregon. 2. Comprehensive physics-based simulations. American Journal of Science, 307, 678‐708. https://doi.org/10.2475/04.2007.03.

Ebel, B. A., Rengers, F. K., & Tucker, G. E. (2016). Observed and simulated hydrologic response for a first-order catchment during extreme rainfall 3 years after wildfire disturbance. Water Resources Research, 52, 9367‐9389. https://doi.org/10.1002/2016WR019110

Falke, J. A., Fausch, K. D., Magelky, R., Aldred, A., Durnford, D. S., Riley, L. K., et al. (2011). The role of groundwater pumping and drought in shaping ecological futures for stream fishes in a dryland river basin of the western Great Plains, USA. Ecohydrology, 4(5), 682‐697. https://doi.org/10.1002/eco.158

Fatichi, S., Vivoni, E., Ogden, F. L., Ivanov, V. Y., Mirus, B., Gochis, D., et al. (2016). An overview of current applications, challenges, and future trends in distributed process-based models in hydrology. Journal of Hydrology, 537, 45‐60. https://doi.org/10.1016/ j.jhydrol.2016.03.026

Fekete, B. M., & Vörösmarty, C. J. (2007). The current status of global river discharge monitoring and potential new technologies complementing traditional discharge measurements. IAHS Publication, 309, 129–136.

Freeman, M. C., Pringle, C. M., & Jackson, C. R. (2007). Hydrologic connectivity and the contribution of stream headwaters to ecological integrity at regional scales. Journal of the American Water Resources Association, 43(1), 5–14. https://doi.org/10.1111/j.1752-1688.2007.00002.x

Freeze, R. A. (1974). Streamflow generation. Reviews of Geophysics, 12(4), 627‐647. https://doi.org/10.1029/RG012i004p00627

Freeze, R. A., & Harlan, R. L. (1969). Blueprint for a physically-based, digitally-simulated

hydrologic response model. Journal of Hydrology, 9(3), 237‐258. https://doi.org/10.1016/ 0022-1694(69)90020-1

Frei, S., & Fleckenstein, J. H. (2014). Representing effects of micro-topography on runoff generation and sub-surface flow patterns by using superficial rill/depression storage height variations. Environmental Modelling and Software, 52, 5‐18. https://doi.org/10.1016/j.envsoft.2013.10.007

Frei, S., Lischeid, G., & Fleckenstein, J. H. (2010). Effects of micro-topography on surface‐subsurface exchange and runoff generation in a virtual riparian wetland-A modeling study. Advances in Water Resources, 33(11), 1388‐1401. https://doi.org/10.1016/j.advwatres.2010.07.006

Frisbee, M. D., Phillips, F. M., Campbell, A. R., Liu, F., & Sanchez, S. A. (2011). Streamflow generation in a large, alpine watershed in the southern Rocky Mountains of Colorado: Is streamflow generation simply the aggregation of hillslope runoff responses? Water Resources Research, 47, 1‐18. https://doi.org/10.1029/2010WR009391 W06512

Fritz, K. M., Hagenbuch, E., D'Amico, E., Reif, M., Wigington, P. J., & Leibowitz, et al. (2013). Comparing the extent and permanence of headwater streams from two field surveys to values from hydrographic databases and maps. Journal of the American Water Resources Association, 49(4), 867‐882. https://doi.org/10.1111/jawr.12040

Fritz, K. M., Johnson, B. R., & Walters, D. M. (2008). Physical indicators of hydrologic permanence in forested headwater streams. Journal of the North American Benthological Society, 27(3), 690‐704. https://doi.org/10.1899/07-117.1

Godsey, S. E., & Kirchner, J. W. (2014). Dynamic, discontinuous stream networks: Hydrologically driven variations in active drainage density, flowing channels and stream order. Hydrological Processes, 28, 5791‐5803. https://doi.org/10.1002/hyp.10310

Goulsbra, C., Evans, M., & Lindsay, J. (2014). Temporary streams in a peatland catchment: Pattern, timing, and controls on stream network expansion and contraction. Earth Surface Processes and Landforms, 39(6), 790‐803. https://doi.org/10.1002/esp.3533

Goulsbra, C. S., Lindsay, J. B., & Evans, M. G. (2009). A new approach to the application of electrical resistance sensors to measuring the onset of ephemeral streamflow in wetland environments. Water Resources Research, 45, 1‐7. https://doi.org/10.1029/

2009WR007789

Guilbert, J., Betts, A. K., Rizzo, D. M., Beckage, B., & Bomblies, A. (2015). Characterization of increased persistence and intensity of precipitation in the northeastern United States. Geophysical Research Letters, 42, 1888‐1893. https://doi.org/10.1002/2015GL063124

Gungle, Bruce, 2006, Timing and duration of flow in ephemeral streams of the Sierra Vista Subwatershed of the Upper San Pedro Basin, Cochise County, southeastern Arizona: U.S. Geological Survey Scientific Investigations Report 2005–5190, 47 p.

Gutierrez-Jurado, K. Y., Partington, D., Batelaan, O., Cook, P., & Shanafield, M. (2019). What triggers streamflow for Intermittent Rivers and Ephemeral Streams in Low-Gradient Catchments in Mediterranean Climates. Water Resources Research, 55, 9926–9946. https://doi.org/10.1029/2019WR025041

Hall, J. A. S., Maschmedt, D. J., & Billing, B. (2009). The soils of southern South Australia. Department of Water, Land and Biodiversity Conservation, Government of South Australia.

Hallema, D. W., Moussa, R., Sun, G., & Mcnulty, S. G. (2016). Surface storm flow prediction on hillslopes based on topography and hydrologic connectivity. Ecological Processes, 5(1), 1‐13. https://doi.org/10.1186/s13717-016-0057-1

Haria, A. H., & Shand, P. (2004). Evidence for deep sub-surface flow routing in forested upland Wales: Implications for contaminant transport and stream flow generation. Hydrology and Earth System Sciences, 8(3), 334‐344. https://doi.org/10.5194/hess-8-334-2004

Harrington, G. A. (2002). Recharge mechanisms to Quaternary sand aquifers in the Willunga Basin, South Australia. Department of Water, Land and Biodiversity Conservation.

Hathaway, D.L., Ha, T.S., and Hobson, A. (2002). Transient Riparian Aquifer and Stream Exchanges along the San Joaquin Stream. In Proceedings of the Ground Water/Surface Water Interactions, AWRA 2002 Summer Specialty Conference, July 1-3, 2002, Colorado, 169-174.

Head, L., Adams, M., Mcgregor, H. V., & Toole, S. (2014). Climate change and Australia. Wiley Interdisciplinary Reviews: Climate Change, 5, 175‐197. https://doi.org/10.1002/wcc.255

Heppner, C. S., & Loague, K. (2008). A dam problem: Simulated upstream impacts for a Searsville-like watershed. Ecohydrology, 1(4), 408‐424. https://doi.org/10.1002/eco.34

Heppner, C. S., Loague, K., & VanderKwaak, J. E. (2007). Long-term InHM simulations of

hydrologic response and sediment transport for the R-5 catchment. Earth Surface Processes and Landforms, 32(9), 1273-1292. https://doi.org/10.1002/esp.1474

Hewlett, J. D., & Hibbert, A. R. (1967). Factors affecting the response of small watersheds to precipitation in humid areas. In W. E. Sopper, & H. W. Lull (Eds.), International Symposium on Forest Hydrology, (pp. 275-290). Oxford, UK: Pergamon.

Hopp, L., & McDonnell, J. J. (2009). Connectivity at the hillslope scale: Identifying interactions between storm size, bedrock permeability, slope angle and soil depth. Journal of Hydrology, 376, 378-339. https://doi.org/10.1016/j.jhydrol.2009.07.047

Horton, R. E. (1932). Drainage-basin characteristics. Eos, Transactions American Geophysical Union, 13(1), 350-361. https://doi.org/10.1029/TR013i001p00350

Horton, R. E. (1945). Erosional development of streams and their drainage basins; hydrophysical approach to quantitative morphology. Bulletin of the Geological Society of America, 56(3), 275-370. https://doi.org/10.1130/0016-7606(1945)56[275:EDOSAT]2.0.CO;2

Huntington, J. L., & Niswonger, R. G. (2012). Role of surface-water and groundwater interactions on projected summertime streamflow in snow dominated regions: An integrated modeling approach. Water Resources Research, 48, 1-20. https://doi.org/10.1029/2012WR012319W11524

Irvine, M. (2016). Using tracers to determine groundwater fluxes in a coastal aquitard-aquifer system. Doctoral dissertation, Flinders University, School of the Environment.

Ivanov, V. Y., Vivoni, E. R., Bras, R. L., & Entekhabi, D. (2004). Preserving high-resolution surface and rainfall data in operational-scale basin hydrology: A fully-distributed physically-based approach. Journal of Hydrology, 298(1-4), 80-111. https://doi.org/10.1016/j.jhydrol.2004.03.041

Jeffrey, S. J., J. O. Carter, K. B. Moodie, and A. R. Beswick (2001). Using spatial interpolation to construct a comprehensive archive of Australian climate data, Environ. Modell. Software, 16(4), 309–330. https://doi.org/10.1016/S1364-8152(01)00008-1

Jensen, C. K., McGuire, K. J., McLaughlin, D. L., & Scott, D. T. (2019). Quantifying spatiotemporal variation in headwater stream length using flow intermittency sensors. Environmental Monitoring and Assessment, 191(226). https://doi.org/10.1007/s10661-

019-7373-8

Jensen, C. K., McGuire, K. J., & Prince, P. S. (2017). Headwater stream length dynamics across four physiographic provinces of the Appalachian Highlands. Hydrological Processes, 31, 3350‐3363. https://doi.org/10.1002/hyp.11259

Jones, J. P., Sudicky, E. A., Brookfield, A. E., & Park, Y.-J. (2006). An assessment of the tracer-based approach to quantifying groundwater contributions to streamflow. Water Resources Research, 42, W02407. https://doi.org/10.1029/2005WR004130

Jones, J. P., Sudicky, E. A., & Mclaren, R. G. (2008). Application of a fully-integrated surface-subsurface flow model at the watershed-scale: A case study. Water Resources Research, 44(W03407), 1–13. https://doi.org/10.1029/2006WR005603

Käser, D., Graf, T., Cochand, F., Mclaren, R., Therrien, R., & Brunner, P. (2014). Channel Representation in Physically Based Models Coupling Groundwater and Surface Water: Pitfalls and How to Avoid Them. Groundwater, 52(6), 827–836. https://doi.org/10.1111/gwat.12143

Kennard, M. J., Pusey, B. J., Olden, J. D., MacKay, S. J., Stein, J. L., & Marsh, N. (2010). Classification of natural flow regimes in Australia to support environmental flow management. Freshwater Biology, 55(1), 171‐193. https://doi.org/10.1111/j.13652427.2009.02307.x

Keppel, R. V., & Renard, K. G. (1962). Transmission losses in ephemeral stream beds. Journal of the Hydraulics Division, 88(3), 59-68.

Kollet, S., Sulis, M., Maxwell, R. M., Paniconi, C., Putti, M., Bertoldi, G., et al. (2017). The integrated hydrologic model intercomparison project, IH-MIP2: A second set of benchmark results to diagnose integrated hydrology and feedbacks. Water Resources Research, 53, 867‐890. https://doi.org/10.1002/2016WR019191

Kristensen, K. J., & Jensen, S. E. (1975). A model for estimating actual evapotranspiration from potential evapotranspiration. Hydrology Research, 6(3), 170-188. https://doi.org/10.2166/nh.1975.0012

Lange, G. M. (1998). An approach to sustainable water management in Southern Africa using natural resource accounts: the experience in Namibia. Ecological Economics, 26(3), 299–311. https://doi.org/10.1016/S0921-8009(97)00119-5

Larned, S. T., Datry, T., Arscott, D. B., & Tockner, K. (2010). Emerging concepts in temporary-

river ecology. Freshwater Biology, 55(4), 717-738. https://doi.org/10.1111/j.1365-2427.2009.02322.x

Levick, L. R., Goodrich, D. C., Hernandez, M., Fonseca, J., Semmens, D. J., Stromberg, J., et al. (2008). The ecological and hydrological significance of ephemeral and intermittent streams in the arid and semi-arid American Southwest. U.S. Environmental Protection Agency and USDA/ARS Southwest Watershed Research Center. EPA/600/R-08/134, ARS/233046.

Li, L., Lambert, M. F., Maier, H. R., Partington, D., & Simmons, C. T. (2015). Assessment of the internal dynamics of the Australian Water Balance Model under different calibration regimes. Environmental Modelling & Software, 66, 57-68. https://doi.org/10.1016/j.envsoft.2014.12.015

Li, L., Maier, H. R., Lambert, M. F., Simmons, C. T., & Partington, D. (2013). Framework for assessing and improving the performance of recursive digital filters for baseflow estimation with application to the Lyne and Hollick filter. Environmental Modelling and Software, 41, 163-175. https://doi.org/10.1016/j.envsoft.2012.11.009

Li, L., Maier, H. R., Partington, D., Lambert, M. F., & Simmons, C. T. (2014). Performance assessment and improvement of recursive digital baseflow filters for catchments with different physical characteristics and hydrological inputs. Environmental Modelling and Software, 54, 39-52. https://doi.org/10.1016/j.envsoft.2013.12.011

Liu, F., Parmenter, R., Brooks, P. D., Conklin, M. H., & Bales, R. C. (2008). Seasonal and interannual variation of streamflow pathways and biogeochemical implications in semi-arid, forested catchments in Valles Caldera, New Mexico. Ecohydrology, 1(3), 239-252. https://doi.org/10.1002/eco.22

Loague, K., Heppner, C. S., Ebel, B. A., & VanderKwaak, J. E. (2010). The quixotic search for a comprehensive understanding of hydrologic response at the surface: Horton, Dunne, Dunton, and the role of concept-development simulation. Hydrological Processes, 24(17), 2499-2505. https://doi.org/10.1002/hyp.7834

Loague, K., Heppner, C. S., Mirus, B. B., Ebel, B. A., Ran, Q., Carr, A. E., et al. (2006). Physics-based hydrologic-response simulation: Foundation for hydroecology and hydrogeomorphology. Hydrological Processes, 20(5), 1231-1237. https://doi.org/

10.1002/ hyp.6179

Luce, C. H., & Cundy, T. W. (1994). Parameter identification for a runoff model for forest roads. Water Resources Research, 30(4), 1057‐1069. https://doi.org/10.1029/ 93WR03348

Martin, R. R. (1998). Willunga Basin- Status of Groundwater Resources 1998. Primary Industries and Resources, SA, Adelaide, pp. 1-27. Retrieved from www.scopus.com

Martin, R. R. (2006). Hydrogeology and Numercial Groundwater Flow Model for the McLaren Vale Prescribed Wells Area Summary Report. REM, Adelaide and Mount Lofty Ranges Natural Resource Management Board.

Maxwell, R. M. (2010). Infiltration in arid environments: Spatial patterns between subsurface heterogeneity and water-energy balances. Vadose Zone Journal, 9(4), 970‐983. https://doi.org/10.2136/ vzj2010.0014

Maxwell, R. M., & Kollet, S. J. (2008). Quantifying the effects of three-dimensional subsurface heterogeneity on Hortonian runoff processes using a coupled numerical, stochastic approach. Advances in Water Resources, 31(5), 807‐817. https://doi.org/10.1016/ j.advwatres.2008. 01.020

McDonough, O. T., Hosen, J. D., & Palmer, M. A. (2011). Temporary streams: The hydrology, geography, and ecology of non-perennially flowing waters. In H. S. Elliot, & L. E. Martin (Eds.), River Ecosystems: Dynamics, Management and Conservation, (pp. 259‐290). Inc: Nova Science Publishers.

Measurement Engineering Australia. (2019). Weather station data. Retrieved March 28, 2019, from https://weather-mclarenvale.info/observations

Meyerhoff, S. B., & Maxwell, R. M. (2011). Quantifying the effects of subsurface heterogeneity on hillslope runoff using a stochastic approach. Hydrogeology Journal, 19(8), 1515‐1530. https://doi.org/10.1007/s10040-011-0753-y

Mirus, B. B., Ebel, B. A., Heppner, C. S., & Loague, K. (2011). Assessing the detail needed to capture rainfall-runoff dynamics with physics based hydrologic response simulation. Water Resources Research, 47, 1‐18. https://doi.org/10.1029/2010WR009906 W00H10

Mirus, B. B., & Loague, K. (2013). How runoff begins (and ends): Characterizing hydrologic response at the catchment scale. Water Resources Research, 49, 2987‐3006.

https://doi.org/10.1002/wrcr.20218

Mirus, B. B., Loague, K., Cristea, N. C., Burges, S. J., & Kampf, S. K. (2011). A synthetic hydrologic-response dataset. Hydrological Processes, 25(23), 3688‐3692. https://doi.org/ 10.1002 /hyp.8185

Mirus, B. B., Loague, K., VanderKwaak, J. E., Kampf, S. K., & Burges, S. J. (2009). A hypothetical reality of Tarrawarra-like hydrologic response. Hydrological Processes, 23(7), 1093‐1103. https://doi.org/10.1002/hyp.7241

Mosley, M. P. (1979). Streamflow generation in a forested watershed, New Zealand. Water Resources Research, 15(4), 795‐806. https://doi.org/10.1029/WR015i004p00795

Nabhan, G. P. (1979). The ecology of floodwater farming in arid southwestern North America. Agro-Ecosystems, 5(3), 245–255. https://doi.org/10.1016/0304-3746(79)90004-0

Nadeau, T. L., & Rains, M. C. (2007). Hydrological connectivity between headwater streams and downstream waters: How science can inform policy. Journal of the American Water Resources Association, 43(1), 118–133. https://doi.org/10.1111/j.17521688.2007. 00010.x

NOAA's National Weather Service. (2018). Precipitation Frequency Data Server (PFDS). Retrieved August 31, 2018, from https://hdsc.nws. noaa.gov/hdsc/pfds/

Panday, S., & Huyakorn, P. S. (2004). A fully coupled physically-based spatially-distributed model for evaluating surface/subsurface flow. Advances in Water Resources, 27(4), 361‐382. https://doi.org/10.1016/j.advwatres.2004.02.016

Park, Y.-J., Sudicky, E. A., Brookfield, A. E., & Jones, J. P. (2011). Hydrologic response of catchments to precipitation: Quantification of mechanical carriers and origins of water. Water Resources Research, 47, 1‐11. https://doi.org/10.1029/2011WR010075 W12515

Partington, D., Brunner, P., Frei, S., Simmons, C. T., Werner, A. D., Therrien, R., et al. (2013). Interpreting streamflow generation mechanisms from integrated surface-subsurface flow models of a riparian wetland and catchment. Water Resources Research, 49, 5501‐5519. https://doi.org/10.1002/wrcr.20405

Partington, D., Brunner, P., Simmons, C. T., Therrien, R., Werner, A. D., Dandy, G. C., & Maier, H. R. (2011). A hydraulic mixing-cell method to quantify the groundwater component of stream flow within spatially distributed fully integrated surface water-

groundwater flow models. Environmental Modelling and Software, 26(7), 886‐898. https://doi.org/10.1016/ j.envsoft.2011.02.007

Partington, D., Brunner, P., Simmons, C. T., Werner, A. D., Therrien, R., Maier, H. R., & Dandy, G. C. (2012). Evaluation of outputs from automated baseflow separation methods against simulated baseflow from a physically based, surface water-groundwater flow model. Journal of Hydrology, 458‐459, 28‐39. https://doi.org/10.1016/j.jhydrol.2012.06.029

Partington, D., Shanafield, M., & Turnadge C. (in prep). Comparing methods of identifying non-stationary, non-linear processes from hydrological time series data.

Pearce, A. J. (1990). Streamflow generation processes: An Austral view. Water Resources Research, 26(12), 3037‐3047. https://doi.org/10.1029/WR026i012p03037

Pedregosa, F., Varoquaux, G., Gramfort, A., Michel, V., Thirion, B., Grisel, O., et al. (2011). Scikit-learn: Machine learning in Python. Journal of Machine Learning Research, 12, 2825‐2830.

Peirce, S. E., & Lindsay, J. B. (2015). Characterizing ephemeral streams in a southern Ontario watershed using electrical resistance sensors. Hydrological Processes, 29(1), 103‐111. https://doi.org/10.1002/hyp.10136

Penna, D., Tromp-Van Meerveld, H. J., Gobbi, A., Borga, M., & Dalla Fontana, G. (2011). The influence of soil moisture on threshold runoff generation processes in an alpine headwater catchment. Hydrology and Earth System Sciences, 15(3), 689‐702. https://doi.org/ 10.5194/hess-15-689-2011

Pierini, N. A., Vivoni, E. R., Robles-Morua, A., Scott, R. L., & Nearing, M. A. (2014). Using observations and a distributed hydrologic model to explore runoff thresholds linked with mesquite encroachment in the Sonoran Desert. Water Resources Research, 50, 8191‐8215. https://doi.org/10.1002/2014WR015781

Poff, N. L. R., Bledsoe, B. P., & Cuhaciyan, C. O. (2006). Hydrologic variation with land use across the contiguous United States: Geomorphic and ecological consequences for stream ecosystems. Geomorphology, 79(3–4), 264–285. https://doi.org/10.1016/j.geomorph. 2006.06.032

Prancevic, J. P., & Kirchner, J. W. (2019). Topographic controls on the extension and retraction of flowing streams. Geophysical Research Letters, 46, 2084‐2092. https://doi.org/

10.1029/2018GL081799

Ragan, R.M., 1968. An experimental investigation of partial area contributions. In: Hydrological Aspects of the Utilization of Water, vol. II, Proceedings of the General Assembly of Bern, IAHS Publication No. 76. International Association of Hydrological

Rhif, M., Abbes, Ben Abbes, A., Farah, I. R., Martínez, B., & Sang, Y. (2019). Wavelet transform application for/in non-stationary time-series analysis: A review. Applied Sciences, 9(7), 1345. https://doi.org/10.3390/app9071345

Sandor, J.A., Norton, J.B., Homburg, J.A., Muenchrath, D.A., White, C.S., Williams, S.E., Havener, C.I. and Stahl, P.D. (2007), Biogeochemical studies of a Native American runoff agroecosystem. Geoarchaeology, 22: 359-386. doi:10.1002/gea.20157

Saft, M., Peel, M. C., Western, A. W., & Zhang, L. (2016). Predicting shifts in rainfall-runoff partitioning during multiyear drought: Roles of dry period and catchment characteristics. Water Resources Research, 52, 9290‐9305. https://doi.org/10.1002/2016WR019525

Sang, Y. F., Wang, D., Wu, J. C., Zhu, Q. P., & Wang, L. (2013). Improved continuous wavelet analysis of variation in the dominant period of hydrological time series. Hydrological Sciences Journal, 58(1), 118–132. https://doi.org/10.1080/02626667.2012.742194

Schaap, M. G., Leij, F. J., & van Genuchten, M. T. (2002). ROSETTA: a computer program for estimating soil hydraulic parameters with hierarchical pedotransfer functions. Journal of Hydrology, 251(3-4), 163–176. https://doi.org/10.1016/S0022-1694(01)00466-8.

Sebben, M. L., Werner, A. D., Liggett, J. E., Partington, D., & Simmons, C. T. (2013). On the testing of fully integrated surface‐subsurface hydrological models. Hydrological Processes, 27(8), 1276‐1285. https://doi.org/10.1002/hyp.9630

Seely, M., Henderson, J., Heyns, P., Jacobson, P., Nakale, T., Nantanga, K., Schachtschneider, K., 2003. Ephemeral and endoreic river systems: Relevance and management challenges. Transboundary Rivers, Sovereignty and Development. Hydropolitical Drivers in the Okavango River basin, Pretoria, 187-212.

Sereda, A., & Martin, R. R. (2000). Willunga groundwater basin observation well network monitoring and trends in aquifers.

Shanafield, M., & Cook, P. G. (2014). Transmission losses, infiltration and groundwater recharge through ephemeral and intermittent streambeds: A review of applied methods. Journal of Hydrology, 511, 518‐529. https://doi.org/10.1016/j.jhydrol.2014.01.068

Shanafield, M., Bourke, S., Zimmer, M. (in prep) A primer on the hydrology of non-perennial water ways: Our current understanding, methodologic challenges, knowledge gaps, and research directions

Shanafield, M., Niswonger, R. G., Prudic, D. E., Pohll, G., Susfalk, R., & Panday, S. (2014). A method for estimating spatially variable seepage and hydraulic conductivity in channels with very mild slopes. Hydrological Processes, 28(1), 51–61. https://doi.org/10.1002/hyp.9545

Shangguan, W., Hengl, T., Mendes de Jesus, J., Yuan, H., & Dai, Y. (2017). Mapping the global depth to bedrock for land surface modeling. Journal of Advances in Modeling Earth Systems, 9, 65-88. https://doi.org/10.1002/2016MS000686

Sheldon, F., Bunn, S. E., Hughes, J. M., Arthington, A. H., Balcombe, S. R., & Fellows, C. S. (2010). Ecological roles and threats to aquatic refugia in arid landscapes: Dryland river waterholes. Marine and Freshwater Research, 61(8), 885-895. https://doi.org/10.1071/MF09239

SILO, Australian Climate Data. (2019). Station 232729 climate records. Retrieved March 28, 2019, from https://www.longpaddock.qld.gov.au/silo/

Skoulikidis, N. T., Sabater, S., Datry, T., Morais, M. M., Buffagni, A., Dörflinger, G., et al. (2017). Non-perennial Mediterranean Rivers in Europe: Status, pressures, and challenges for research and management. Science of the Total Environment, 577, 1-18. https://doi.org/10.1016/j.scitotenv.2016.10.147

Smith, R. E., & Hebbert, R. H. B. (1979). A Monte Carlo analysis of the hydrologic effects of spatial variability of infiltration. Water Resources Research, 15(2), 419-429. https://doi.org/10.1029/WR015i002p00419

Smith, R. E., & Hebbert, R. H. B. (1983). Mathematical simulation of interdependent surface and subsurface hydrologic processes. Water Resources Research, 19(4), 987-1001. https://doi.org/10.1029/WR019i004p00987

Smith, R. E., & Woolhiser, D. A. (1971). Overland flow on an infiltrating surface. Water Resources Research, 7(4), 899-913. https://doi.org/10.1029/WR007i004p00899

Snelder, T. H., Datry, T., Lamouroux, N., Larned, S. T., Sauquet, E., Pella, H., & Catalogne, C. (2013). Regionalization of patterns of flow intermittence from gauging station records. Hydrology and Earth System Sciences, 17(7), 2685-2699. https://doi.org/10.5194/hess-

17-2685-2013

Sophocleous, M. (2002). Interactions between groundwater and surface water: The state of the science. Hydrogeology Journal, 10(1), 52‑67. https://doi.org/10.1007/s10040-001-0170-8

Steward, A. L., von Schiller, D., Tockner, K., Marshall, J. C., & Bunn, S. E. (2012). When the river runs dry: Human and ecological values of dry riverbeds. Frontiers in Ecology and the Environment, 10(4), 202‑209. https://doi.org/10.1890/110136

Stubbington, R., Chadd, R., Cid, N., Csabai, Z., Miliša, M., Morais, M., et al. (2018). Biomonitoring of intermittent rivers and ephemeral streams in Europe: Current practice and priorities to enhance ecological status assessments. Science of the Total Environment, 618, 1096–1113. https://doi.org/10.1016/j.scitotenv.2017.09.137

Sudicky, E. A., Jones, J. P., Park, Y., Brookfield, A. E., & Colautti, D. (2008). Simulating complex flow and transport dynamics in an integrated surface-subsurface modeling framework. Geosciences Journal, 12(2), 107‑122. https://doi.org/10.1007/s12303-008-0013-x

Thoma, M. J., Barrash, W., Cardiff, M., Bradford, J., & Mead, J. (2014). Estimating unsaturated hydraulic functions for coarse sediment from a field-scale infiltration experiment. Vadose Zone Journal, 13(3), 1‑17. https://doi.org/10.2136/vzj2013.05.0096

Thomas, B. F., Behrangi, A., & Famiglietti, J. S. (2016). Precipitation intensity effects on groundwater recharge in the southwestern United States. Watermark, 8(3), 90. https://doi.org/ 10.3390/w8030090

Trenberth, K. E., Dai, A., Rasmussen, R. M., & Parsons, D. B. (2003). The changing character of precipitation. Bulletin of the American Meteorological Society, 84(9), 1205‑1217. https://doi.org/10.1175/BAMS-84-9-1205

Trudel, M., Leconte, R., & Paniconi, C. (2014). Analysis of the hydrological response of a distributed physically-based model using postassimilation (EnKF) diagnostics of streamflow and in situ soil moisture observations. Journal of Hydrology, 514, 192‑201. https://doi.org/ 10.1016/j.jhydrol.2014.03.072

Tzoraki, O., & Nikolaidis, N. P. (2007). A generalized framework for modeling the hydrologic and biogeochemical response of a Mediterranean temporary river basin. Journal of

Hydrology, 346(3-4), 112-121. https://doi.org/10.1016/j.jhydrol.2007.08.025

van Genuchten, M. T. (1980). A closed-form equation for predicccting hydraulic conductivity of unsaturated soils. Soil Science Society of America Journal, 44, 892-898. https://doi.org/doi:10.2136/sssaj1980.03615995004400050002x

VanderKwaak, J. E. (1999). Numerical simulation of flow and chemical transport in integrated surface-subsurface hydrologic systems. Ontario, Canada. Retrieved from: Ph. D thesis. University of Waterloo. http://hdl.handle.net/10012/412

VanderKwaak, J. E., & Loague, K. (2001). Hydrologic-response simulations for the R-5 catchment with a comprehensive physics-based model. Water Resources Research, 37(4), 999-1013. https://doi.org/10.1029/2000WR900272

VanderKwaak, J. E., & Sudicky, E. A. (2000). Application of a physically-based numerical model of surface and subsurface water flow and solute transport. In ModelCARE'99 Conference, (pp. 515-523). Zurich, Switzerland: IAHS-AISH Publication. Retrieved from: https://www.scopus.com/record/display.uri?eid=2s2.0033785150&origin=inward&txGid=d2 64a8f17fe4a371ff1b48f10e3f4e0a

Vivoni, E. R., Entekhabi, D., Bras, R. L., & Ivanov, V. Y. (2007). Controls on runoff generation and scale-dependence in a distributed hydrologic model. Hydrology and Earth System Sciences, 11(5), 1683-1701. https://doi.org/10.5194/hess-11-1683-2007

Ward, A. S., Schmadel, N. M., & Wondzell, S. M. (2018). Simulation of dynamic expansion, contraction, and connectivity in a mountain stream network. Advances in Water Resources, 114, 64-82. https://doi.org/10.1016/j.advwatres.2018.01.018

AMLR, Water Data Services (2019). Pedler Creek @ Stump Hill Road - A5030543. Retrieved March 10, 2019, from: https://amlr.waterdata.com.au/Flow.aspx?sno=A5030543&Report=trSummary

Weill, S., Altissimo, M., Cassiani, G., Deiana, R., Marani, M., & Putti, M. (2013). Saturated area dynamics and streamflow generation from coupled surface-subsurface simulations and field observations. Advances in Water Resources, 59, 196-208. https://doi.org/10.1016/j.advwatres. 2013.06.007

Whiting, J. A., & Godsey, S. E. (2016). Discontinuous headwater stream networks with stable flowheads, Salmon River basin, Idaho. Hydrological Processes, 30(13), 2305–2316.

https://doi.org/10.1002/hyp.10790

Wigington, P. J., Jr, Moser, T. J., & Lindeman, D. R. (2005). Stream network expansion: A riparian water quality factor. Hydrological Processes, 19(8), 1715–1721. https://doi.org/10.1002/hyp.5866

Wigmosta, M. S., Vail, L. W., and Lettenmaier, D. P. (1994). A distributed hydrology-vegetation model for complex terrain, Water Resour. Res., 30(6), 1665– 1679, doi:10.1029/94WR00436.

Zehe, E., & Sivapalan, M. (2009). Threshold behaviour in hydrological systems as (human) geo-ecosystems: manifestations, controls, implications. Hydrology and Earth System Sciences, 13(7), 1273‐1297. https://doi.org/10.5194/hess-13-1273-2009

Zimmer, M. A., & McGlynn, B. L. (2017). Bidirectional stream‐groundwater flow in response to ephemeral and intermittent streamflow and groundwater seasonality. Hydrological Processes, 31(22), 3871‐3880. https://doi.org/10.1002/hyp.11301

Zimmer, M. A., & McGlynn, B. L. (2018). Lateral, vertical, and longitudinal source area connectivity drive runoff and carbon export across watershed scales. Water Resources Research, 54(3), 1576‐1598. https://doi.org/10.1002/2017WR021718

Zimmermann, B., Zimmermann, A., Turner, B. L., Francke, T., & Elsenbeer, H. (2014). Connectivity of overland flow by drainage network expansion in a rain forest catchment. Water Resources Research, 50, 1457‐1473. https://doi.org/10.1002/2012WR012660